

AIR FORCE MISSILE DEVELOPMENT CENTER TECHNICAL REPORT

AD 667514

PREDICTED FORCING FUNCTIONS AND FORCE
MEASUREMENTS ON AN OUTRIGGER ROCKET SLED
TRAVELING THROUGH A BLAST ENVIRONMENT

Daniel J. Krupovage

Distribution of this document is unlimited.



DDX
APR 16 1968
HOLLoman

December 1967

**HOLLOMAN AIR FORCE BASE
NEW MEXICO**

Reproduced by the
CLEARINGHOUSE
for Federal Scientific & Technical
Information Springfield, Va. 22151

MDC-TR-62-7

PREDICTED FORCING FUNCTIONS AND FORCE
MEASUREMENTS ON AN OUTRIGGER ROCKET SLED
TRAVELING THROUGH A BLAST ENVIRONMENT

Daniel J. Krupovage

Distribution of this document is unlimited.

December 1967

AIR FORCE MISSILE DEVELOPMENT CENTER
DIRECTORATE OF TEST TRACK
AIR FORCE SYSTEMS COMMAND
WOLFWAN AIR FORCE BASE, NEW MEXICO 80380

FOREWORD

This report was prepared in the Engineering Division of the Test Track Directorate under Projects 6876 (Track Facility Development) and 5710 (Nuclear Weapons Effects Research and Testing).

The author is indebted to the following persons: Hans J. Rasmussen, Technical Director of the Test Track, for his technical advice concerning sled aerodynamics and blast wave phenomena; to Paul H. Sonnenburg formerly of the Track Engineering Division who initiated the computer program, set up the initial approximations used in the computer solutions, and designed the force transducer; to Peter Cook and Richard A. Ward of the Digital Computation Division of AFMPC (MOR) who set up the numerical solution techniques and programmed the equations of the CEC 3000 computer.

PUBLICATION REVIEW

This technical report has been reviewed and is approved.


TYLER A. REDFIELD
Colonel, USAF
Director, Test Track

ABSTRACT

A technique was developed for predicting the aerodynamic forcing functions acting on an outrigger rocket sled as it traversed a blast environment. This technique was programmed on the CDC 3600 computer. In order to computerize the technique, the time histories of the blast parameters were approximated by first and third order polynomial equations. The sled trajectory was transformed into the scaled time and distance coordinates of the blast parameters. The steady state aerodynamic coefficients as a function of Mach number obtained from wind tunnel tests were approximated by third order polynomials. These steady state coefficients were used at discrete times to define the aerodynamic forces acting on the vehicle as it traversed the blast environment.

The report also describes the load transducer used to measure the lateral forces acting on the front slipper of the outrigger rocket sled. The time history of these measured forces and lateral acceleration data is discussed. A maximum force on the front slipper of 76,000 pounds was recorded on one of the runs. Also included is information on the vehicle structural vibration frequencies, which was obtained from reduction of test data in the form of power spectral density.

TABLE OF CONTENTS

	<u>Page</u>
Foreword	ii
Abstract	iii
List of Illustrations	v
List of Symbols	ix
Section I. Introduction	1
Section II. Blast Wave Phenomena	3
Section III. Equipment and Procedures	5
1. Procedure for Predicting Sled Aerodynamic Forcing Functions	5
2. Adaptation of the Procedure for Predicting Sled Aerodynamic Forcing Functions to a Computer	9
3. Force Transducer	12
4. Accelerometer	15
5. Power Spectral Density Computations	15
Section IV. Discussion and Results	17
1. Computer Calculated Aerodynamic Forcing Functions	17
2. Force Measurements	19
3. Predicted Forcing Functions and Measured Response	22
4. Acceleration Measurements	23
5. Power Spectral Density Plots	24
Section V. Conclusions	26
References	27
Appendix	91

LIST OF ILLUSTRATIONS

<u>FIGURE</u>		<u>PAGE</u>
1	Schematic of Modified Track Cross-Section in Blast Test Area	28
2	Schematic of a Blast Overpressure on a Ground Fixed Object	29
3	Three Stage Outrigger Rocket Sled	30
4	Schematic of Velocity and Force Vectors Acting on the Rocket Sled	31
5	Time Histories of the Density Ratio ρ_B/ρ_0 Gen- erated by a Free Field TNT Explosion	32
6	Schematic of the Force Transducer and Strain Gage Locations	33
7	Slipper Installation Cross Section	34
8	Port Side Applied Load Versus Bridge Output	35
9	Starboard Side Applied Load Versus Bridge Output	36
10	Blast Environment Vertical Force Versus Time (Group I)	37
11	Blast Environment Lateral Force Versus Time (Group I)	38
12	Blast Environment Axial Force Versus Time (Group I)	39
13	Blast Environment Rolling Moment Versus Time (Group I)	40
14	Blast Environment Pitching Moment Versus Time (Group I)	41
15	Blast Environment Yawing Moment Versus Time (Group I)	42
16	Blast Environment Vertical Force Versus Time (Group II)	43
17	Blast Environment Lateral Force Versus Time (Group II)	44

<u>FIGURE</u>		<u>PAGE</u>
18	Blast Environment Axial Force Versus Time (Group II)	45
19	Blast Environment Rolling Moment Versus Time (Group II)	46
20	Blast Environment Pitching Moment Versus Time (Group II)	47
21	Blast Environment Yawing Moment Versus Time (Group II)	48
22	Blast Environment Vertical Force Versus Time (Group III)	49
23	Blast Environment Lateral Force Versus Time (Group III)	50
24	Blast Environment Axial Force Versus Time (Group III)	51
25	Blast Environment Rolling Moment Versus Time (Group III)	52
26	Blast Environment Pitching Moment Versus Time (Group III)	53
27	Blast Environment Yawing Moment Versus Time (Group III)	54
28	Forward Slipper Lateral Force as a Function of Time for 1,552 Pounds of TNT	55
29	Forward Slipper Lateral Force as a Function of Time for 2,672 Pounds of TNT	56
30	Forward Slipper Lateral Force as a Function of Time for 4,000 Pounds of TNT	57
31	Permanent Track Deflection in Blast Test Area	58
32	Sled Lateral Acceleration as a Function of Time	59
33	Sled Lateral Acceleration as a Function of Time in the Blast Environment	60
34	Velocity and Longitudinal Acceleration as a Function of Time for Sled Run 5B-G1	61

<u>FIGURE</u>		<u>PAGE</u>
35	Sanborn Power Versus Time (Run 5B-F1 - Port)	62
36	Sanborn Power Versus Time (Run 5B-F1 - Starboard)	63
37	Sanborn Power Versus Time (Run 5B-F1 - Acceleration)	64
38	Power Spectral Density (Port - 4 to 5 seconds)	65
39	Power Spectral Density (Port - 5 to 6 seconds)	66
40	Power Spectral Density (Starboard - 4 to 5 seconds)	67
41	Power Spectral Density (Starboard - 5 to 6 seconds)	68
42	Power Spectral Density (Acceleration - 4 to 5 sec)	69
43	Power Spectral Density (Acceleration - 7.5 to 8.5 seconds)	70
44	Power Spectral Density (Acceleration - 4 to 5 sec)	71
45	Power Spectral Density (Acceleration - 5 to 6 sec)	72
46	Power Spectral Density (Acceleration - 7.5 to 3.5 seconds)	73
47	Power Spectral Density (Acceleration - 9 to 10 sec)	74
48	Sanborn Power Versus Time (Run 5B-G1 - Port)	75
49	Sanborn Power Versus Time (Run 5B-G1 - Starboard)	76
50	Sanborn Power Versus Time (Run 5B-G1 - Acceleration)	77
51	Power Spectral Density (Port - 5 to 6 seconds)	78
52	Power Spectral Density (Starboard - 5 to 6 sec)	79
53	Power Spectral Density (Acceleration - 5 to 6 sec)	80
54	Power Spectral Density (Acceleration - 6.5 to 7.5 seconds)	81
55	Power Spectral Density (Port - 6.5 to 7.5 sec)	82
56	Power Spectral Density (Port - 8.5 to 9.5 sec)	83
57	Power Spectral Density (Starboard - 6.5 to 7.5 sec)	84

<u>FIGURE</u>		<u>PAGE</u>
58	Power Spectral Density (Acceleration 8.5 to 9.5 seconds)	85
59	Sanborn Power Versus Time (Run 6B-A1 - Acceleration)	86
60	Power Spectral Density (Acceleration - 4 to 5 sec)	87
61	Power Spectral Density (Acceleration - 5 to 6 sec)	88
62	Power Spectral Density (Acceleration - 6 to 7 sec)	89
63	Power Spectral Density (Acceleration - 9 to 10 sec)	90

LIST OF SYMBOLS

A	3.1416 ft ²	Reference Area
a	ft/sec	Speed of Sound
AA thru IIII		Constants for Aerodynamic Coefficient Polynomial
C		Constant for Power Curves
c		Sled Aerodynamic Coefficient
D	lbs	Drag Force
D ₁ , D ₂ , D ₃ ...etc		Constants for the Polynomial Relating the Power Curve Constants
$\frac{dV}{dt}$	ft/sec ²	Sled Acceleration
F	lbs	Force
F, G, H, Q		When subscripted, represents constants for the polynomial equation relating to the power curve constants.
g	32.2 ft/sec ²	Acceleration Constant
Hz	cycles/sec	Hertz
J		Blast Parameters in Computer Program
ℓ	7 ft	Moment Reference Length
II		Mach Number
I ₁ , I ₂ , I ₃ ...etc		Moment in Foot Pounds.
OC thru RR		Constants for Aerodynamic Coefficient Polynomials
P	lb/in ²	Pressure
PDC	Per degree	Computer Term for $\frac{\partial C}{\partial \psi}$
R	ft	Radial Distance from Ground Zero (See Figure 4)
r		Ground Reflection Factor

S	Ft	Track Station
THETA	degrees	Computer Term for ψ
t	sec	Time
U	ft/sec	Shock Front Velocity
u	ft/sec	Particle Velocity (See Figure 4)
V	ft/sec	Sled Velocity with Respect to Ground (See Figure 4)
W	lbs	Weight of TNT Charge
w	lbs	Weight of Rocket Sled
Y	sec/lb ^{1/3}	Scaled Time
Z	ft/lb ^{1/3}	Scaled Distance
λ	lb ^{1/3}	Scale Factor
ϕ	degrees	Angle of Intercept (See Figure 4)
ρ	$\frac{\text{lb-sec}^2}{\text{ft}^4}$	Density
ψ	degrees	Angle of Yaw (See Figure 4)
$\frac{\partial c}{\partial \psi}$	per degree	Slope of Force or Moment Coefficient Versus Angle of Yaw

Subscripts

B	In Blast Environment
b	Instant of Charge Detonation
D	Drag Force
E	Equivalent
i	Initial or Intercept Point
j	Angle of Yaw for Zero Aerodynamic Force or Moment

I	Rolling Moment
II	Pitching Moment
m	Points of Computation for Particular Variable (m = 1, 2,...etc)
II	Vertical Force
n	Yawing Moment
O	Ambient Conditions, or Perpendicular Distance from Track to Ground Zero
R	Reflected
r	Relative
s	Side-on
SH	Immediately Behind Shock
SL	Sea Level
1.	Blast Pressure, Vertical Force or Polynomial Coefficients
2.	Blast Pressure, Lateral Force, or Polynomial Coefficients
3.	Particle Velocity, Longitudinal Force or Polynomial Coefficients
4.	Particle Velocity, Rolling Moment or Polynomial Coefficients
5.	Blast Density, Pitching Moment or Polynomial Coefficients
6.	Blast Density, Yawing Moment or Polynomial Coefficients

BLANK PAGE

SECTION I

INTRODUCTION

In 1963 the Holloman High Speed Test Track initiated the development of a rocket sled capable of carrying an externally mounted payload of approximately 300 pounds through a blast environment generated by track-side HE detonation. The charge was to be detonated near the ground at a distance of approximately 160 feet to one side of the track. The external payload was mounted on the sled to experience free stream aerodynamic conditions; i.e., the flow field around the payload was not to be influenced by flow disturbances or shock waves generated by the rocket sled or the ground. The sled was designed for a maximum free stream Mach number of 3.0. An outrigger vehicle was considered to be an acceptable configuration. This configuration allowed for the payload to be suspended sufficiently high above the ground to eliminate flow interference while minimizing sled frontal area. The height above the ground was selected to prevent the reflection of the shock wave generated by the external payload from impinging on this payload at speeds above Mach 2.0. A series of wind tunnel tests was conducted at Arnold Engineering Development Center, Tennessee, to determine the aerodynamic characteristics of the selected vehicle configuration. The results of these tests are reported in Reference 1, 2 and 3.

In the blast test area the track configuration was modified to provide a clean blast environment for the sled, i.e., an environment which is free of debris and blast shock front reflections. In order to achieve this, it was necessary to asphalt the ground in the immediate area of the blast. In the test area the track rail was located approximately 19 inches above ground level. Shock tube tests conducted at Massachusetts Institute of Technology (reference 4) showed that this would cause detrimental interference with the blast environment. It was, therefore, decided to provide a ramp from the ground to the level of the rail top surface as schematically shown in Figure 1. Also, the shock tube tests showed that the trough (i.e., the area between and below the rails) would cause additional interference. Therefore, the trough was filled to six inches below the top surface of the rail in the sled blast intercept area. A ramp of 200 foot length was installed at both ends of this area in order to minimize the abrupt changes in sled aerodynamic loading and structural response which would have been caused by a single step up to the height of the filled trough.

A method was developed for predicting the forces which the sled, the rail and the track foundation would experience as the sled traversed the blast environment. The method used was a static force analysis at discreet times during sled blast intercept. The location and size of the explosive charge, angle of sled-shock front intercept and sled velocity were specified. Based on these initial conditions, the incremental time history of the blast parameters (i.e., pressure, density and particle velocity) was determined

through the use of References 5 and 6. After the sled-blast environment conditions were determined, the resultant aerodynamic forces were calculated from the aerodynamic coefficients obtained from the wind tunnel tests. This technique was programmed for the CDC 3600 computer.

The sled aerodynamic forces predicted this way are a part of the sled forcing functions. Professor M. M. Cottrell of the University of New Mexico developed a technique for predicting the sled structural response to these aerodynamic forcing functions. A technical report (Reference 7) has been prepared describing this technique.

In order to validate the previously mentioned techniques, efforts were made to measure forces on the vehicle. As a first approach strain gages were layed on critical points of the vehicle. However, during the calibration and after a few low velocity runs, it became evident that the cross-talk was too severe and it did not allow determination of the direction of the loading. Another approach, which was finally adopted, employed the load unit described in Section III of this report.

SECTION II

BLAST WAVE PHENOMENA

The detonation of an explosive charge in a gaseous medium, such as air, is followed by abrupt changes in the state of the medium. The detonation wave in an explosive charge, such as TNT, travels at approximately 22,000 feet per second. Following the detonation of the charge an essentially spherical blast wave emanates from the center of the explosion. This blast wave initially travels at velocities above the speed of sound in the unaffected region of air but rapidly approaches the velocity of sound. The wave front velocity in air is given by the following equation (Reference 6):

$$U = a_0 \left(1 + \frac{6\Delta P_s}{7P_0}\right)^{1/2} \quad (1)$$

Other changes in the medium effected by the detonation are characterized by a change in the velocity of the particles of the medium called particle velocity and a change in the density of the medium. The magnitudes of these changes immediately behind the shock front are given by the following equations (Reference 6):

$$u_{SH} = \frac{5a_0\Delta P_s}{7P_0} \left(1 + \frac{6\Delta P_s}{7P_0}\right)^{-1/2} \quad (2)$$

and

$$\rho_{SH} = \rho_0 \left(7 + \frac{6\Delta P_s}{P_0}\right) / \left(7 + \frac{\Delta P_s}{P_0}\right) \quad (3)$$

If the charge is detonated near the ground, the magnitudes of the quantities previously described are increased. This is due to the reflection of the original blast wave from the ground surface. The reflected wave is traveling in an environment of increased pressure generated by the explosion, and rapidly overtakes the original hemispherical blast wave front. When this takes place, a Mach stem begins to form at ground level (Reference 8). The stem increases in height as the combined front moves away from ground zero. The point above the ground at which the reflected blast wave, the initial blast wave front and the Mach stem intersect is termed the triple point. The location of this point at various distances from ground zero is reported in Reference 9. This enhancement of the blast environment by the blast wave reflection was a desirable effect in the rocket sled tests. It allowed

for higher pressures, densities and particle velocities with less charge weight than free air blast conditions require.

The time history of the pressure fluctuation a ground fixed object experiences as a blast wave traverses its location is schematically shown in Figure 2. The object first experiences the impingement of the high pressure (side-on pressure, P_s) of the blast wave on its forward surface. This pressure rises almost instantaneously to a pressure above the side-on pressure. This pressure is called the reflected pressure (P_R), and has a magnitude dependent on the shape of the object. As the side-on and reflected pressures are being developed, the object also experiences a dynamic pressure effect $C_D(q)$ which is equal to $C_D(1/2\rho_B u^2)$. Here ρ_B is the density in the blast and u is the particle velocity. The object is now experiencing the pressure at point b on the pressure time history curve of Figure 2. The reflected pressure exists for the time it takes a shock wave, moving at the speed of sound in the blast environment, to traverse the distance h (see Figure 2a). The pressure on the object has now decayed to point c in Figure 2. As the blast front engulfs the object (see Figure 2c) and diffracts (see Figure 2d) around the back surface, the pressure differential between the forward and rear surfaces essentially becomes zero for relatively small objects, such as a rocket sled vehicle. The pressure on the object has now decayed to point e in Figure 2. As time proceeds, the object experiences a decay in pressure, air density (ρ_B) and particle velocity (u). These quantities decay to ambient conditions with the decay in particle velocity slightly lagging that of the pressure. Following this, these three quantities decrease below ambient conditions and return to ambient conditions when the blast wave has completely traversed the object (point f in Figure 2).

An object moving relative to ground zero and thus to an expanding blast field will experience similar phenomena. However, if the velocity of the object is in the same order of magnitude as the blast wave particle velocity both must be added vectorially. The resultant velocity determined this way is used to calculate the dynamic pressure forces on the object. In this report, the aerodynamic forcing functions generated in a blast environment are determined by means of vector addition of the component velocities. The resultant velocity and angle of attack are used to determine the appropriate aerodynamic force and moment coefficients from the steady state coefficients obtained from wind tunnel tests.

SECTION III

EQUIPMENT AND PROCEDURES

1. PROCEDURE FOR PREDICTING SLED AERODYNAMIC FORCING FUNCTIONS

In order to calculate the aerodynamic forcing functions acting on the outrigger rocket sled (see Figure 3) as it traverses a blast environment, excluding the initial engulfment of the sled in the blast wave, the following parameters must be specified (see Figure 4):

- a. The angle (ϕ_f) between a line drawn from ground zero perpendicular to the track and a line drawn from ground zero and the point of blast wave and sled interception.
- b. Perpendicular distance (R_0) from ground zero to the track.
- c. Weight (W) of TNT charge.
- d. Velocity (V) of the sled as it traverses the blast environment relative to a ground fixed coordinate system.
- e. Sled aerodynamic force and moment coefficients as functions of time and angle of yaw (ψ - rotation about a vertical axis through the sled).

These parameters are not the only way of defining a desired sled-blast wave environment. For example, the environment could be defined by specifying blast overpressure and duration. However, these can easily be converted to charge weight and intercept point.

Before proceeding to the details of the procedure a comment concerning the sled velocity is necessary. It was previously stated that the time history of the sled velocity relative to the ground was required. For the test series for which this procedure was set up, the sled was in a zero thrust condition (i.e., deceleration) during blast interception and, therefore, the velocity depends on the air drag. The drag under this condition can be described by the following equation:

$$D = c_D A (1/2) \rho V^2 = \frac{W}{g} \frac{dV}{dt} \quad (4)$$

The effects of friction between the sled slipper and the rail can be neglected at the velocity under study without significant loss in accuracy. To use this equation, the drag coefficient (c_D) as a function of Mach number ($M = V/a$) must be available. If the sled is decelerating or the speed of sound (a) in the blast environment has changed, c_D is not constant. However, since only small changes in Mach number occur during

blast intercept, C_D was assumed constant. Likewise, the drag is affected by the changes in density which occur during blast wave interception. However, since the time interval over which the density changes occurred was very short (less than 0.1 seconds) the effect of this on the velocity of the sled relative to the ground was neglected. Therefore, with these assumptions, the velocity of the sled relative to the ground was assumed to be constant.

In order to obtain a time history of the blast parameters (i.e., particle velocity (u), density (ρ_3) and overpressure (P) and the resulting forcing functions the sled trajectory must first be mapped into the scaled time and distance plane on which these parameters are described. These parameters on the scaled time distance plane are plotted in Reference 5 or 6. Reference 6 was used in this report.

Step 1

Select a time interval (e.g., 4 milliseconds) to step the parameters. Using the initial parameters and the following equation, the location (radial distance) of the sled relative to ground zero as a function of time t_m is determined (see Figure 4).

$$R_m = R_0 / \sin \left[\tan^{-1} \frac{R_0}{(R_0 / \tan \phi_i - V t_m)} \right] \quad (5)$$

The scaled time and distance can now be determined from the following equation.

$$Z_{T_m} = \frac{R_m}{\lambda} \quad (\text{scaled distance}) \quad (6)$$

$$Y_{T_m} = \frac{t_m \bar{a}}{\lambda} \quad (\text{scaled time}) \quad (7)$$

where:

$$\lambda = \left(\frac{W_E}{\bar{P}} \right)^{1/3}$$

$$W_E = rW$$

For Holloman conditions (at 68°F)

$$\bar{p} = \frac{P_0}{P_{SL}} = \frac{12.7}{14.7} = 0.8639$$

$$\bar{a} = \frac{a_0}{a_{SL}} = \frac{1126}{1117} = 1.00806$$

The quantity r is the ground reflection factor which must be included to convert the blast parameters obtained from free-field data in Reference 6 to the parameters which exist if a reflecting plane is present. This value is in the order of 1.8.....1.9. This is the approximate value of the reflection factor obtained from a small number of pressure measurements made at the Holloman Track Facility.

Step 2

Using the values of Z and Y just obtained in the curves of Reference 6, the time history of the blast parameters (P , u , ρ_0) can be tabulated. Figure 5 shows a typical blast parameter time history curve of Reference 6 with two sled trajectories mapped onto it.

Step 3

It is necessary to obtain the angle of yaw, ψ , and relative velocity, V_r , (see Figure 4). These parameters can be obtained from the following equations:

$$\psi_m = \tan^{-1} \left[\frac{u_m \sin \phi_m}{V + u_m \cos \phi_m} \right] \quad (\text{angle of yaw}) \quad (8)$$

$$V_{rm} = \frac{V + u_m \cos \phi_m}{\cos \psi_m} \quad (\text{relative velocity}) \quad (9)$$

where:

$$\phi_r = \sin^{-1} \frac{R_0}{R_r}$$

Step 4

In order to relate the previous parameters to Mach number it is necessary to obtain the speed of sound in the blast environment.

This is calculated from the following equations:

$$a_{rm} = a_0 \left[(1 + \Delta P_{Bm}/P_0) / (\rho_{Bm}/\rho_0) \right]^{1/2} \quad \begin{array}{l} \text{(Relative speed} \\ \text{of sound)} \end{array} \quad (10)$$

$$M_{rm} = \frac{V_{rm}}{a_{rm}} \quad \begin{array}{l} \text{(Relative Mach Number)} \end{array} \quad (11)$$

For Holloman conditions (at 68°F)

$$\rho_0 = 2.017 \times 10^{-3} \frac{\text{lb-sec}^2}{\text{ft}^4}$$

$$P_0 = 12.7 \text{ lb/in}^2$$

$$a_0 = 1126 \text{ ft/sec}^2$$

Step 5

For the previously determined relative Mach numbers and angles of yaw at the selected instances of time (t_m) in the blast environment, the aerodynamic force and moment coefficients are then obtained from wind tunnel data. For the vehicle under consideration, the aerodynamic coefficients as function of Mach number and angle of yaw were taken for configuration $P_1 D_{mod_0}$ as defined in Reference 3.

These coefficients are:

c_{z1} = vertical force coefficient

c_{y1} = side force coefficient

c_{D1} = axial force coefficient

c_{l1} = rolling moment coefficient

c_{m1} = pitching moment coefficient

c_{n1} = yaw moment coefficient

The force and moment coefficients were referenced to a point between the forward and aft most slippers on the main body (see Figure 4). The reference area is the cylindrical cross-sectional area at this point (i.e., $A = 3.1416 \text{ ft}^2$). The reference length is the distance between the track rail centerlines (i.e., $\ell = 7 \text{ ft}$).

Step 6

Using the previously determined information, the sled aerodynamic forcing functions can now be obtained from the following typical force and moment equations for each time:

$$F_{()} = \frac{\partial c_{()} }{\partial \psi} [\psi_m - \psi_j] A(1/2) \rho_{Bm} V_{rm}^2 \quad (12)$$

$$M_{()} = \frac{\partial c_{()} }{\partial \psi} [\psi_m - \psi_j] A\ell(1/2) \rho_{Bm} V_{rm}^2 \quad (13)$$

where:

ψ_j = The angle of yaw at which zero force or moment occurs.

$\frac{\partial c_{()} }{\partial \psi}$ = The slope of the force or moment coefficient versus angle of yaw.

$()$ = Indicates subscript of force or moment coefficient (i.e., H, Y, D, l, M and n)

2. ADAPTATION OF THE PROCEDURE FOR PREDICTING SLED AERODYNAMIC FORCING FUNCTIONS TO A COMPUTER

In order to program the calculations for obtaining the aerodynamic forcing functions of the sled on the CDC 3600 computer, certain approximations were made. These approximations will be discussed in the order of the steps described in the previous section.

Step 1 - Approximation

The curve representing the shock front in Reference 6 (see Figure 5 as typical example) is approximated by the following equation:

$$z^{C11y} = C_{2i} \quad (14)$$

Introducing this approximation into the combined Z and Y equation (Equations 6 and 7 combined) results in:

$$t_i = R_i C_{2i} / \bar{a} Z_i (1 + C_{1i}) \quad (15)$$

where: i - is used to designate the intercept of the blast front by the sled at the preselected point on the track.

$$C_{1i} = -1.390$$

$$C_{2i} = 0.2090$$

The computer program is now made to step backward in time a total of t_i milliseconds and locate the track station (S_b) at which the sled will be when the charge of TIT is detonated. In the computer program the time $t = 0$ is the time of detonation designated by t_b . The computer program now calculates values of Z_m and Y_m by equations 5, 6, and 7, starting at the time t_b . However, the values of Z_m and Y_m have no physical meaning up to time t_i (sled blast wave intercept). The program also computes the time when the sled leaves the blast front. This time is called t_{out} . It is calculated by comparing each successive value of time t_m with the values of t_i calculated from equation 15 using Z_m and R_m at the time t_m in place of Z_i and R_i . In this case t_{out} equals t_m when t_m equals t_i and is the arrival time of the blast front at the point on the track where the sled traverses the blast front again.

Step 2 - Approximations:

In order to obtain the blast parameters (P , u , ρ_B) the values of Z_m and Y_m are determined. The parameters P , u , and ρ_B are represented as J_1 , J_2 , and J_3 respectively in the computer program. A given set Z_m and Y_m at a time t_m has only one value each of P , u , or ρ_B . The following technique was used to obtain the appropriate value: first, the lines of constant P , u , ρ_B were approximated by power curves of the form

$$Z^{C_1} Y = C_2 \quad (16)$$

One power curve was developed for each constant value of J_1 , J_2 or J_3 represented in Reference 6. This resulted in one value of C_1 and one value of C_2 for each value J_1 . Similarly one value of C_3 , C_4 for each constant value of J_2 and C_5 , C_6 for J_3 , was obtained. Second, C_2 was expressed as a function of C_1 by approximating a straight line to the values of C_2 and C_1 (i.e., $C_2 = 0.44615 C_1 + 0.94153$). Also, C_1 was expressed as a function of J_1 by approximating several straight lines. In the case of J_2 and J_3 , the equations $C_4 = f(C_3)$; $C_6 = f(C_5)$; and $C_3 = f(J_2)$,

$C_5 = f(J_3)$ were expressed as third order polynomials by least squares approximation. A typical polynomial is of the form

$$Y_m Z_m^3 = C_4 = F_4 C_3^3 + F_3 C_3^2 + F_2 C_3 + F_1 \quad (17)$$

where: F_1, F_2, F_3 and F_4 are the coefficients of the polynomial approximation. The equation is now solved for the roots, C_3 . If the computer is programmed to select the largest root, then the appropriate value of C_3 is obtained. Third, using the following equation and the root C_3 , values of J_2 can be obtained for each set of Z_m and Y_m .

$$J_{2m} = G_4 C_3^3 + G_3 C_3^2 + G_2 C_3 + G_1 \quad (18)$$

where: G_4, G_3, G_2 and G_1 are the coefficients of the polynomial approximations. Similarly values of J_3 can be obtained. For J_1 the approximations are straight lines; so there is no problem with root selection. Therefore, with the four polynomials and the straight line approximations the blast parameters (P, u, p_B) are described. These polynomial and straight line approximations introduce errors greater than 10 percent as the following limits are exceeded: $20 < Z < 6$ and $19 < Y < 1.9$.

In case the sled leaves the blast environment through the tail of the shock (indicated by the second shock in Figure 5), the value of the time of exit must be obtained by hand computation. This can be done by referring to the minimum value of Z_m obtained from the computer program. Taking the minimum value of Z_m tabulated by the computer and referring to the time history curves in Reference 6 the computer tabulated values of Y_m can be compared to the Y_m of the curves. If the computer value of Y_m is larger than the value of Y_m for which the sled arrives on the second shock line, then the sled exited the blast environment. Computer solutions from the time of exit of the second shock to the re-entrance by way of the second shock are meaningless.

Step 3 and 4 - Approximations

No approximations were required in these steps. Equations 9 through 11 were solved in the computer.

Step 5 - Approximations

The aerodynamic force and moment coefficients were put into the computer through the use of third order polynomial approximations. That is the derivative $ac(\gamma)/a\psi_m$ (called $PDC(\gamma)_m$ in the computer) as a function of Mach number was fitted by the method of least squares to a third order polynomial. Likewise, for each polynomial of $PDC(\gamma)_m$ a polynomial of

ψ_j (called THETA $()_m$ in the computer) as a function Mach number was fitted by the method of least squares to another third order polynomial. The polynomials take the form of

$$\text{THETA } 1_m = AA_4 M_{rm}^3 + AA_3 M_{rm}^2 + AA_2 M_{rm} + AA_1 \quad (19)$$

where: AA_4 , AA_3 , AA_2 and AA_1 are the coefficients of the polynomial approximation for the aerodynamic coefficients.

$$\text{PDC } 1_m = BB_4 M_{rm}^3 + BB_3 M_{rm}^2 + BB_2 M_{rm} + BB_1 \quad (20)$$

where: BB_4 , BB_3 , BB_2 and BB_1 are the coefficients of the polynomial approximation. The values of M_r are calculated from equation 11 using the appropriate values obtained from the solutions of equations 9 and 10. The axial force was found to be very sensitive to changes in PDC 3. In order to improve the complete time history curve of the axial force a straight line approximation was made for values of PDC 3 above Mach 2.45. The curve for PDC 3 as a function of Mach number curved rather abruptly in the area of Mach 2.45 and as the Mach number increased it approached a straight line. This approximation does not give completely satisfactory results in the computer computation of the axial force curve. However, time did not permit further improvement and the inaccuracy was not considered to be too severe. The previous approximations are valid in the Mach number range from 2.0 to 3.0.

Step 6 - Approximations

The final step required no approximations. Equations of the form of 12 and 13 were solved directly with the values obtained from steps 1 through 5.

3. FORCE TRANSDUCER

Figure 6 shows the force transducer used to measure the side force applied to the rail by the vehicle. The transducer is located on the forward slipper of the outrigger sled. Figure 7 shows a schematic of the transducer installation on the slipper. Four strain gages of each boss were used to form two Wheatstone bridges. Each strain gage had a 120 ohm resistance and thus each bridge resulted in a 240 ohm bridge. The two bridges were designed to measure the compressive load as applied from one side or the other by the sled on the respective boss. The strain gages used were eight BLH rosette, type FABX-12-12 S-6. The gages were bonded as close to the edge of the boss as possible. The gage locations are schematically shown in Figure 6.

The transducer was calibrated at the University of New Mexico under the direction of Dr. William C. Baker. The loading of the unit was done on a Tinius Olson testing machine. The bridge output was read with a Budd Model P-350 strain indicator. The calibration loads were applied for the following four load distributions: uniformly distributed over the total circular surface (see Figure 6), uniformly distributed load over the outer periphery of the circular surface, and the two preceding conditions with only 180 degrees of the circular surface loaded. Also, load was applied with the transducer in four different angular positions in the testing machine.

It was found that there was no cross talk between the two bridges under these test conditions. It was also noted that the output of the bridges was highly dependent on the way the load was applied. Based on the bridge output information obtained from these load tests, "calibrate resistors" were selected to electrically represent certain loads. It was found later, during calibration of the transducer on the sled, that the calibrate resistors did not represent the loads indicated during the laboratory calibrations. This discrepancy was attributed to the difference in load condition generated by the actual sled surfaces and structure as compared to the way the loads were applied in the laboratory.

The load unit was checked at the University of New Mexico for the temperature compensation effectiveness of the bridge. This test consisted of heating the tapered calibration plug (the plug simulates the cone on the slipper - see Figure 7) to 420°F, and then placing the transducer, which was at room temperature, on the plug. A one megaohm calibrate resistor was used to determine the force equivalent to the output of the bridge due to temperature variation. The bridge output caused by temperature increase in the load unit was recorded for 60 seconds. The largest increase in bridge output occurred in the first ten seconds. During this time, the bridge indicated an equivalent force increase of approximately 700 pounds which is approximately 1% of the anticipated loads to be measured. For the remaining 50 seconds the bridge indicated an additional equivalent force increase of approximately 100 pounds. It should be noted that the previously described heating of the force transducer is considerably more severe than actual sled run conditions will produce.

Prior to a sled run, the load unit was installed in the sled and was not removed until the sled run had been completed. The bolt connecting the slipper and load unit to the sled was torqued to approximately 200 foot-pounds. The torquing produced a precompressed condition in the load unit. This was done to insure that the sled surfaces which contact the boss of the force transducer were bearing on the boss circular surface. Then the system was statically calibrated using the electrical circuitry in the sled that was to be used on the run to record the calibrations. During calibration, the zero bridge output was set up to be the precompressed value produced by the torquing. The calibration data

were recorded on the on-board Genesco tape recorder which was used on the run. The readings obtained from a digital volt meter during the static calibration were compared with those recorded and found to be the same.

Statical loads were applied to the bolt head of the sled slipper support structure. The load was applied in the lateral direction by a 50 ton Blackhawk hydraulic jack. The force applied by the jack was measured and indicated by a Revere load cell and indicator. The loads were first applied to the side that would be facing the blast (port side). Then the loads were applied to the starboard side. The load was applied in 10,000 pound increments and an effort was made to relieve the load in 10,000 pound increments. However, the hydraulic jack could not be regulated to drop exactly to the right load step. This necessitated going below the predetermined load step and jacking back up to it. After the 10,000 pound steps were applied and relieved, one step equal to the maximum calibration load was applied and relieved. The foregoing procedure was then repeated on the port side. Prior to each of the four sled runs, the load unit calibration was redone as previously described. The results of one of these calibration tests are shown in Figures 8 and 9 and are representative of the other calibration tests. It should be noted that the cross talk on the starboard side bridge from a load applied on the port side was considerable. No effort was made to reduce this since this was not the critical load side and time did not permit the effort involved in reducing this cross talk. Figure 9 shows that cross talk on the port side is not significant. These figures also indicate that the bridge output for the initial 10,000 pound step is non-linear. This is attributed to the effects on the load unit due to torquing. The calibrate resistors used to represent an equivalent force were 14.7 K ohm and 59 K ohm on the port and starboard side, respectively. These resistors resulted in indicating equivalent forces of 30,000 and 25,000 pounds, respectively as shown in Figures 8 and 9. These values were set to represent approximately 60% (e.g., 30,000 pounds equals 3 volts of a maximum output of 5 volts of full scale deviation during the runs). It was previously mentioned that these calibrate resistors would not be indicative of these loads if the values obtained in the laboratory for the various load distributions were used.

In the calibration check before the first sled run a vertical up-load was statically applied to the sled to check cross talk on the boss. The load was applied by wrapping a nylon strap (10,000 pound tensile strength) around the cantilevered payload and pulling vertically up with a crane. A Hydroset was attached between the crane hook and the nylon strap to measure the magnitude of the applied load. The attitude of the crane boom limited the maximum vertical up-load to be applied for this cross talk check to 7,500 pounds. The results were similar to those observed in the lateral load calibration. Cross talk on the port side bridge was not significant above a 2,500 pound vertical up-load. This 2,500 pound vertical up-load resulted in a 2,000 pound load indication

in the lateral direction. The starboard bridge indicated cross talk up to a 7,500 pound vertical upload. A 5,000 pound upload resulted in a 2,000 pound indication in the lateral direction. A loading fixture was not available for a vertical download check. This was not considered critical since the sled primarily experiences a nose up pitch attitude. Due to limitations in local structural strength, loads were not applied at other points on the vehicle to check for additional cross talk.

4. ACCELEROMETER

A uniaxial accelerometer was used to measure lateral acceleration. The accelerometer used was a Stathar (strain gage bridge type, oil damped) with a range of ± 500 g's Model No. AG9-TC-500-350. This accelerometer was located in a compartment immediately above the front slipper. The front slipper is the one on which the lateral forces were measured. The accelerometer output during the run was recorded with a system capable of responding to 2100 cycles per second on the same Genesco tape recorder as the strain gage data. However, the accelerometer is flat only out to approximately 1500 cycles per second. A calibrate resistor equivalent to approximately 477 g's was used to represent 100% of full scale deviation. The calibrate resistor was selected on the basis of manufacturers data and not from information of calibration tests at the track facility.

5. POWER SPECTRAL DENSITY COMPUTATIONS

The force and acceleration data were reduced to the form of Power Spectral density plots. This reduction resulted in force squared or acceleration squared per cycle per second being plotted as a function of cycles per second (Hz).

For completeness, an explanation of the reduction technique is included. This explanation was taken from one of the Computation Division Data Processing Branch's (MDRCP) vibration data reports and is as follows:

The reduced data consist of mean square (\bar{Y}^2) versus time plots and power spectral density versus frequency plots for selected functions and specific time intervals. To verify MDRCP data processing, a comparison is made by dividing the power from the mean square versus time (S) by the total power from the spectral density versus frequency (D). The limits of this ratio are $0.80 < S/D < 1.20$. If the comparison does not come within the above limits, a statement to that effect is included.

The mean square versus time plots are usually taken over the time interval of X to X + 30 seconds. Data flow at MDRCP for these plots is from an analog magnetic tape machine to a data discriminator to the Dallantine RMS meter to the Sanborn Recorder. The Sanborn records

the Ballantine mean square value output which is the continuous average of the squared signal over twice the time constant of the meter. The meter time constant is approximately 0.1 seconds. The lower frequency limit for these plots is 5 Hz. The full scale value of the mean square value (\bar{Y}^2) for each plot is calculated as follows:

$$\left[\frac{\text{mV RMS}}{T} \right]^2 \cdot S = \bar{Y}^2 \text{ (full scale)}$$

where:

- S = Sanborn recording factor
- mV RMS = Millivolts RMS of the calibration signal
- T = Transducer sensitivity in millivolts per engineering unit.

Data flow for the power spectral density versus frequency plots at DRCP is from an analog magnetic tape machine to a tape loop. Data from the loop are then discriminated and analyzed by the Honeywell 9300 Automatic Wave Analyzer. The analyzer performs an estimate of the power spectral density by measuring the mean square value of the function over a bandwidth B (equal to 10 Hz for some runs). In other instances the bandwidth B was equal to 2 Hz. Dividing the mean square value (\bar{Y}^2) by the filter bandwidth B provides a single point (displayed at the center of the bandwidth) on the X-Y plot for each bandwidth increment being analyzed. The lines connecting the individual points are not data but are included as an aid in determining locations of the points. The full scale mean square value \bar{Y}^2 for the plot is calculated by the previous equation without the Sanborn recording factor (S) included. Dividing \bar{Y}^2 by the bandwidth provides Y-axis scaling in units of mean square value per Hz, which is plotted versus X-axis frequency in Hz. The X-Y plot is then a power spectral density display versus frequency or a power spectrum plot.

SECTION IV
DISCUSSION AND RESULTS

1. COMPUTER CALCULATED AERODYNAMIC FORCING FUNCTIONS

A parametric study was made through the use of the computerized procedure for predicting aerodynamic forcing functions in the blast environment. The study was broken down into three groups. Each group contained five runs. Group I involved a variation in charge weight (W). Group II involved a variation in the sled intercept velocity (V). Group III involved a variation in angle of sled intercept (ϕ_i). The initial conditions for each group are summarized in the following table:

INITIAL CONDITIONS					
	ϕ_i	R_i	S_i	V	λ
Group I	70°	170.26	12959	3300	13.913
	↓	↓	↓	↓	17.777
	↓	↓	↓	↓	20.645
	↓	↓	↓	↓	23.357
	↓	↓	↓	↓	25.276
Group II	70°	170.26	12959	3300	20.645
	↓	↓	↓	3000	↓
	↓	↓	↓	2700	↓
	↓	↓	↓	2400	↓
	↓	↓	↓	2100	↓
Group III	90°	160	13017	3300	20.645
	30°	162.47	13938.8	↓	↓
	70°	170.26	12958.8	↓	↓
	60°	184.75	12940.6	↓	↓
	50°	203.87	12882.74	↓	↓

The equivalent weight $W_E = \lambda^3/\bar{P}$ was intended to be representative of a 5, 7.5, 10, 12.5 and 15 psi side-on pressure condition at intercept for Group I. The ground reflection factor used in this series of computer studies was 1.8.

Figures 10 through 15 present the time history of the six forcing function components for Group I. Figures 16 through 21 present the six

forcing function components for Group II and Figures 22 through 27 present those of Group III. Several of the resultant forcing functions calculated on the computer were compared with forcing functions calculated by hand. In the hand calculations the blast parameters were obtained directly from the curves in Reference 6. The aerodynamic coefficients were obtained directly from wind tunnel data. The comparison showed that the two techniques produced the same shape curves. In the intercept region, the curves were within 10% of each other. As the curves approached ambient conditions the curves, in some cases, varied by approximately 25%. Since the time histories of the blast parameters in Reference 6 are somewhat empirical and thus are approximations, the previous accuracies were considered satisfactory.

2. FORCE MEASUREMENTS

Ground zero was 160 feet perpendicular to track station 13,017 feet on the west side as shown in Figure 4. The sled intercepted the blast front at an angle ϕ_i of approximately 60 degrees. Sled travel was from south to north.

On the four runs conducted, force measurements were taken. However, due to instrumentation malfunction, complete data were not obtained on any one run. The following table shows the times of data acquisition during each run:

	5B-F1 Run	5B-C1 Run	5B-G2 Run	6B-A1 Run
Track 7 (70kc) Port Side Data Acquisition times (sec)	0 to 3	0 to 30	0 to 7 7.5 to 11.4	0 to 3
Track 9 (70kc) Starboard Side Data Acquisition times (sec)	0 to 3	0 to 3	0 to 7 7.5 to 11.4	0 to 12.5

Only the time history of the lateral force on the forward slipper was measured. This slipper and direction were selected since calculations of slipper loading showed it to be the most critical. The calculations were based on a static aerodynamic force analysis. Wind tunnel force data at various angles of yaw were incorporated with the blast parameters (density, particle velocity and pressure) to give a time history of the three aerodynamic force and moment components acting

on the sled while it traversed the blast environment. The components were then reacted at the slippers through the statical force and moment equations. The sled slipper restraint redundancy was removed by assuming that the yawing moment and side force were reacted by only the forward and aft most slippers on the main body. The center slipper on the main body and the outrigger tip slipper were designed to allow for 7/8" gap between the side surface of the slippers and the rail to insure the validity of the previous assumptions. Efforts were made to have the major portion of this gap on the side of the slipper nearest the blast.

The first run is not of interest for obtaining the magnitude of the sled front slipper lateral forces. On this run, the expected velocity was not achieved because two boosters did not ignite and thus blast intercept was not at the desired point. This resulted in no noticeable increase in force as the sled traversed the blast environment. However, the data from the first run were used to obtain the sled frequency information which is discussed under Power Spectral Density Plots.

Figures 28, 29 and 30 present the force measurements taken on the last three runs. The figures mainly show the time history of the sled response in the blast environment. Intercept velocities on the runs were 3,050, 3010, and 3,200 feet per second, successively. From indications of free field trackside pressure measurements and photographic coverage, sled blast intercept on these three runs occurred within + 6 feet of the predicted point of intercept. The force data indicated sled-blast intercept at approximately 8.21 seconds from first noticeable deviation in the data traces. However, analysis of time-distance data for the sled runs shows blast sled intercept to be at approximately 8.61 seconds. The letter "t" just above the IRIG-B time scale (scale at bottom of data traces) indicates the approximate location of blast intercept. Since the recorded force data constitute the sled response to the blast induced forcing functions, the exact location of blast intercept cannot be determined. It is assumed, however, that the intercept occurs within the two milliseconds prior to the sudden rise in the data. The force data prior to blast intercept are representative of the dynamic lateral forces which are exerted by the slipper on the rail under normal run conditions. Normal run conditions are defined as those which exist outside the blast environment.

It should be noted that the filled trough (the area below the outrigger and between the rails) in the blast area did not cause any noticeable change in lateral force indication as the sled traversed this area. A change in lateral force was predicted from wind tunnel force measurements. However, since the deviation of the data was set to measure the large forces encountered in the blast environment, the smaller forces generated by a trough filled condition were not discernible.

Figure 28 presents the port side lateral force versus time data generated by a 1,552 pound TNT charge. As was previously mentioned, the starboard side data channel did not function during blast intercept for

this run. Time history traces of the forces on all runs were recorded on channels with a 2,100 cycle per second frequency response. The uppermost time history trace in Figure 30 was played back through a filter which eliminated frequencies above 700 cycles per second. This trace was compared with a playback made with a 2,100 cycle per second filter and no significant change in amplitude was observed. The middle trace was played back with frequencies above 160 cycles per second filtered out. A reduction in the magnitude of the forces is indicated. The bottom trace was played back with frequencies above 45 cycles per second filtered out. It is apparent from these traces that approximately 50% of the structural response is due to the lower frequencies (below 45 cycles) while the remaining portion of the response is generated by frequencies between 45 and 700 cycles per second.

The characteristic shape of the traces is describable as follows: The bottom trace has four significant rises after the initial major increase in force. The initial increase in force which will be called the first rise, is attributed to the response of the sled to the diffraction period of sled blast wave interception. The diffraction period is considered to be the time from the first point contact of the sled with the blast front to the time when the sled is completely engulfed in the increased pressure environment generated by the blast. This is in essence a sled response generated by the initial pressure differential existing on opposite sides of the sled vertical surfaces. For example, a 5 psi blast environment acting side-on to a sled which has approximately 5,000 square inches of side area will produce a 25,000 pound side loading. If it is assumed that the sled experiences a reflected overpressure in the order of two times the side-on blast pressure, this will rise to a 50,000 pound load. Assume a blast front moving at approximately 1.2 feet per milliseconds intercepts the vehicle, which is two feet wide, directly side-on. The time to envelop the sled will be just under two milliseconds. It is assumed that this is the characteristic of the forcing functions causing the initial rise in the force data.

The second rise is attributed to the sled response due to the density change and particle velocity generated by the blast. The aerodynamic forces acting on a vehicle are functions of density, velocity, angle of attack (e.g., yaw) and configuration. The particle velocity effects a change in the angle of yaw. The density in the blast environment is increased and the velocity becomes the resultant sled velocity composed of the two components sled velocity and particle velocity (see Figure 4). These effects are assumed to lag the diffraction period effects and give rise to the second increase in force observed.

The third rise is considered to be the beginning of the second cycle of the response to the earlier rises. At the time of the third rise, the blast density and particle velocity are near the ambient conditions and

do not result in any significant increase in force. Each boss of the load transducer can measure only compressive loads as the sled oscillates in the lateral direction. Therefore, slipper loading will be measured first on one boss then on the other boss which means that the second half of the first cycle is recorded on the starboard side channel. This can be seen in the data obtained on the following run (Figure 29), which shows information from both channels.

The fourth rise in force in Figure 28 is attributed to the rise in the blast environment parameters as the sled proceeds to exit the blast front. The sled will leave the blast environment since it is traveling considerably faster than the blast front. During the transit of the sled through the blast environment on the last three runs, the sled did not leave the end of the blast wave. On these runs, the sled remained in the blast environment entering the blast front and exiting via the blast front.

The fifth oscillation is again attributed to the beginning of the second cycle of response to the one immediately preceding it. As would be expected, due to damping, the second cycle in both cases is noticeably lower in amplitude.

Figure 29 presents the port and starboard side lateral force versus time data generated by a 2,672 pound TNT charge. The upper traces are the port side force traces played back with frequencies above 790 and 100 cycles per second filtered out. The characteristic shape is very similar to one obtained on the previous run (1,552 pounds of TNT) and describable in the same way. The only significant difference is the increase in amplitude of the second rise. The first rise was of less amplitude but this may be due to a slight phase shift in the frequencies contributing to the structural response. The lower set of traces are the starboard side data. They are played back at the filter frequencies previously described. The cross talk is very distinct, and the response to the oscillation of the sled from one side of the rail to the other is observed.

Figure 30 presents the starboard side lateral force measurements versus time data generated by a 4,000 pound TNT charge (Run Nr 60-A1). As was previously mentioned, the port side channel did not function during the blast intercept. These traces were filtered at the same frequencies as previously described. The characteristic shape of this curve is similar to the one obtained on the starboard side channel recording the 2,672 pound TNT environment. However, a noticeable increase in the amplitude of the cross talk portion of the trace is observed. This indicates that the loading due to the blast was more severe but the magnitudes of the load cannot be accurately determined. A maximum load in the order of 100,000 pounds was anticipated on this last run. However, verification of this is not possible from the existing data.

It is interesting to compare the track deflections shown in Figure 31 with the sled lateral force data. The deflection measurements were taken by the Technical Measurements Branch of the Track, using the standard track surveying techniques. The measurements are those of the master rail which is the one nearest the blast and the one on which the main body of the outrigger sled rides. West is towards ground zero. The abscissa gives track tie down fixture numbers specifically selected for these measurements. Track stations are easily located by noting that tie down fixture 12 is at 13,000 feet and the fixtures are equally spaced 52 inches apart. The sled travels from the lowest numbered tie down fixture to the highest. The deflection measurements were taken at the fixtures shown and not at intermediate points. The uppermost graph represents the measurements taken on the first run (5B-F1). The run did not experience severe loading since the velocity was low as described previously and hence permanent track deflection was not expected. The graphs 5B-G1, 5B-G2 and 6B-A1 represent the 1552, 2672 and 4000 pound TNT environment, respectively. On 6B-A1 a deflection of approximately 0.060 inches was measured at track stations 13,000 and 12,977 feet. If, for example, the sled is traveling at approximately 3.2 feet per millisecond, it would travel 16 feet in five milliseconds. Checking the force measurement in Figures 28 and 29, one finds that the sled experiences the maximum of the first force rise approximately five milliseconds after blast intercept. This corresponds approximately to track station 12,977 where the maximum rail deflection occurs. Reasoning in the same way the rail deflection at track station 13,000 corresponds to the maximum of the second force increase shown in Figures 28 and 29.

3. PREDICTED FORCING FUNCTIONS AND MEASURED RESPONSE

The respective charge weights on each of the last three sled runs were selected to approximate a 5, 7.5 and 10 psi side-on pressure condition at sled-blast intercept. As determined from free field pressure measurements, these pressure conditions were reached within + 0.5 psi. A direct comparison between the related computer calculated forcing functions at 5, 7.5 and 10 psi cannot be made since it was the sled response which was measured. A relationship between the sled forcing function and its response does exist but cannot be completely described with the available information. However, the maximum response does lag behind the maximum applied forcing function. Also, consider the period (τ) of the above-ambient phase forcing function in relation to the period (T) of the estimated lowest mode of vibration of the sled. In reference 11 for a single degree of freedom system with this same relationship of periods (i.e., $0.5 < \tau/T < 1.0$) amplification of the forcing function occurs. The following tables present the estimated forcing function and the measured response.

PRESSURE ENVELOPMENT PHASE

<u>Charge Wt (lbs)</u>	<u>Estimated Lateral Forcing Function (lbs)</u>	<u>Measured Lateral Response (lbs)</u>
1,552	50,000	75,000
2,672	75,000	70,000
4,000	100,000	No Data

DYNAMIC PRESSURE PHASE

1,552	47,900	52,000
2,672	60,700	64,000
4,000	92,000	No Data

The pressure envelopment phase was estimated by assuming a sled side area of 5,000 square inches acted on by a reflected pressure which is twice the side-on pressure. The dynamic pressure phase is based on the particle velocity and density predicted by the computer program.

4. ACCELERATION MEASUREMENTS

Figure 32 shows the lateral acceleration measurements taken for the major portion of the sled trajectory. It can be seen that the acceleration levels build up to + 500 g's during the high velocity portion of the run. It should be kept in mind that the accelerometer was hard mounted in the area of the forward slipper.

Figure 33 shows the expanded acceleration data during the sled-blast intercept.

5. POWER SPECTRAL DENSITY PLOTS

The following table shows the times for which the power spectral density plots included in this report were made.

Run	TIME (seconds)						
	4-5	5-6	6-7	6.5-7.5	7.5-8.5	8.5-9.5	9-10
5B-F1A	7	7					
	9	9					
	12	12			12		12
5B-G1		7		7		7	
		9		9			
		12				12	
6B-A1	12	12	12				

Where:

- 7 - Port side strain gage recorder track
- 9 - Starboard side strain gage recorder track
- 12 - Accelerometer recorder track

Figure 34 shows the velocity and longitudinal acceleration versus time for the time interval from which the power spectral density plots are taken. These velocities and accelerations are representative of runs 5B-G1, 5B-G2, and 6B-A1. Run 5B-F1 is a lower velocity run as previously described. However, the first 6.5 seconds of Figure 34 is representative of run 5B-F1. This time interval is not affected by the booster malfunction on the final stage.

Figures 35, 36 and 37 are the mean square function versus time traces of the related data (see Section III, 5). These traces are representative of pounds squared or acceleration (g's) squared as a function of time. In Figures 35 and 36 there are no data after approximately eight seconds although the trace is continued. These two tracks of information did not operate after eight seconds of the run.

The PSD's (power spectral density) in Figures 38 through 41 show the frequency content of the force data as obtained using a band pass filter of 2 Hz. PSD's of the same time increment of data using a 10 Hz band pass filter showed that with this scaling of the ordinate no significant frequency contribution existed beyond 600 cycles per second. Only a very small amount was noticed between 400 and 600 cycles per second. Therefore, in an effort to better define the frequency content below 400 cycles per second the data were reduced using the 2 Hz band pass filter. In using the 2 Hz band pass filter the number of sample points must be reduced to keep the reduction process within reasonable time limits. This is done by limiting the range of frequency of analysis. In these cases the range was from 0 to 400 Hz.

Figures 42 through 47 are the PSD's obtained from the accelerometer data. Only Figures 42 and 43 were obtained using a 2 Hz band pass filter. It should be noted that the large increase around 2 KHz on the other four figures is attributed to local frequencies arising from the bracket arrangement to which the accelerometer was attached. On later tests (5B-G2 and 6B-A1) the accelerometer mounting arrangement was made more rigid, and the 2 KHz frequency was considerably reduced. It was noticed that on the runs where the rigidity was increased all the levels of frequency contributions were reduced, as indicated by the accelerometer data shown in Figures 60 through 63.

Figures 48 through 63 present the Sanborn traces and resultant PSD's for runs 5B-G1 and 6B-A1. The PSD's from run 5B-G2 are not included since they are very similar to 5B-G1.

Generally the PSD's taken from force transducers data show that the lowest significant natural frequency of the sled system to be approximately 25 Hz.

SECTION V

CONCLUSIONS

1. Computer calculated forcing functions as compared to hand calculated values are within 10% of the initial intercept region and within 25% as ambient conditions are approached.
2. The force transducer will measure loads on the sled to within +5000 pounds according to static calibrations.
3. The maximum sled response measured on the forward slipper attributable to the dynamic pressure phase is approximately 10% greater than the maximum predicted forcing function for the forward slipper.
4. The lateral acceleration levels in the vicinity of the sled forward slipper build up to ± 500 g's in the frequency range from 0 to 1500 Hz.
5. Locations of permanent track rail deflections were found to be coincident with those at which the maximum sled forces were observed.
6. Power Spectral Density plots of force transducer data showed that no significant amplitude contribution was made beyond a frequency of approximately 600 Hz.
7. The first predominate sled frequency noted was approximately 25 Hz.

REFERENCES

1. Jenke, Leroy M. and Lucas, Ernest J., Supersonic Wind Tunnel Tests of Several Outrigger Rocket Sled Models at Small Angles of Yaw, AEDC-TDR-64-248 (December 1964).
2. Jenke, L. M. and Lucas, E. J., Supersonic Wind Tunnel Tests of an Outrigger Rocket Sled and Two Dual Raft Sleds, AEDC-TR-65-168 (August 1965).
3. Jenke, L. M. and Lucas, E. J., Supersonic Wind Tunnel Tests of Outrigger Rocket Sled Models at Small Angles of Yaw, AEDC-TR-65-90 (April 1965).
4. Lewis, Dean S. and Ruetenik, J. Ray, Measurements of the Interference that Various Track Profiles Would Produce on a Blast Wave, MIT-ASRL-TR-131-1 (December 1964), unclassified.
5. Baker, W. E. and Schuman, Jr., W. J., Air Blast Data for Correlation with Moving Airfoil Tests, BRL-TN-1421 (August 1961), unclassified.
6. Mills, R. R., et al, Self-Consistent Blast Wave Parameters, DASA-1559 (October 1964), unclassified.
7. Cottrell, M.M., Bacchus, Charles E. and Ghose Amitava, Dynamic Analysis of Complex Supersonic Sleds, MDC-TR-68-3 (January 1968).
8. U.S. Department of Defense: The Effects of Nuclear Weapons, U.S. Atomic Energy Commission, (June 1957).
9. Bryant, E. J., Eberhard, R. A., Kingery, C. N., Mach Reflection over Hard Packed Dirt and Dry Sand, BRL, Report No. 809 (July 1952).
10. Harris, Cyril M. and Crede, Charles E., Shock and Vibration Handbook, Volume 3, McGraw-Hill Company, Inc (1961).
11. Jacobson, Lydik S. and Ayre, Robert S., Engineering Vibrations, McGraw-Hill, Inc. (1958).

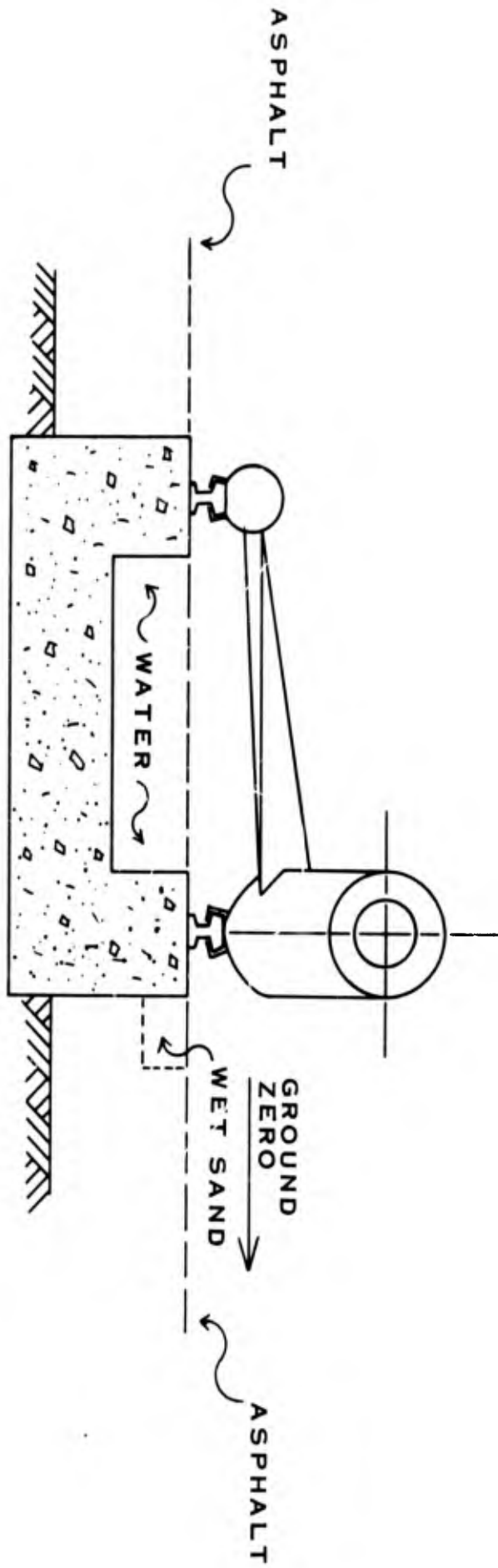


FIGURE 1 SCHEMATIC OF MODIFIED TRACK CROSS-SECTION IN BLAST TEST AREA

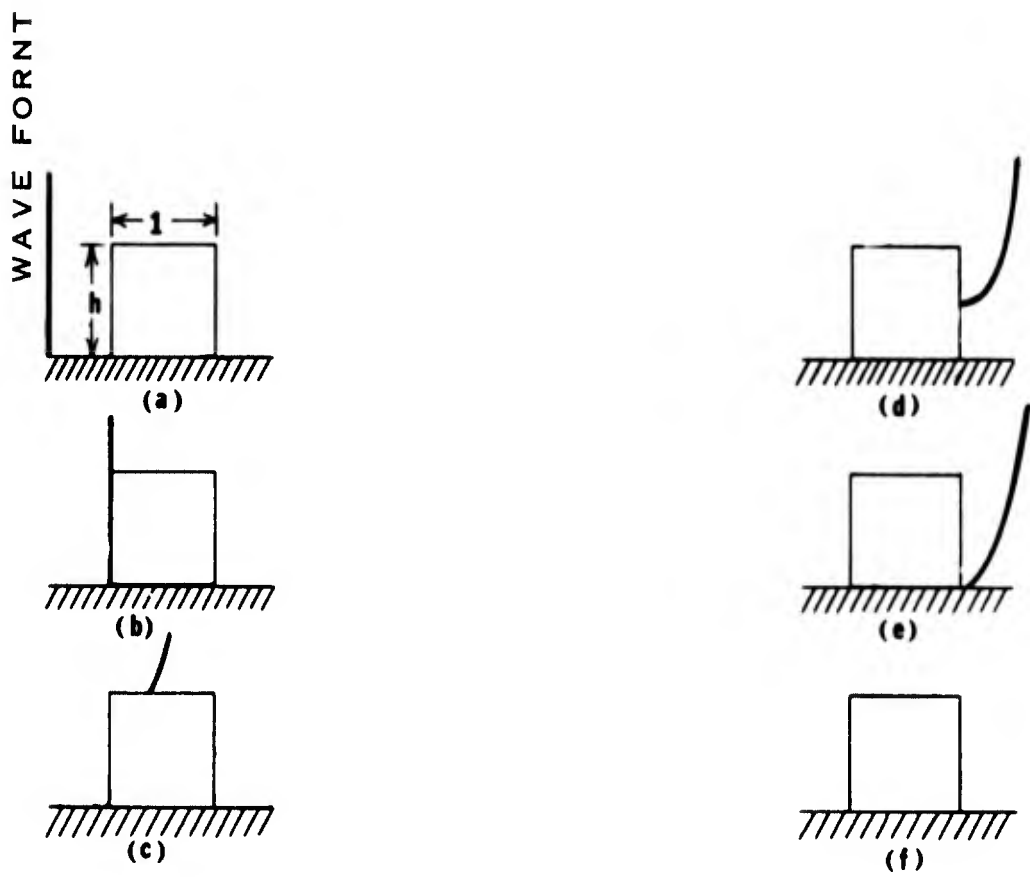
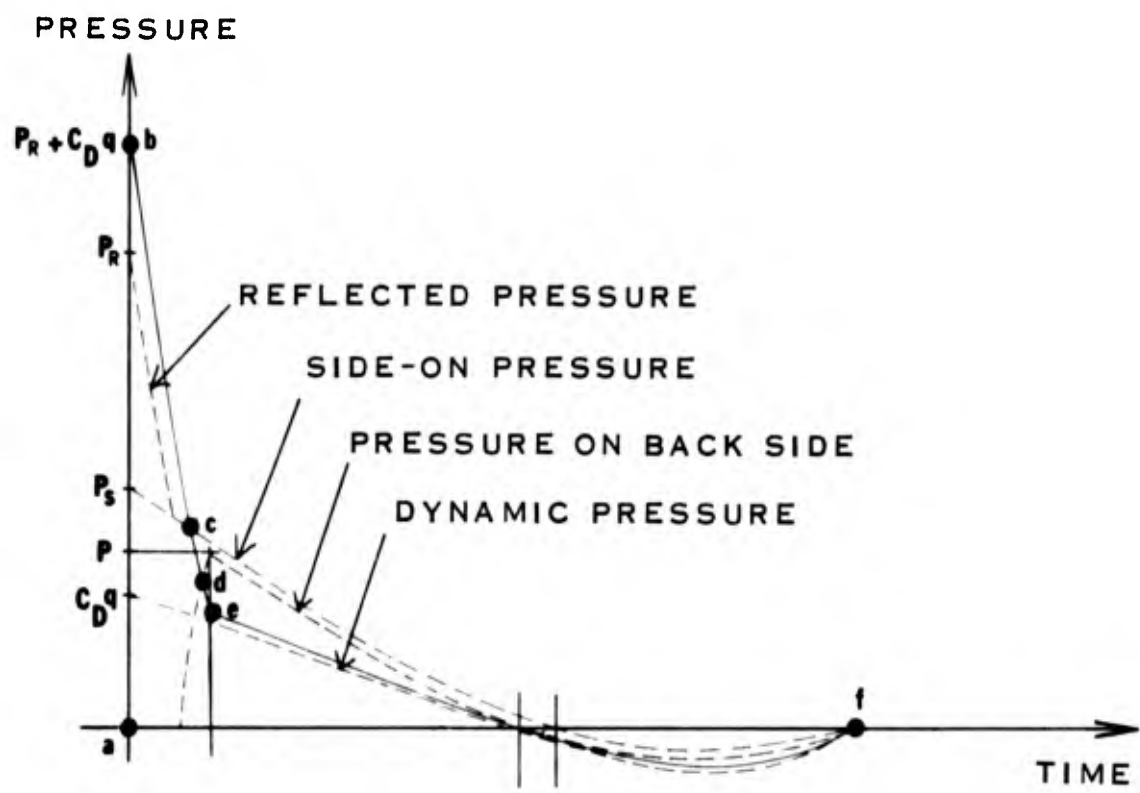


FIGURE 2 SCHEMATIC OF A BLAST OVERPRESSURE ON A GROUND FIXED OBJECT

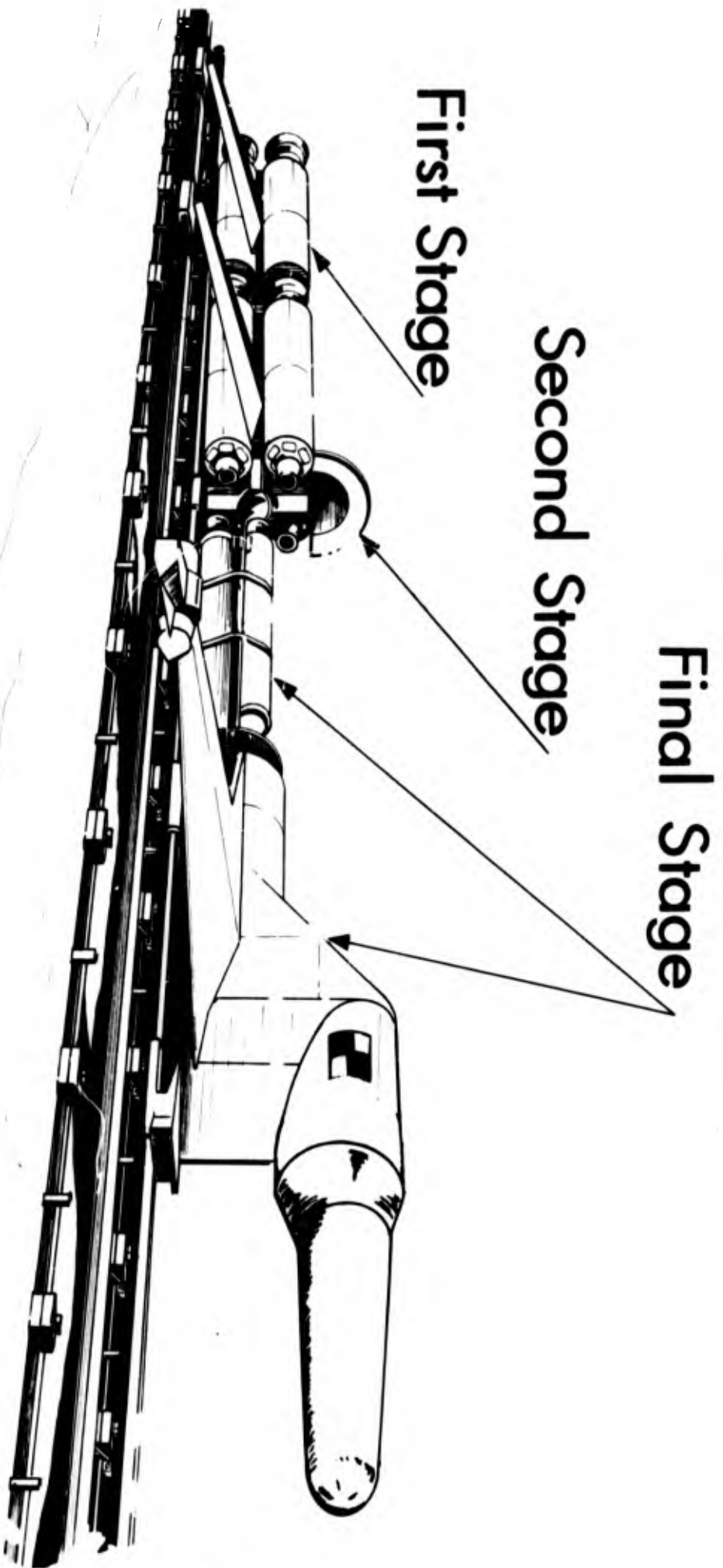
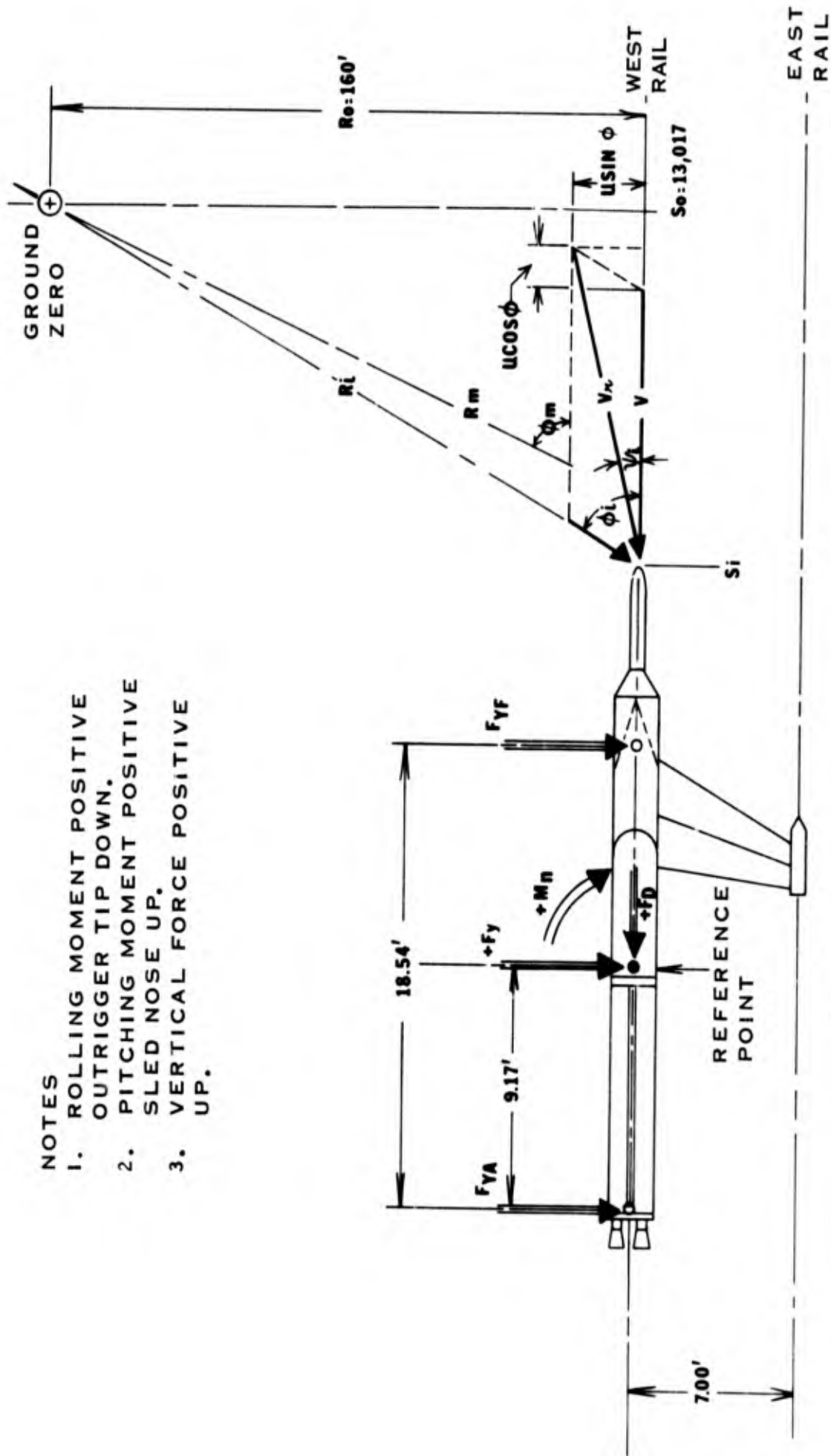


Fig. 3 Three Stage Outrigger Rocket Sled



NOTES

1. ROLLING MOMENT POSITIVE
OUTRIGGER TIP DOWN.
2. PITCHING MOMENT POSITIVE
SLED NOSE UP.
3. VERTICAL FORCE POSITIVE
UP.

FIGURE 4 SCHEMATIC OF VELOCITY AND FORCE VECTORS ACTING ON THE ROCKET SLED

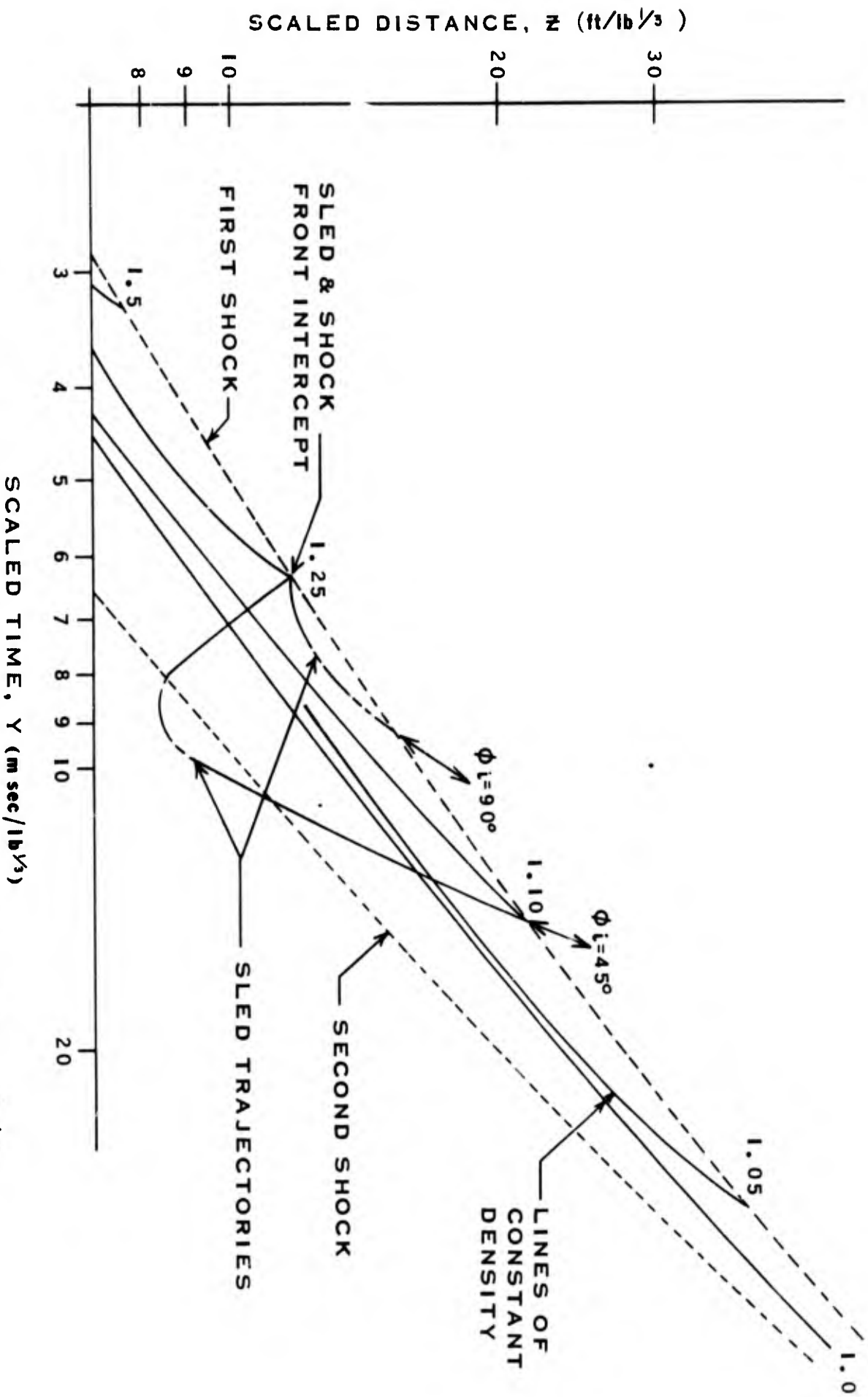


FIGURE 5 TIME HISTORIES OF THE DENSITY RATIO ρ_B/ρ_0 GENERATED BY A FREE FIELD TNT EXPLOSION

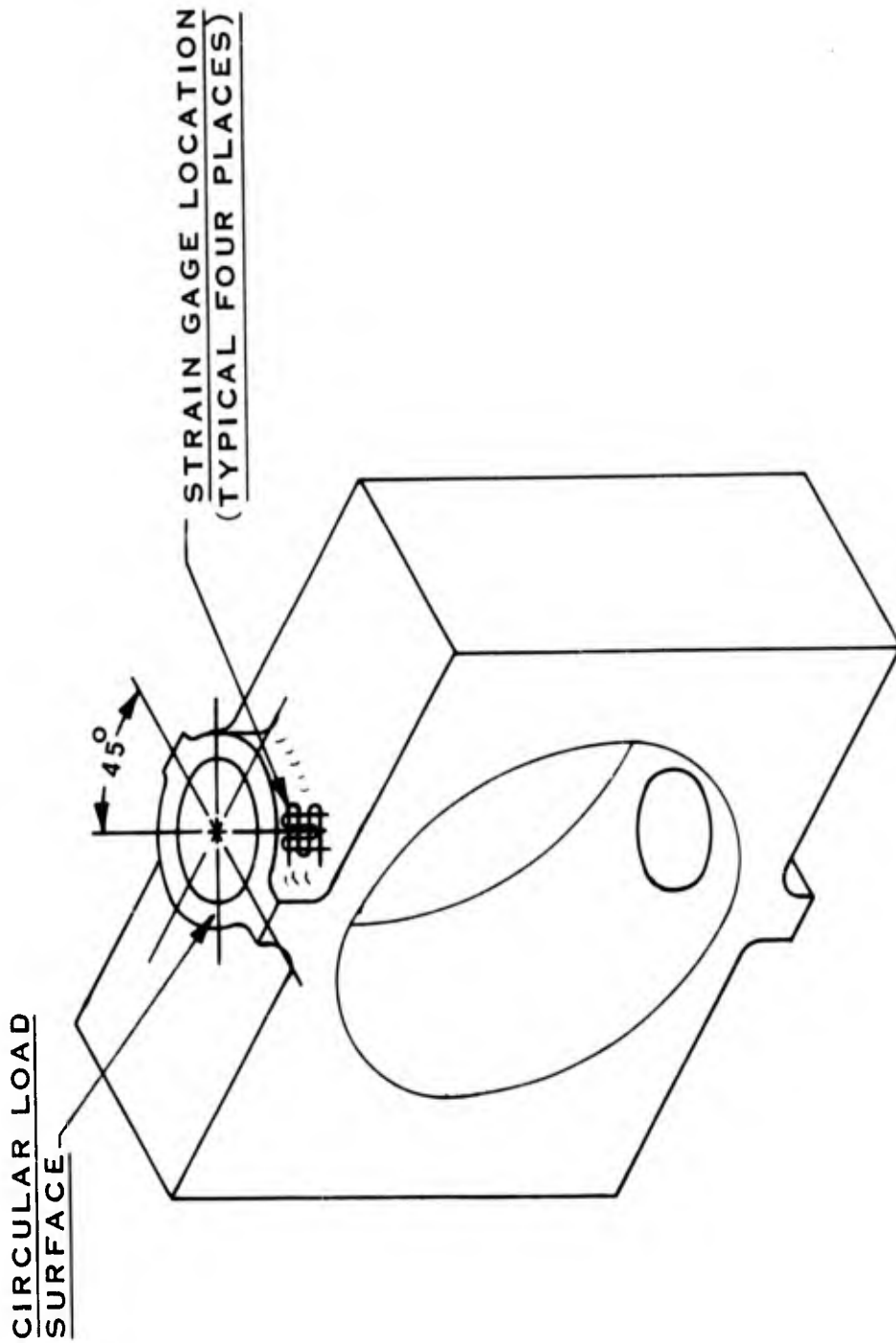


FIGURE 6 SCHEMATIC OF THE FORCE TRANSDUCER AND STRAIN GAGE LOCATIONS

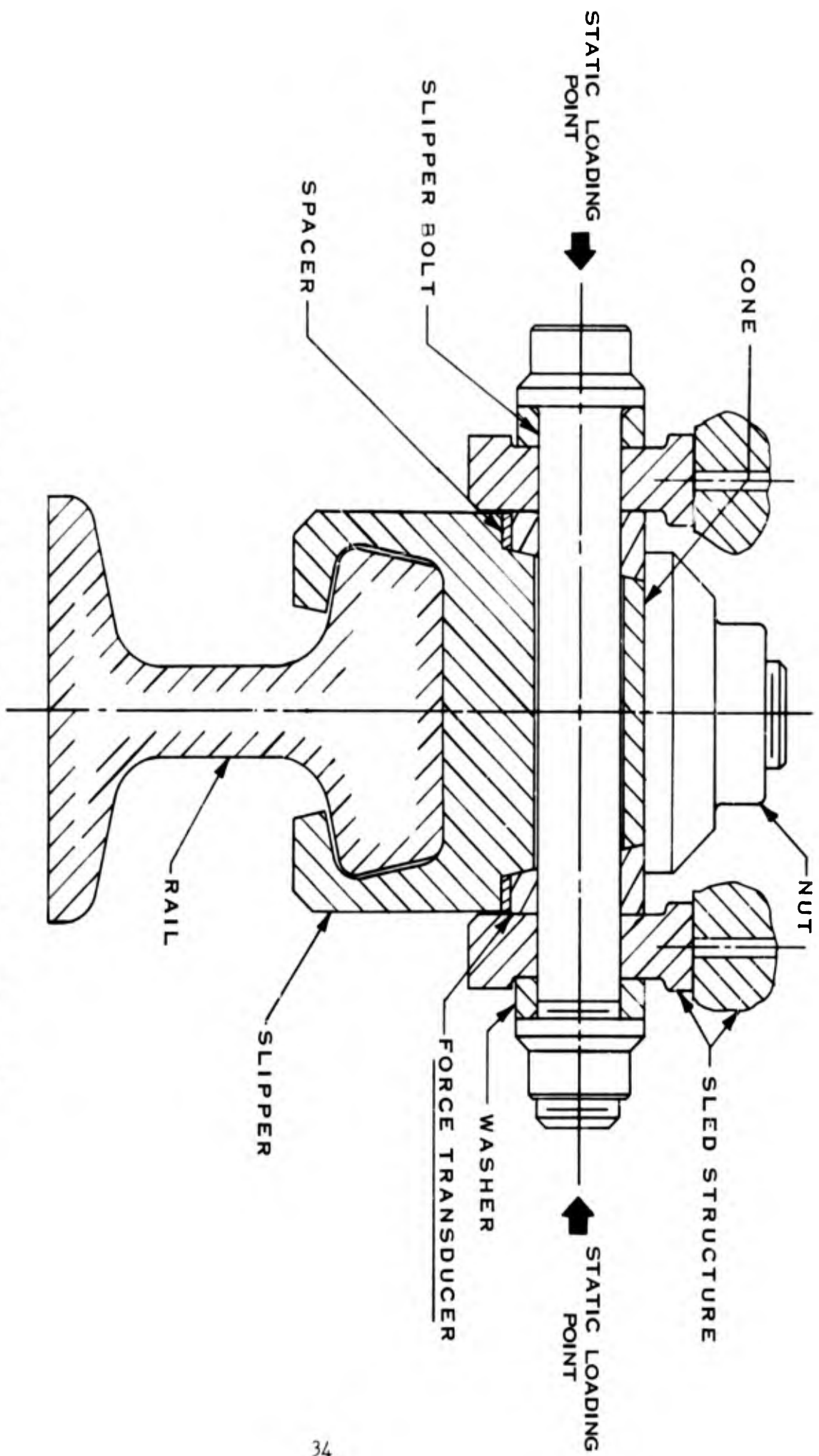


FIGURE 7 SLIPPER INSTALLATION CROSS SECTION

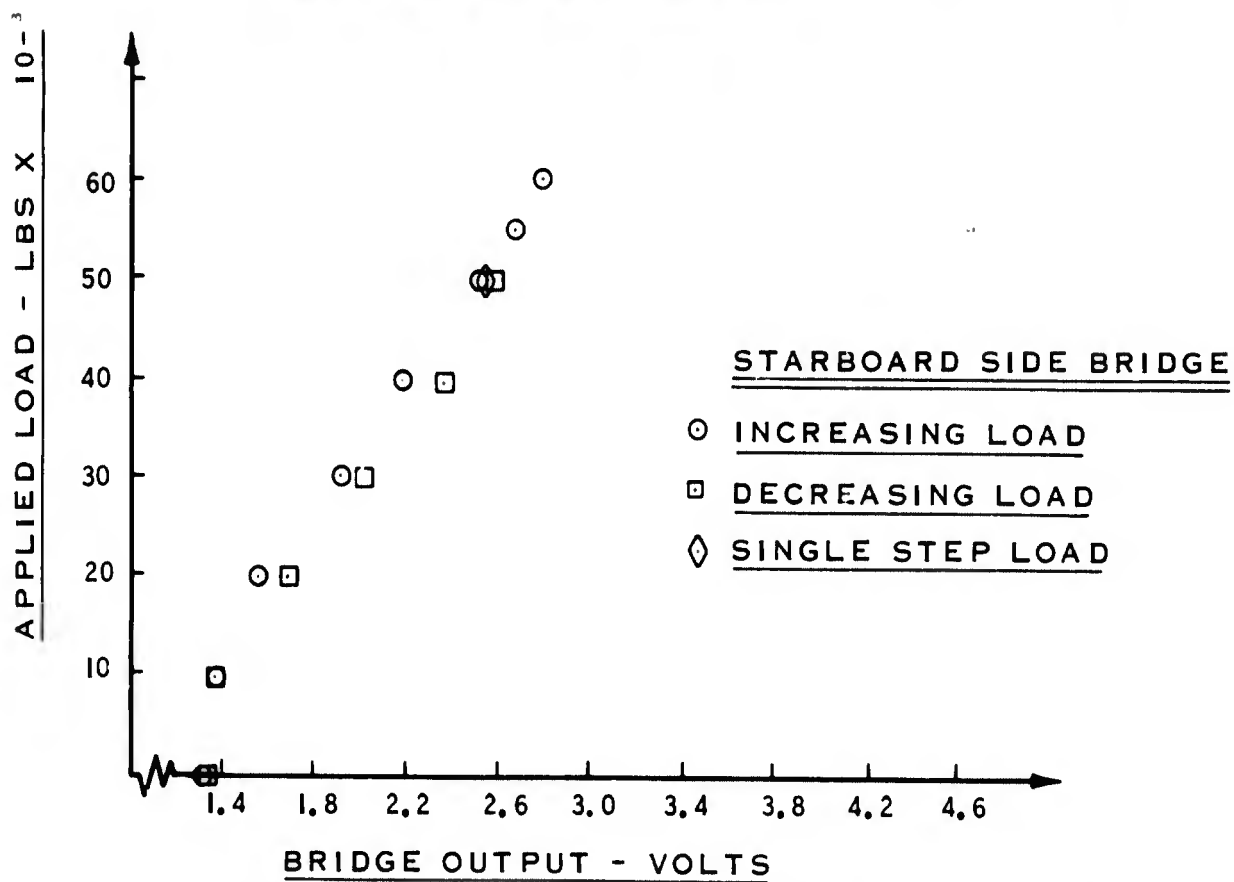
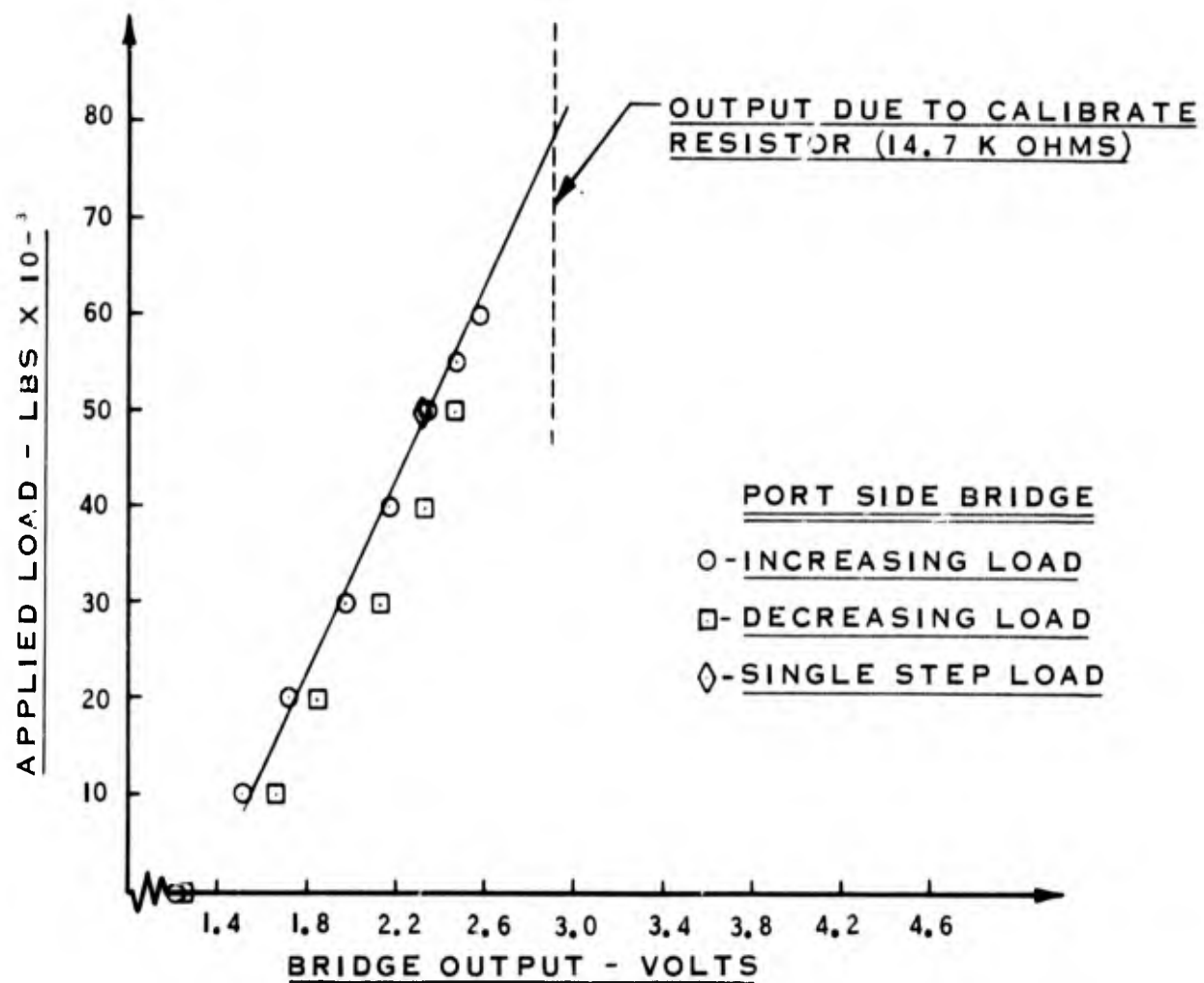


FIGURE 8 PORT SIDE APPLIED LOAD VERSUS BRIDGE OUTPUT

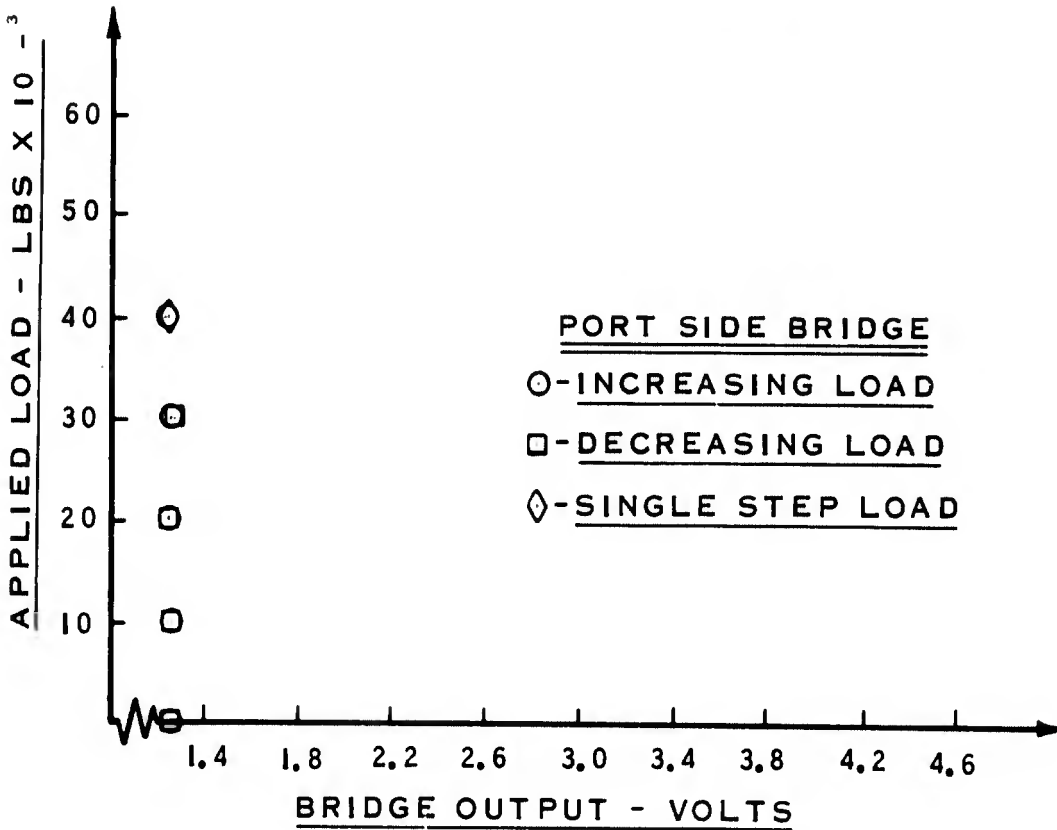
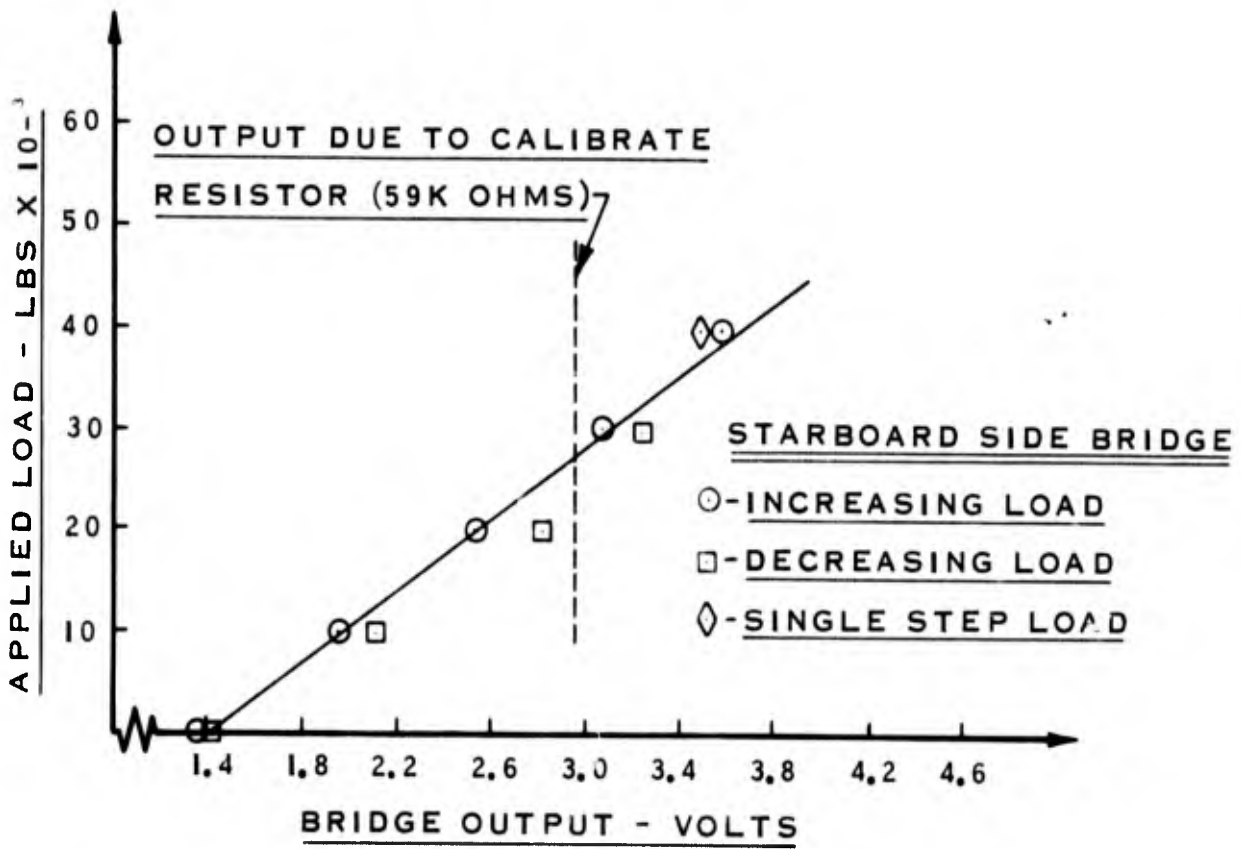
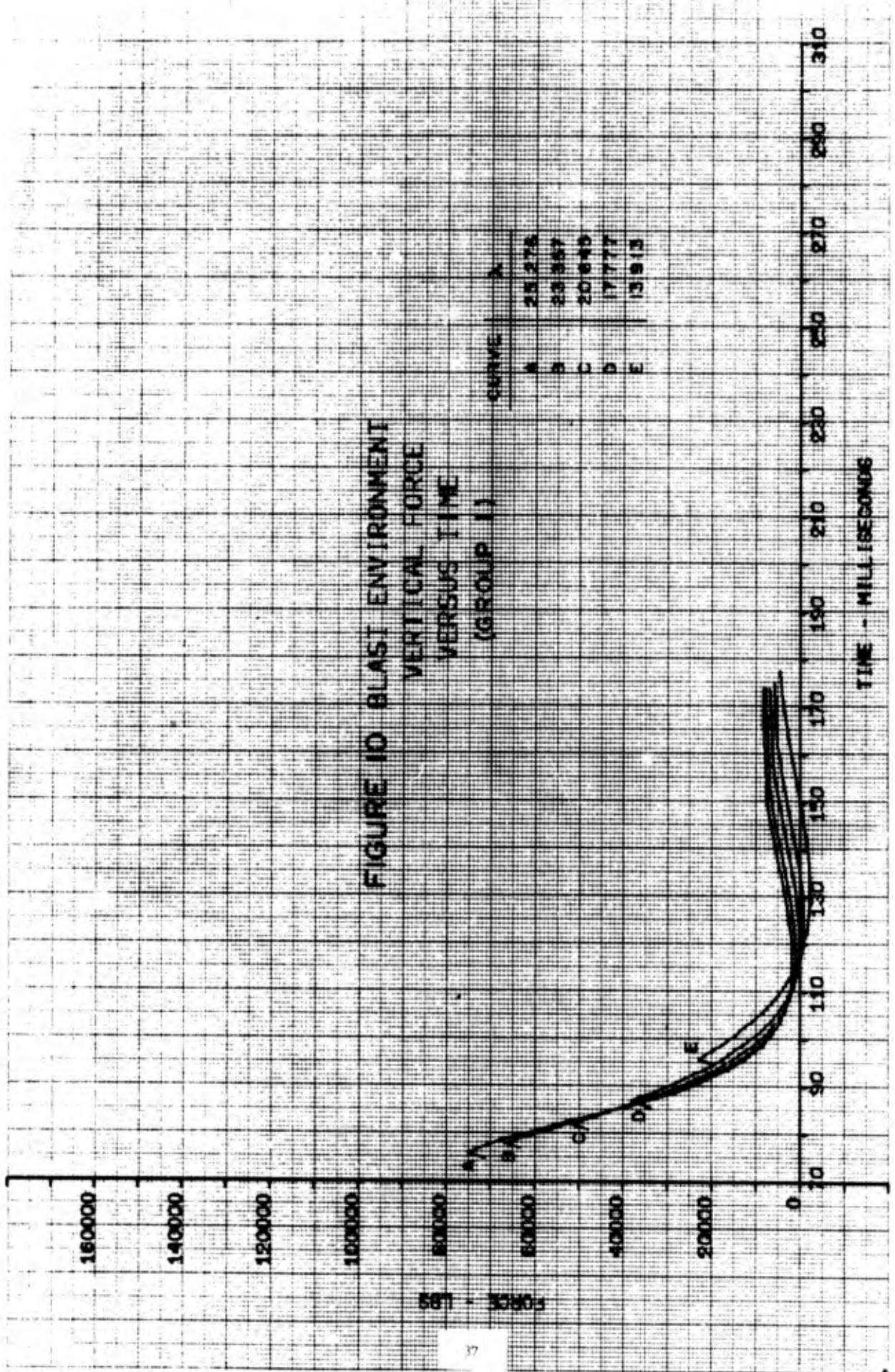


FIGURE 9 STARBOARD SIDE APPLIED LOAD VERSUS BRIDGE OUTPUT



FORCE - LBS

TIME - MILLISECONDS

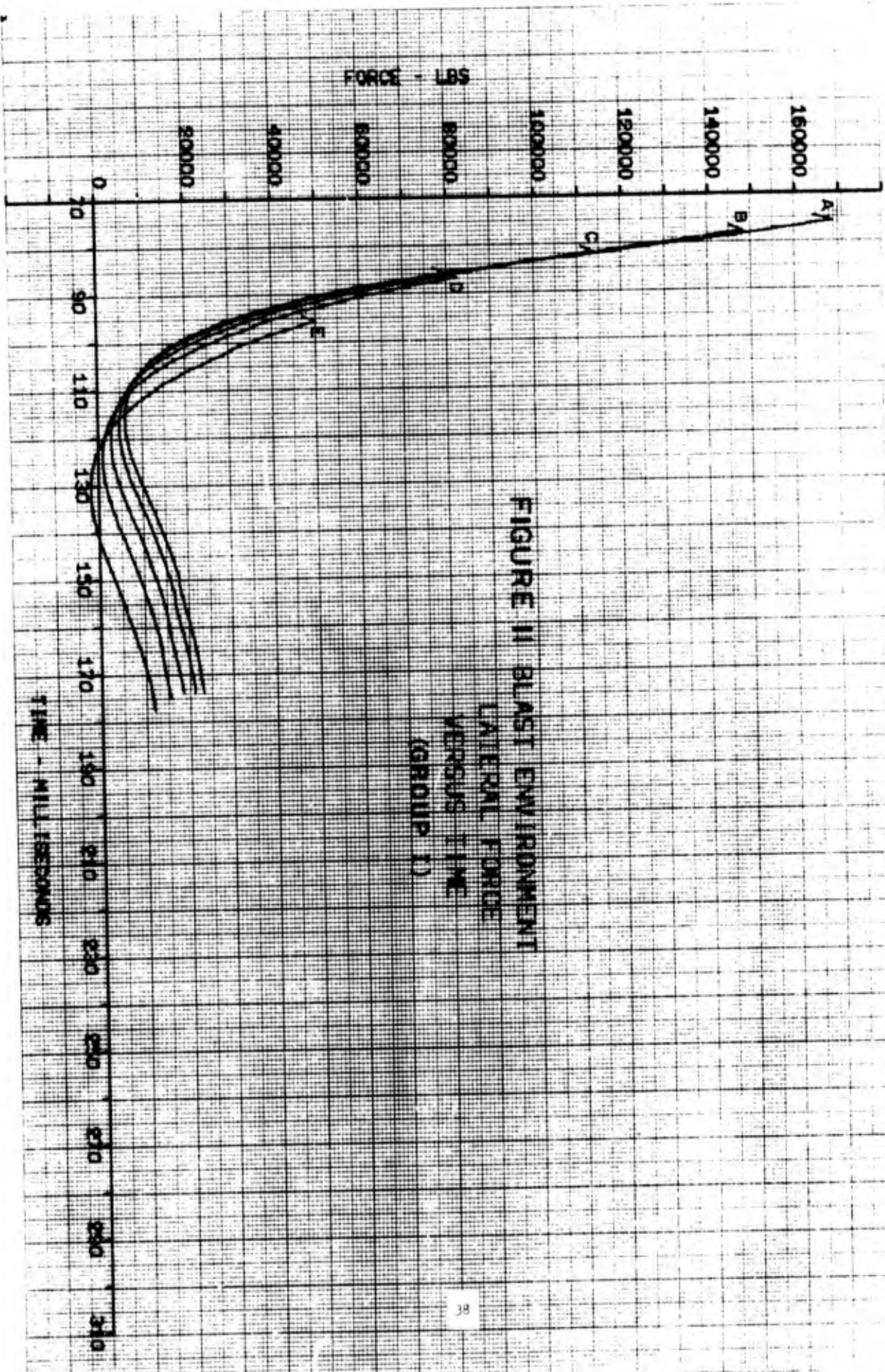
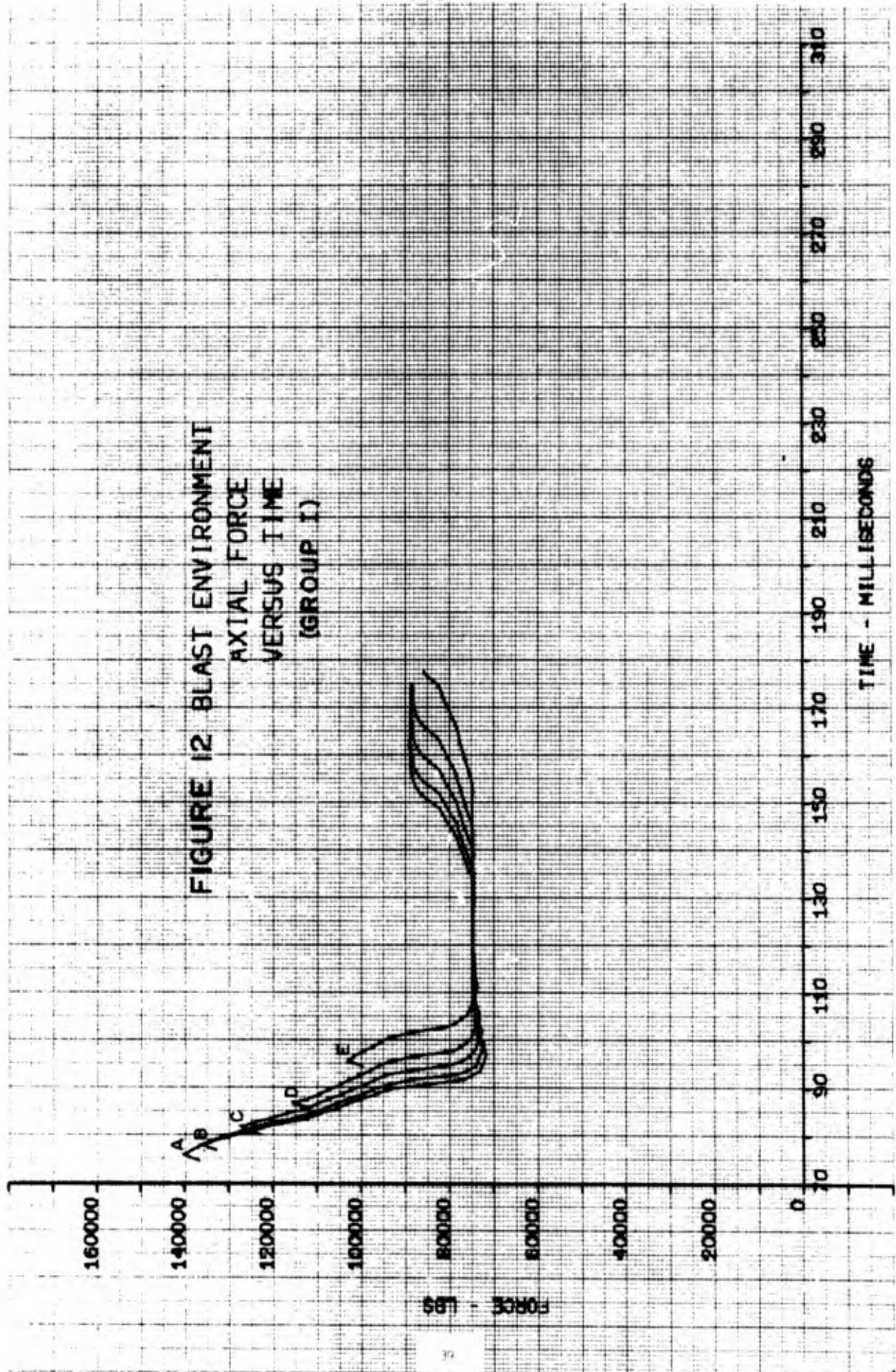
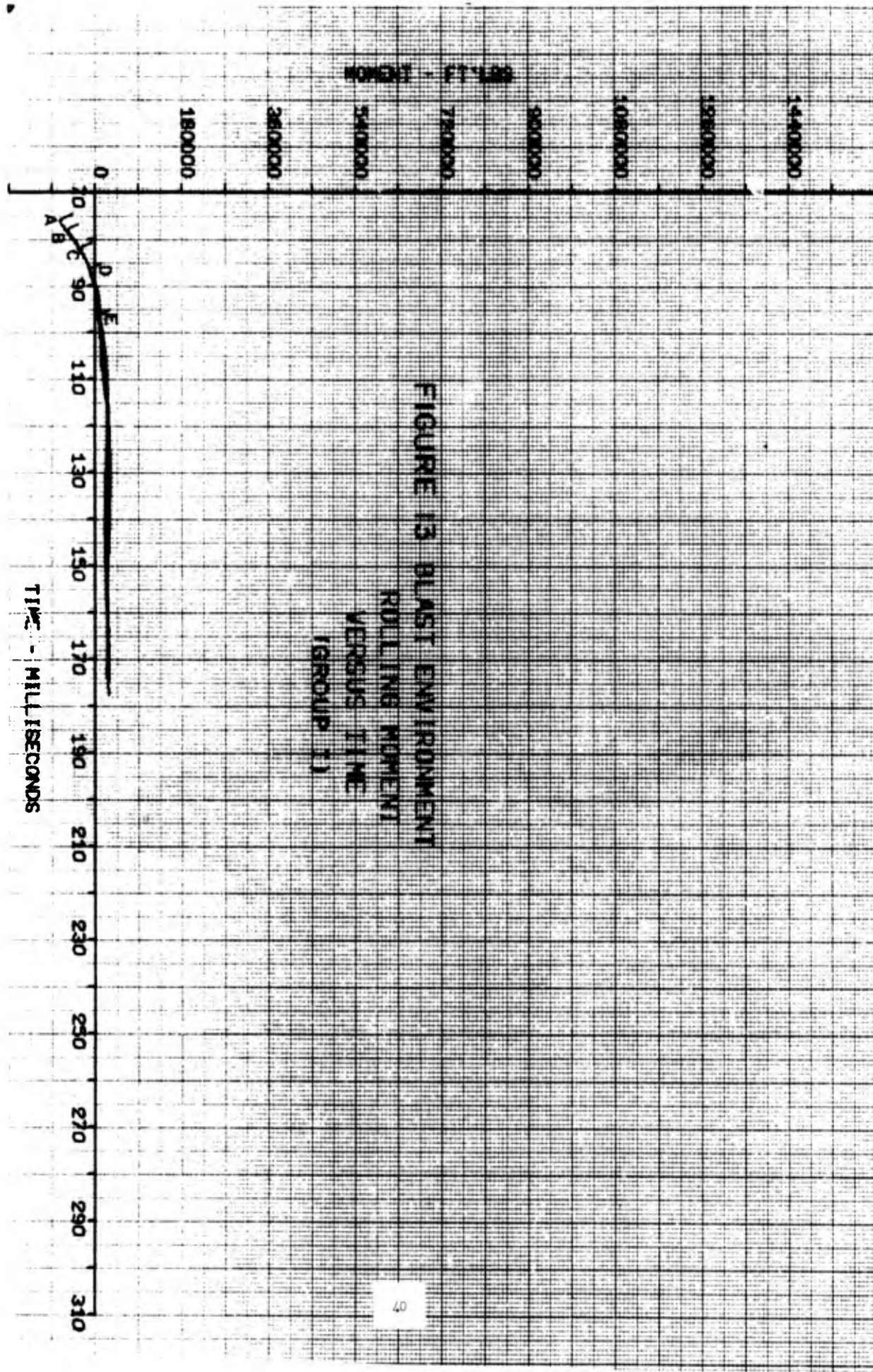


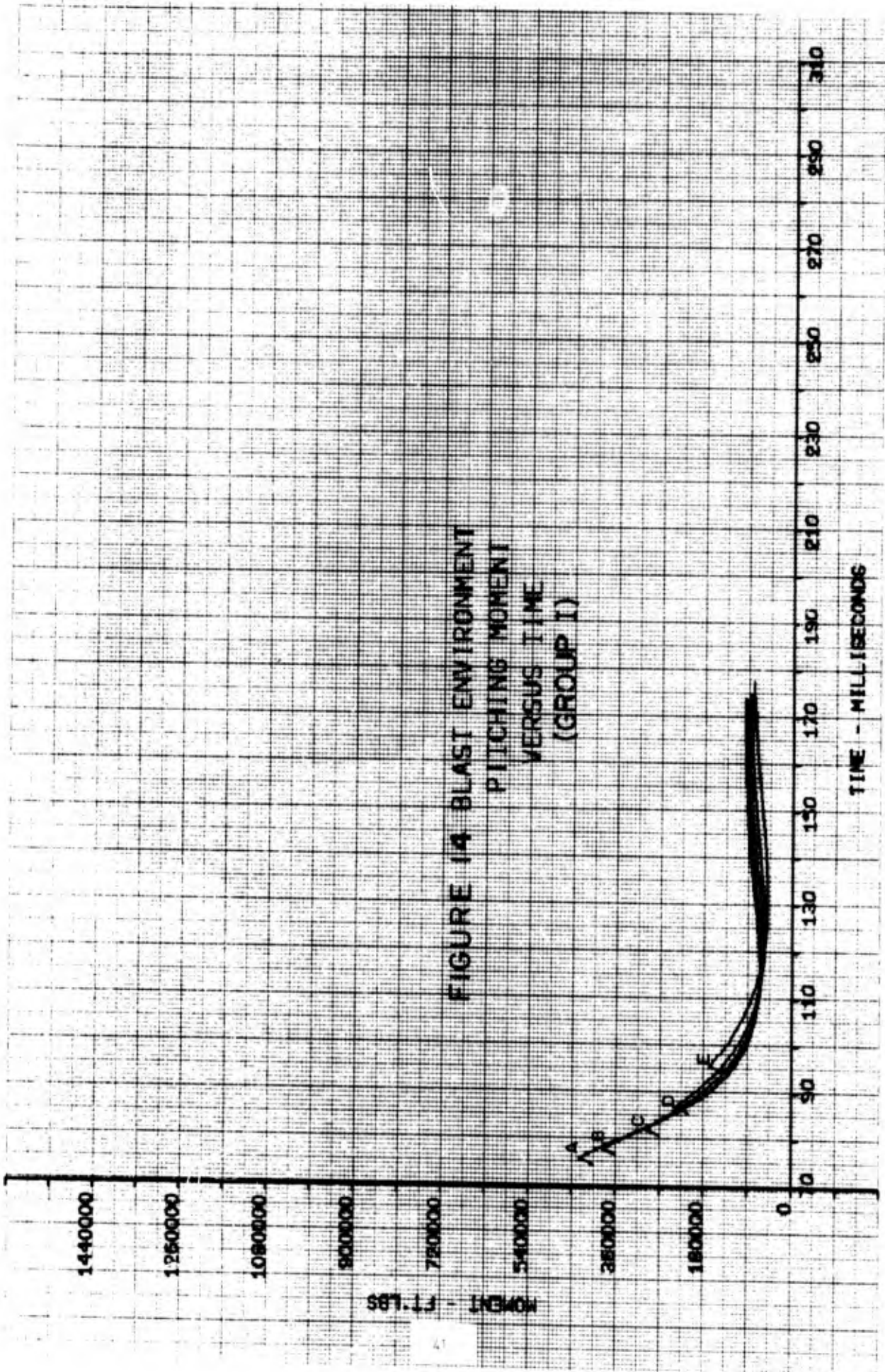
FIGURE 12 BLAST ENVIRONMENT
AXIAL FORCE
VERSUS TIME
(GROUP I)



FORCE - LBS

TIME - MILLISECONDS





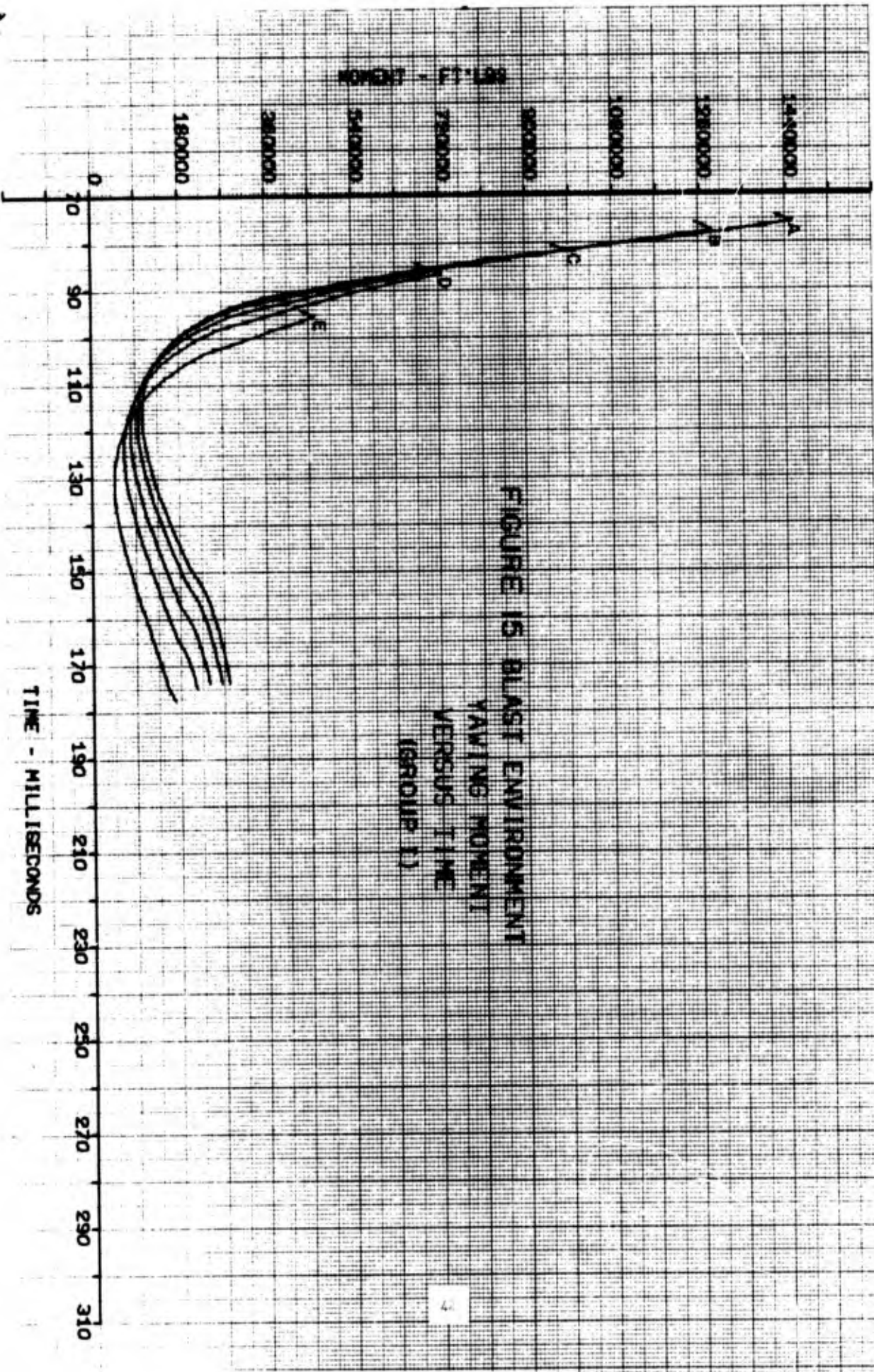
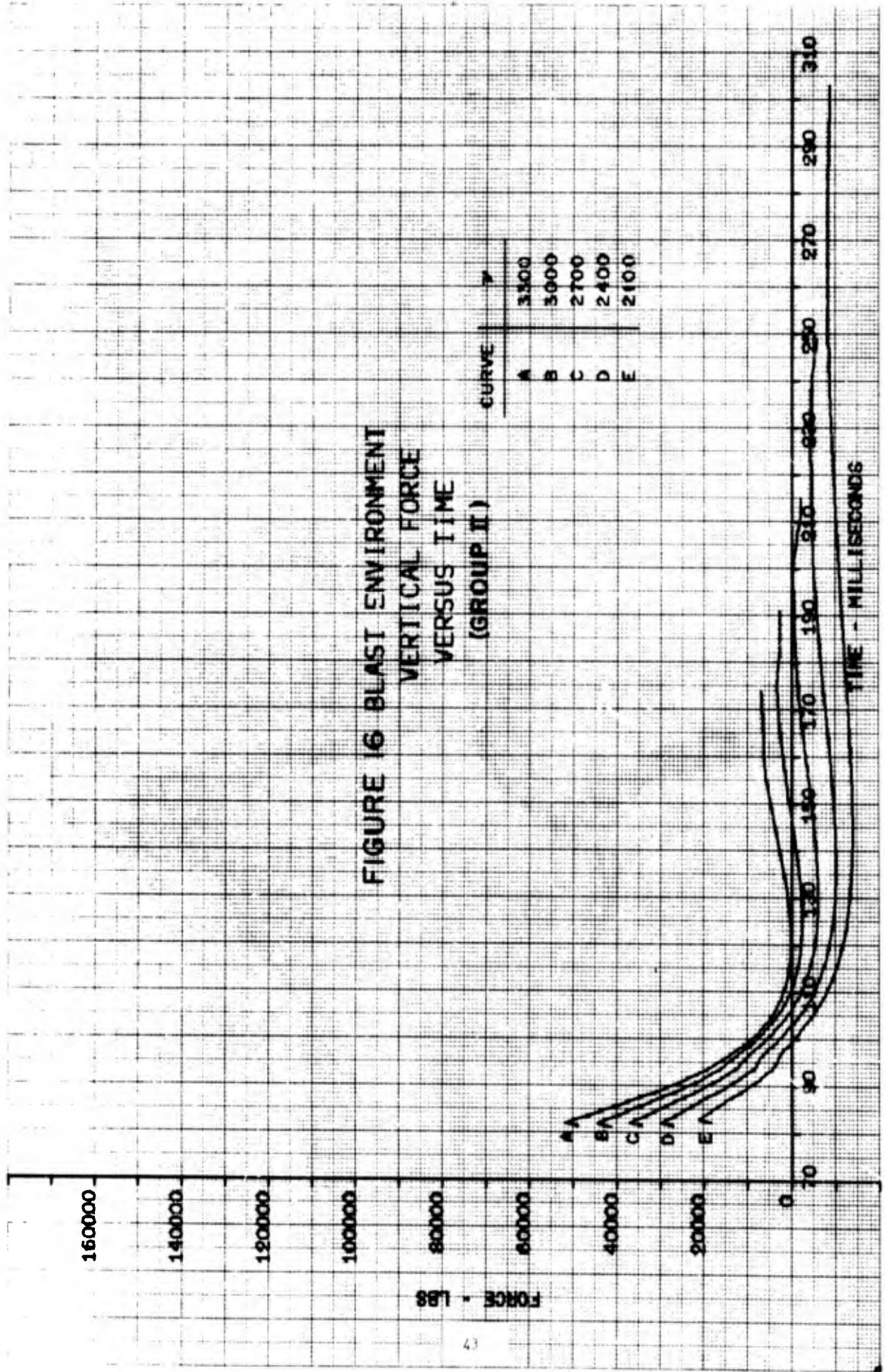


FIGURE 15 BLAST ENVIRONMENT
 YAWING MOMENT
 VERSUS TIME
 (GROUP 1)



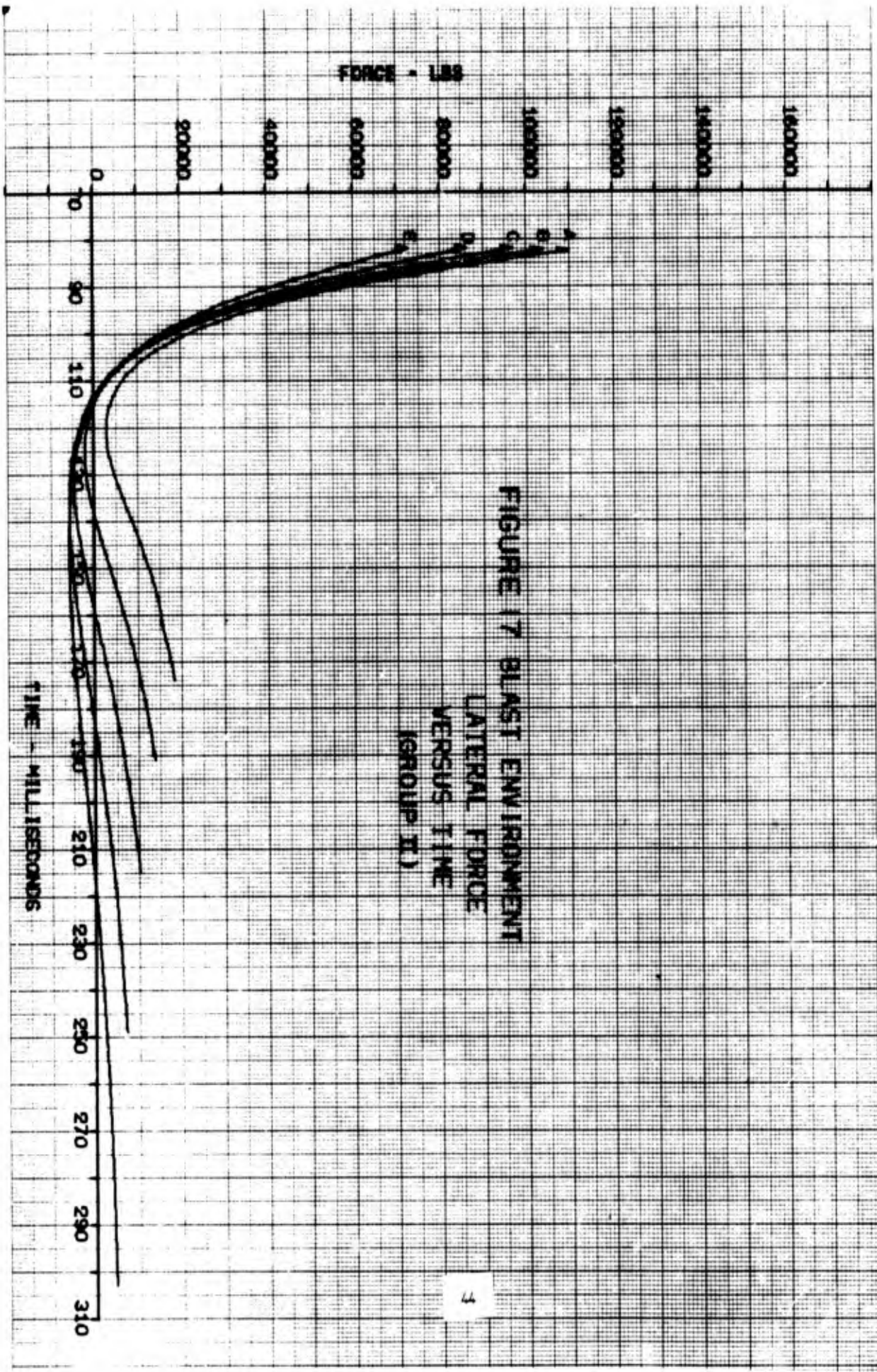
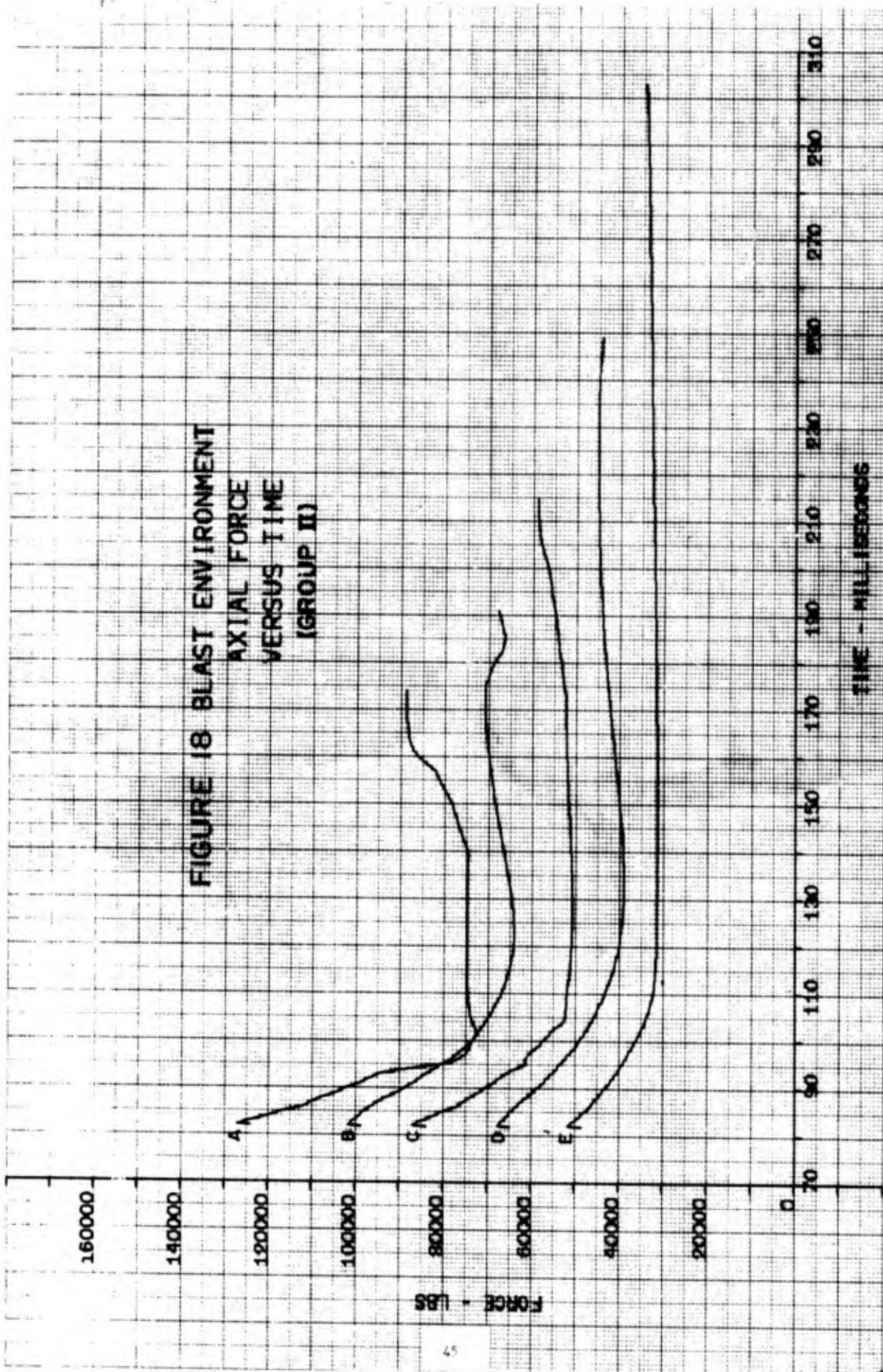


FIGURE 17 BLAST ENVIRONMENT
LATERAL FORCE
VERSUS TIME
(GROUP II)

FIGURE 18 BLAST ENVIRONMENT
AXIAL FORCE
VERSUS TIME
(GROUP II)



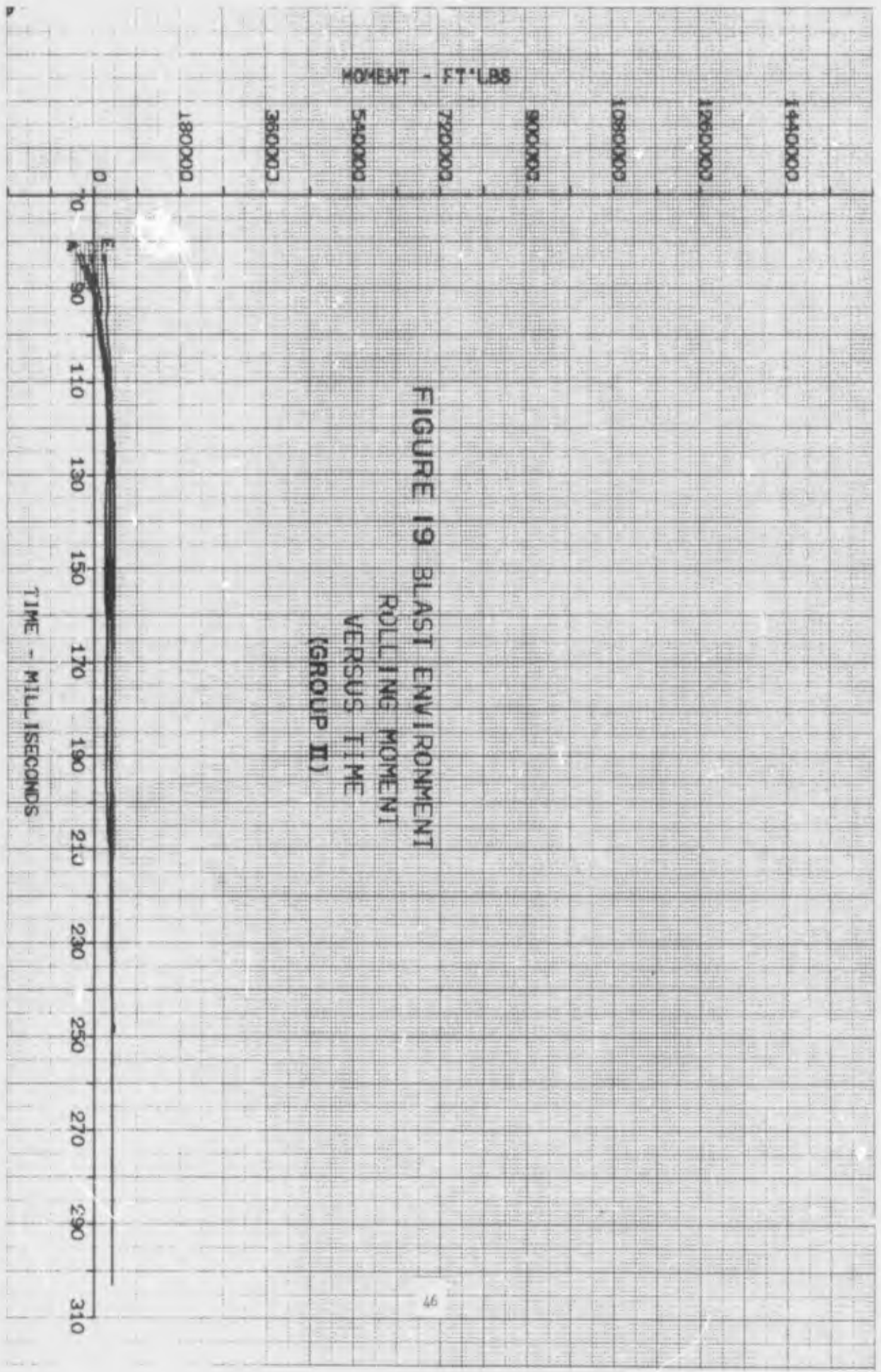


FIGURE 19 BLAST ENVIRONMENT
 ROLLING MOMENT
 VERSUS TIME
 (GROUP II)

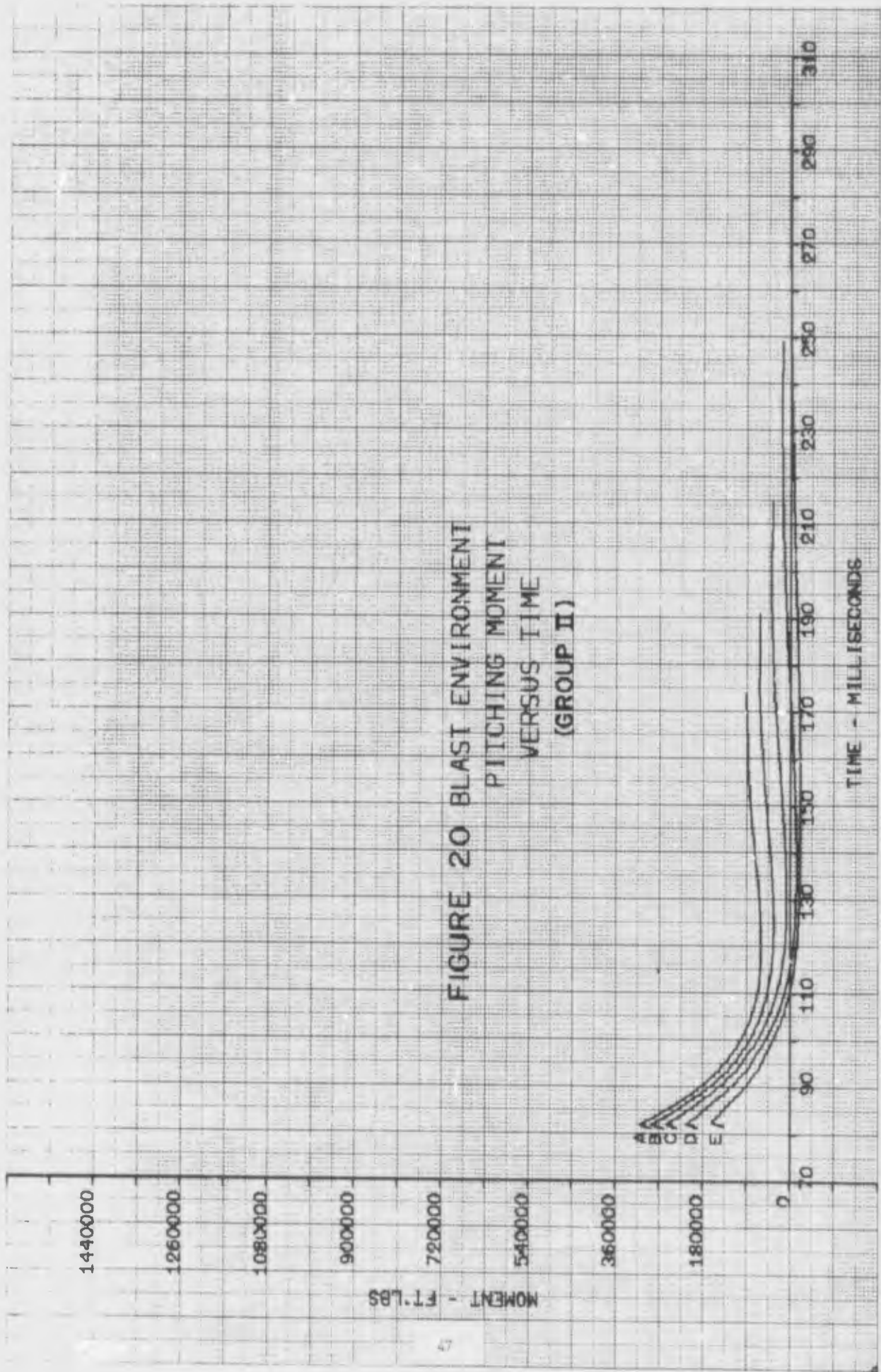


FIGURE 20 BLAST ENVIRONMENT
 PITCHING MOMENT
 VERSUS TIME
 (GROUP II)

MOMENT - FT-LBS

TIME - MILLISECONDS

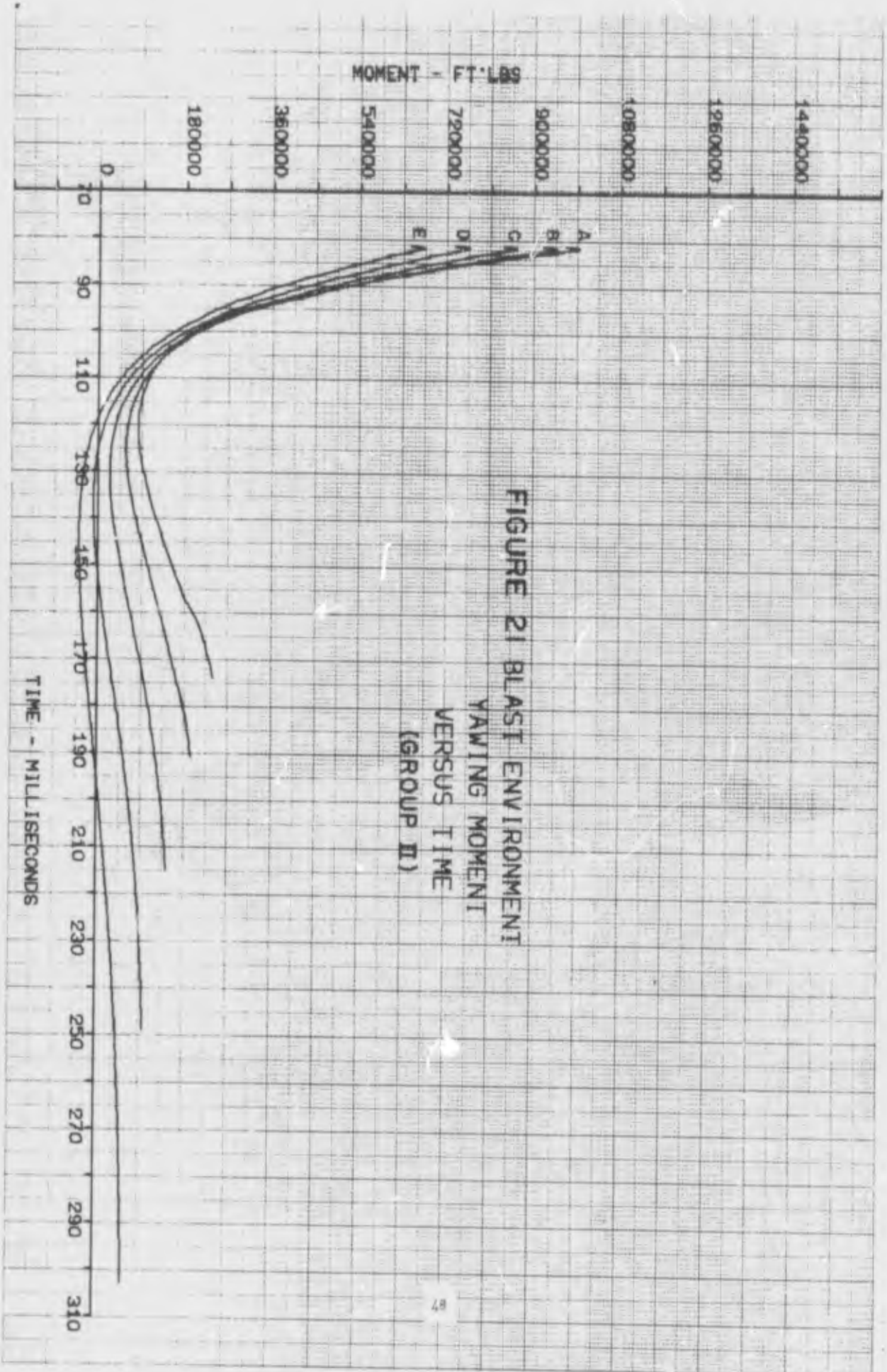
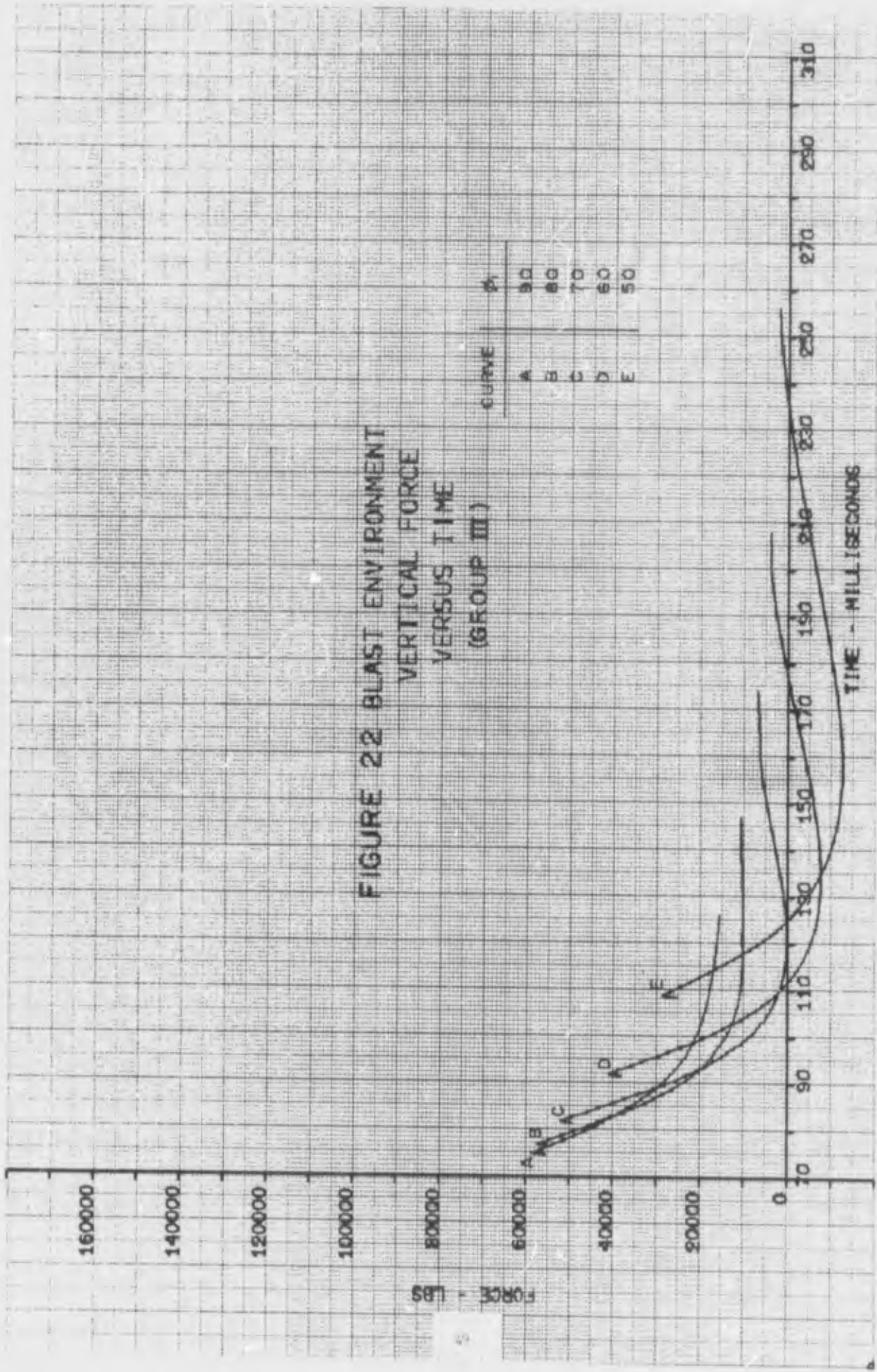


FIGURE 21 BLAST ENVIRONMENT
YAWING MOMENT
VERSUS TIME
(GROUP II)



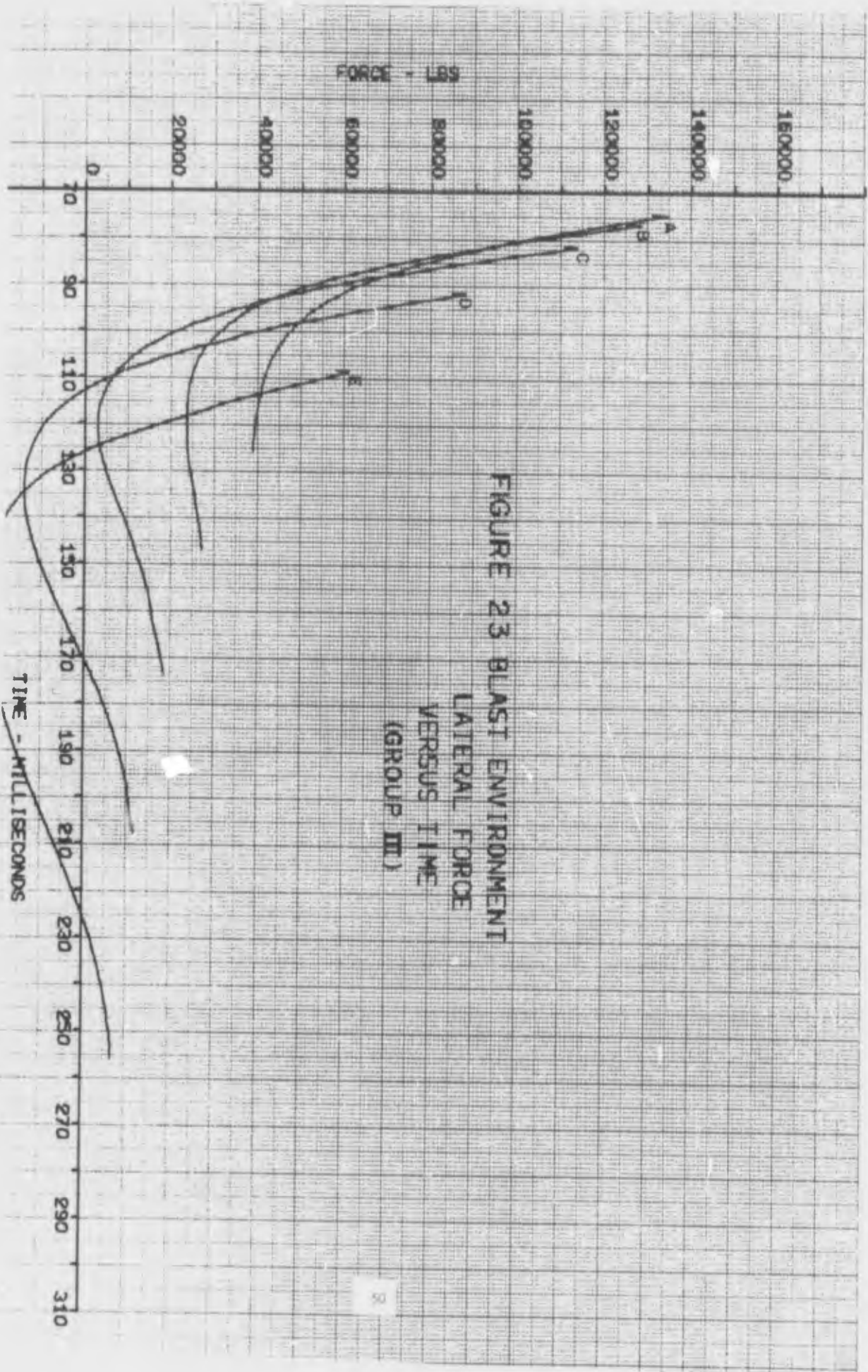


FIGURE 23 BLAST ENVIRONMENT
LATERAL FORCE
VERSUS TIME
(GROUP III)

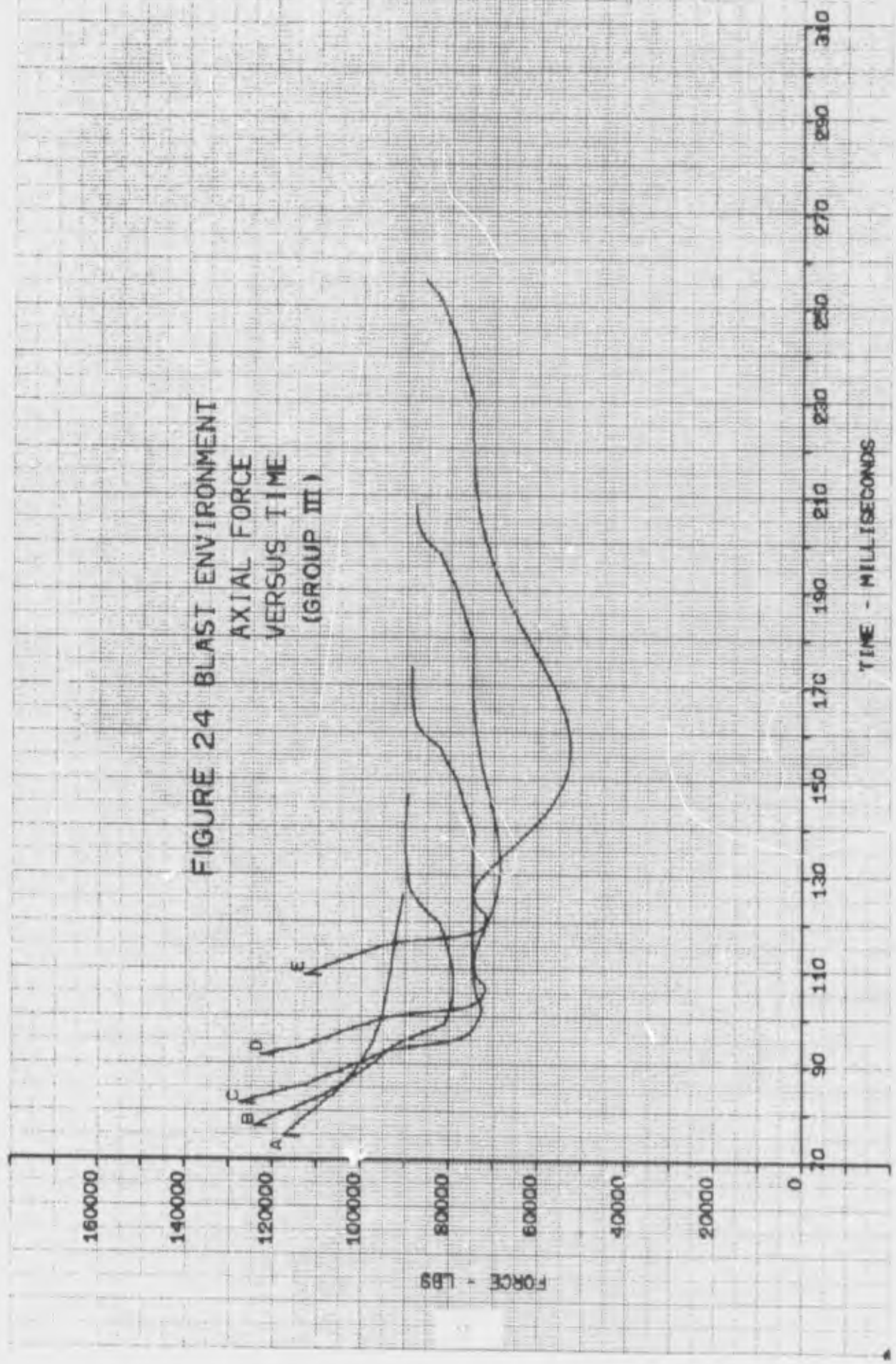


FIGURE 24 BLAST ENVIRONMENT
 AXIAL FORCE
 VERSUS TIME
 (GROUP III)

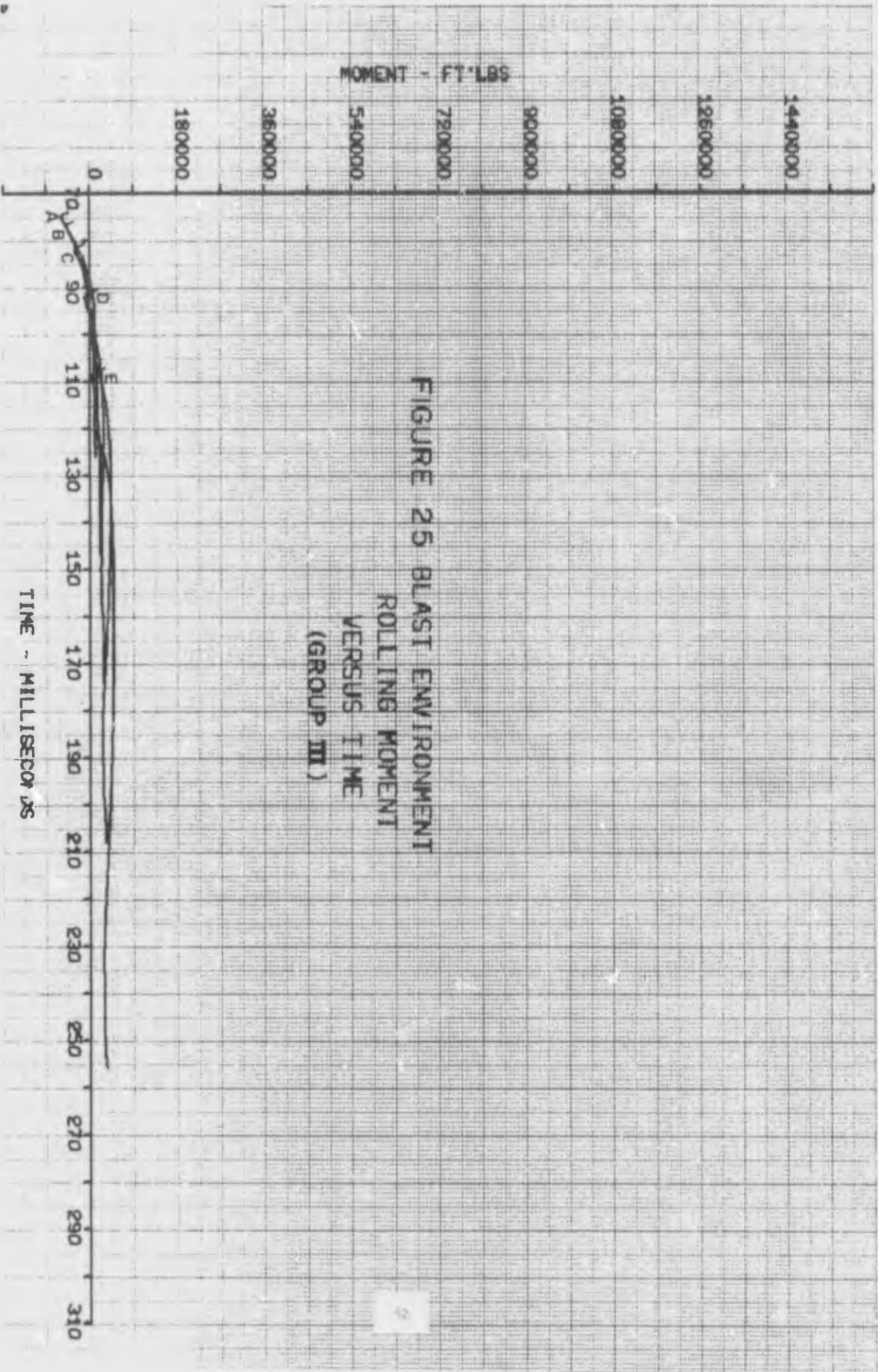
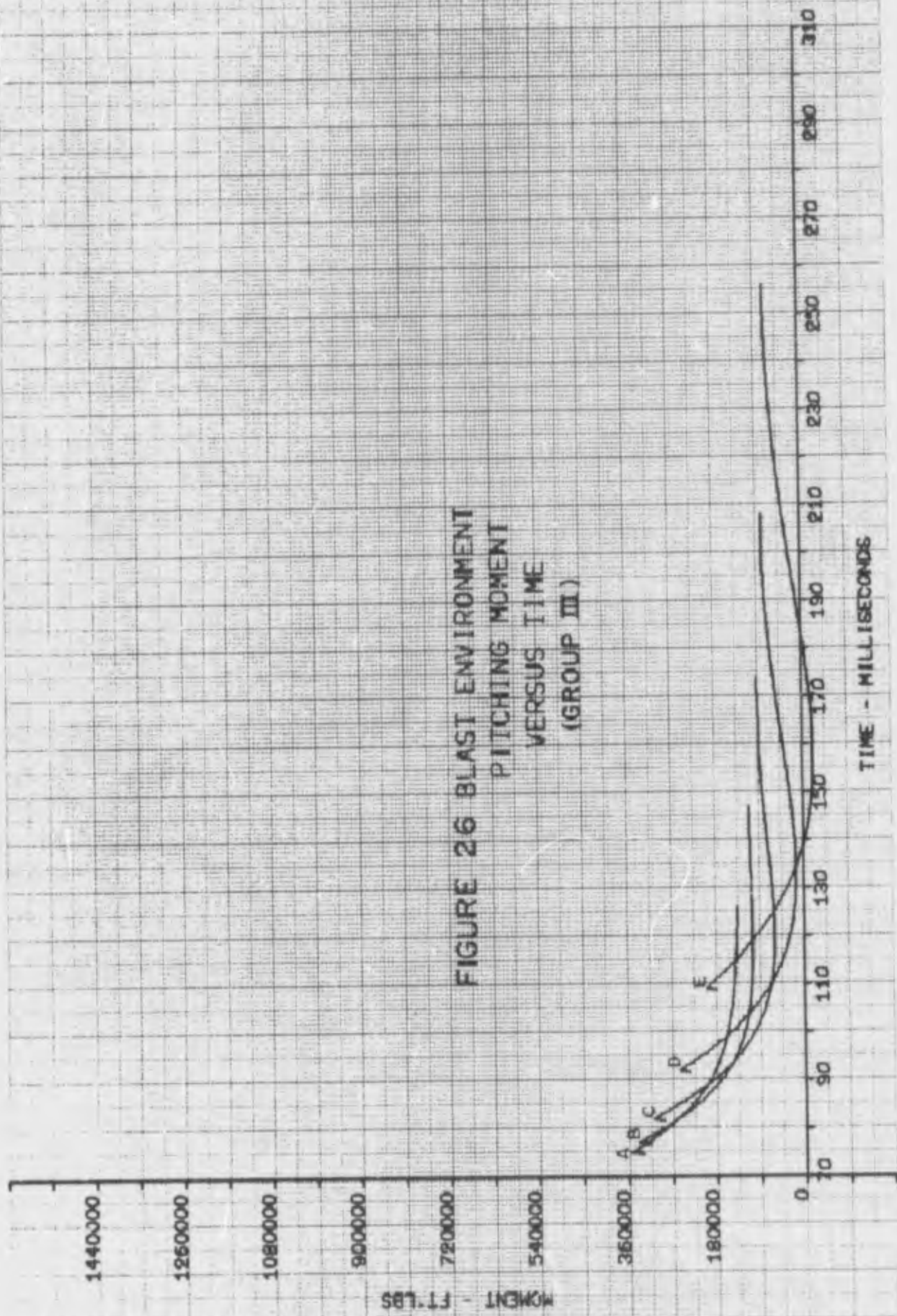


FIGURE 25 BLAST ENVIRONMENT
 ROLLING MOMENT
 VERSUS TIME
 (GROUP III)



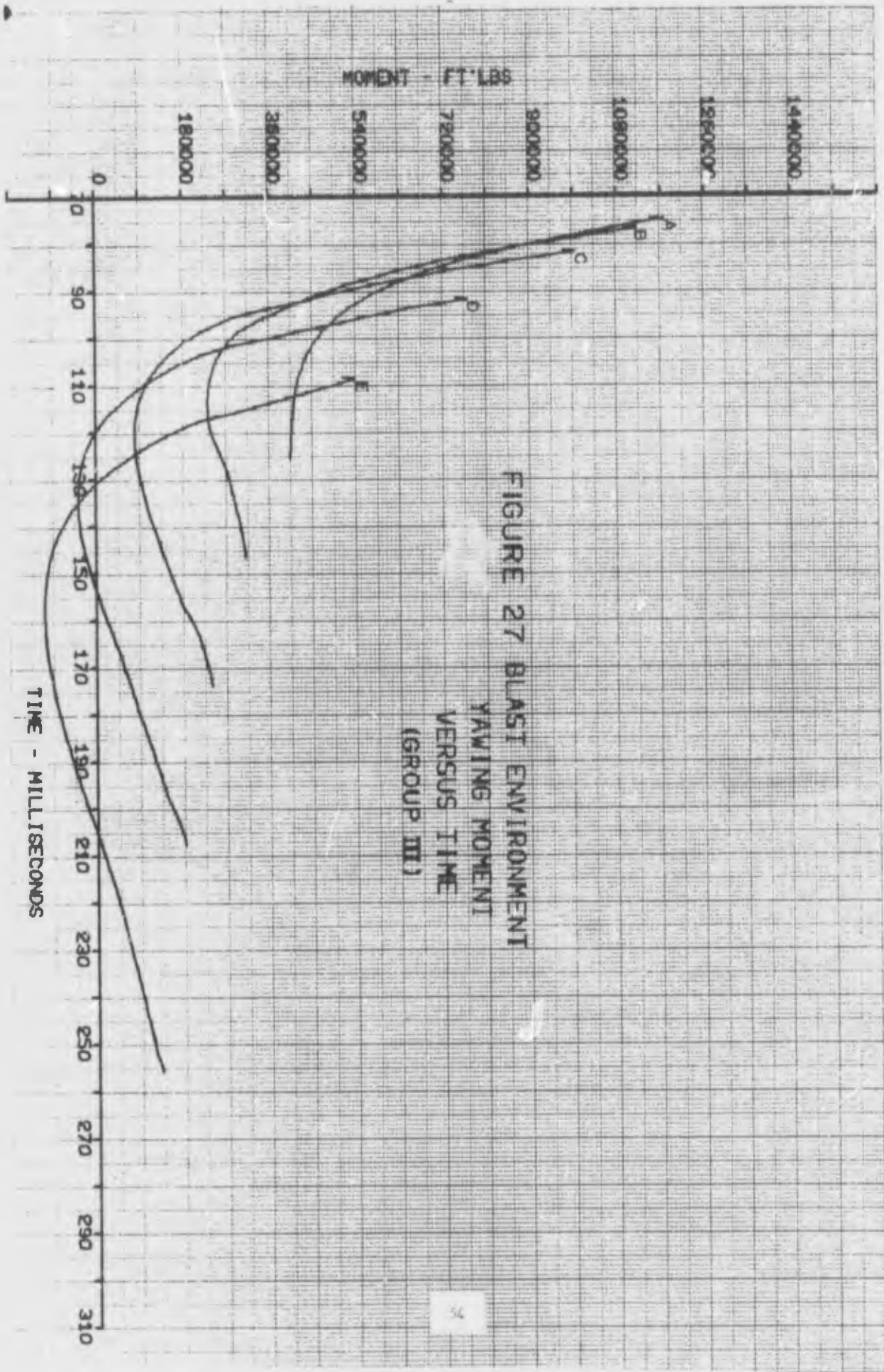


FIGURE 27 BLAST ENVIRONMENT
YAWING MOMENT
VERSUS TIME
(GROUP III)

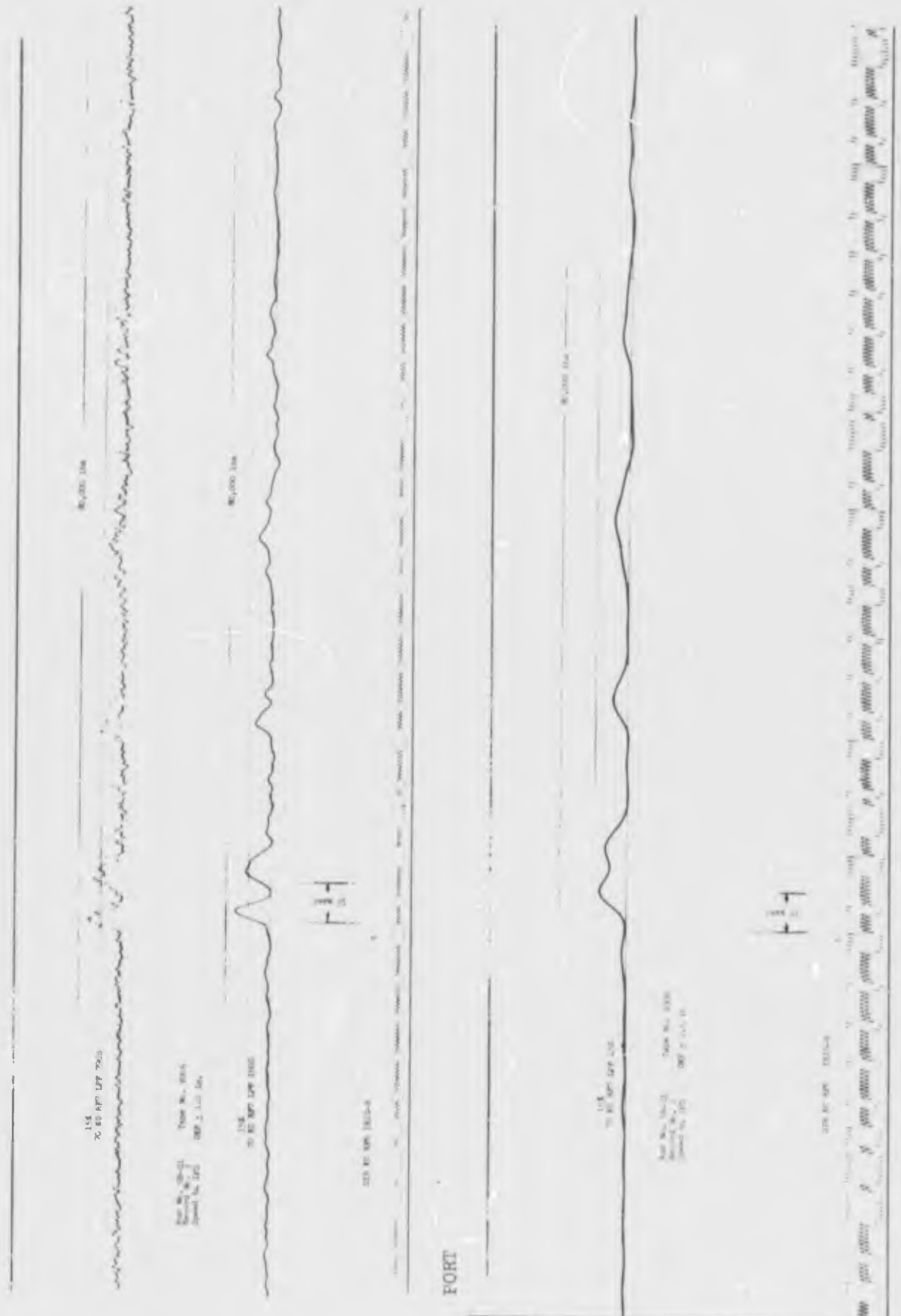
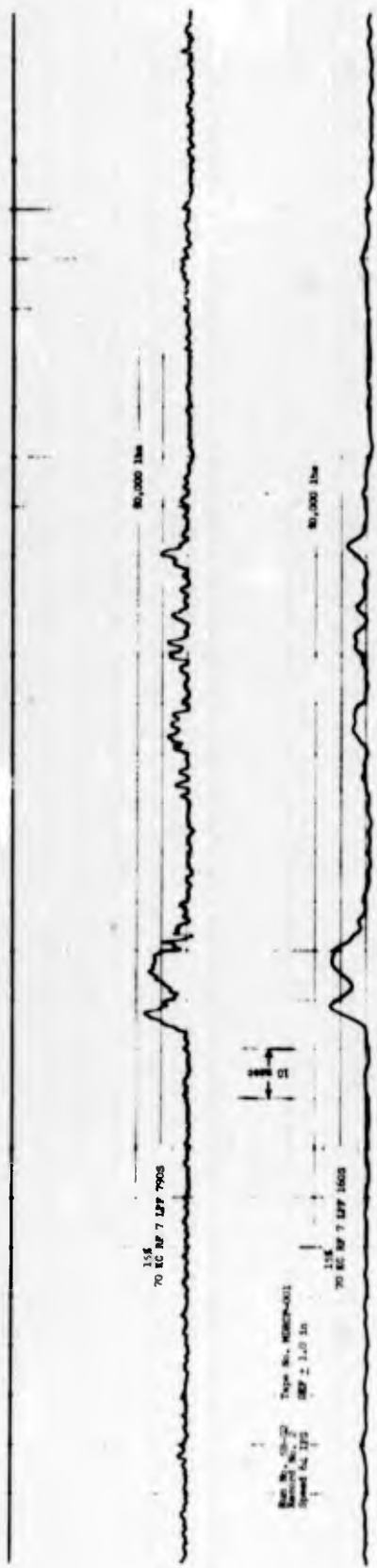


FIGURE 28 FORWARD SLIPPER LATERAL FORCE AS A FUNCTION OF TIME FOR 1552 POUNDS OF TNT



TO EC MP 7 LFF 7905
50,000 lbs

TO EC MP 7 LFF 7405
50,000 lbs

SEE EC MP 7910-8

PORT



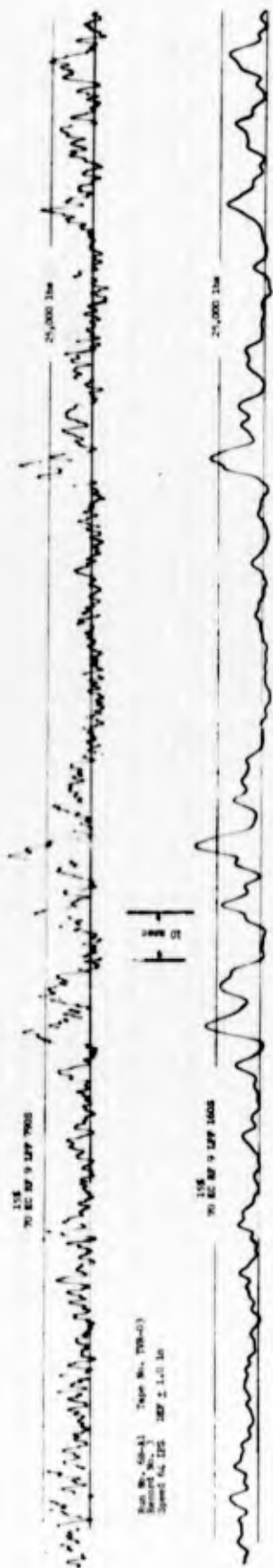
TO EC MP LFF 7905
25,000 lbs

TO EC MP LFF 7405
25,000 lbs

SEE EC MP 7910-8

STARBOARD

FIGURE 29 FORWARD SLIPPER LATERAL FORCE AS A FUNCTION OF TIME FOR 2672 POUNDS OF TNT



STARBOARD

FIGURE 30 FORWARD SLIPPER LATERAL FORCE AS A FUNCTION OF TIME FOR 4000 POUNDS OF TNT

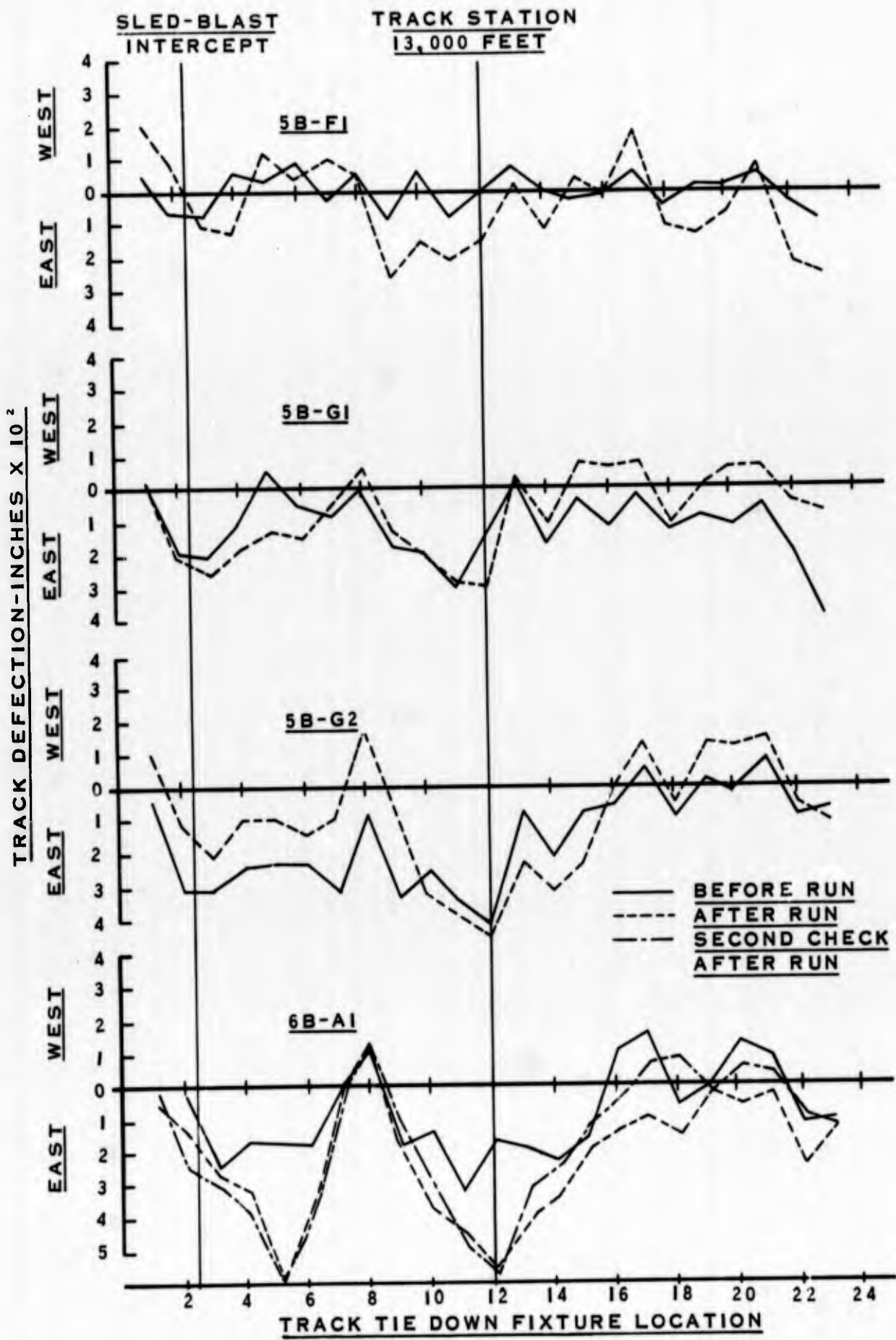


FIGURE 31
 PERMANENT TRACK DEFLECTIONS IN BLAST TEST AREA

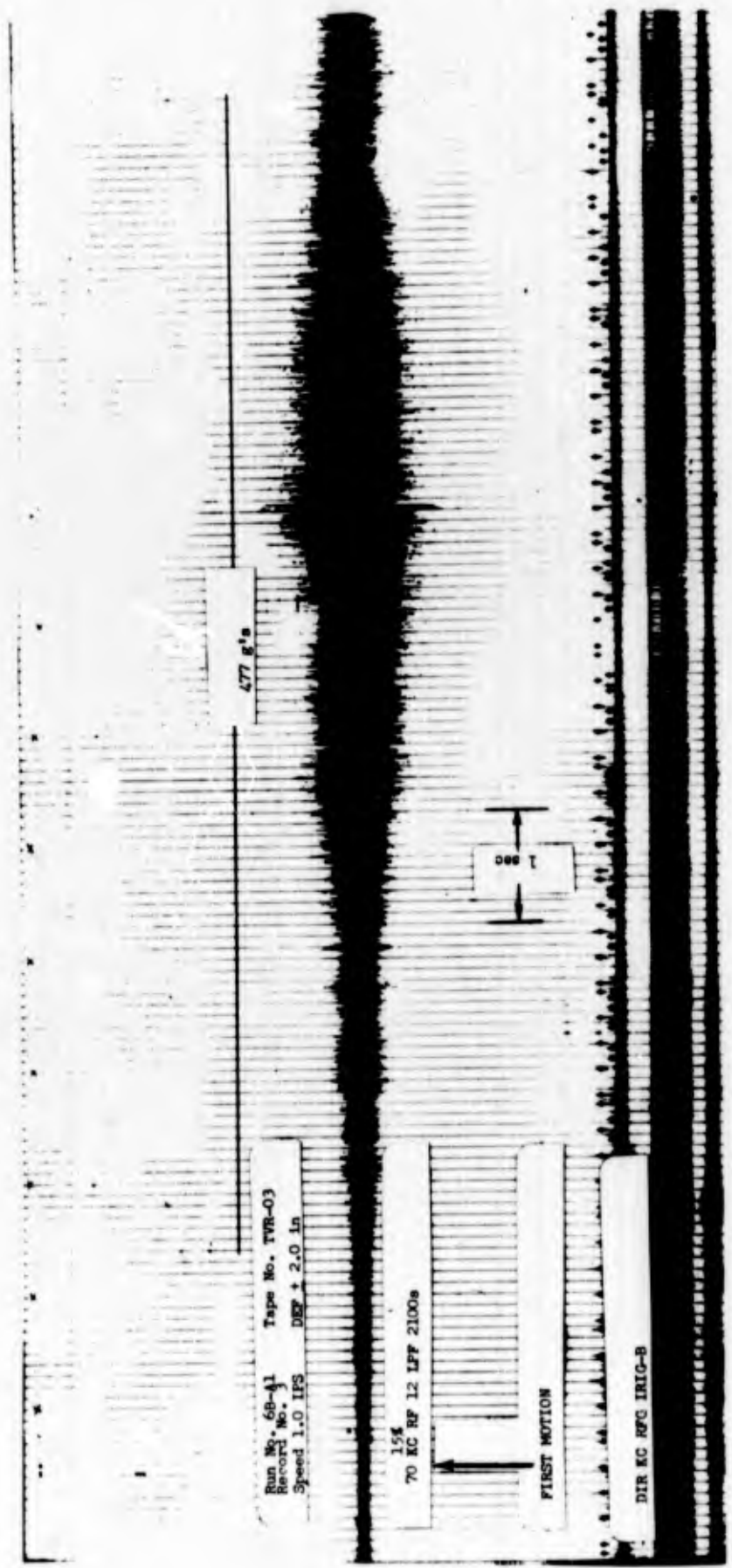


FIGURE 32 SLED LATERAL ACCELERATION AS A FUNCTION OF TIME FOR THE FIRST 13 SECONDS

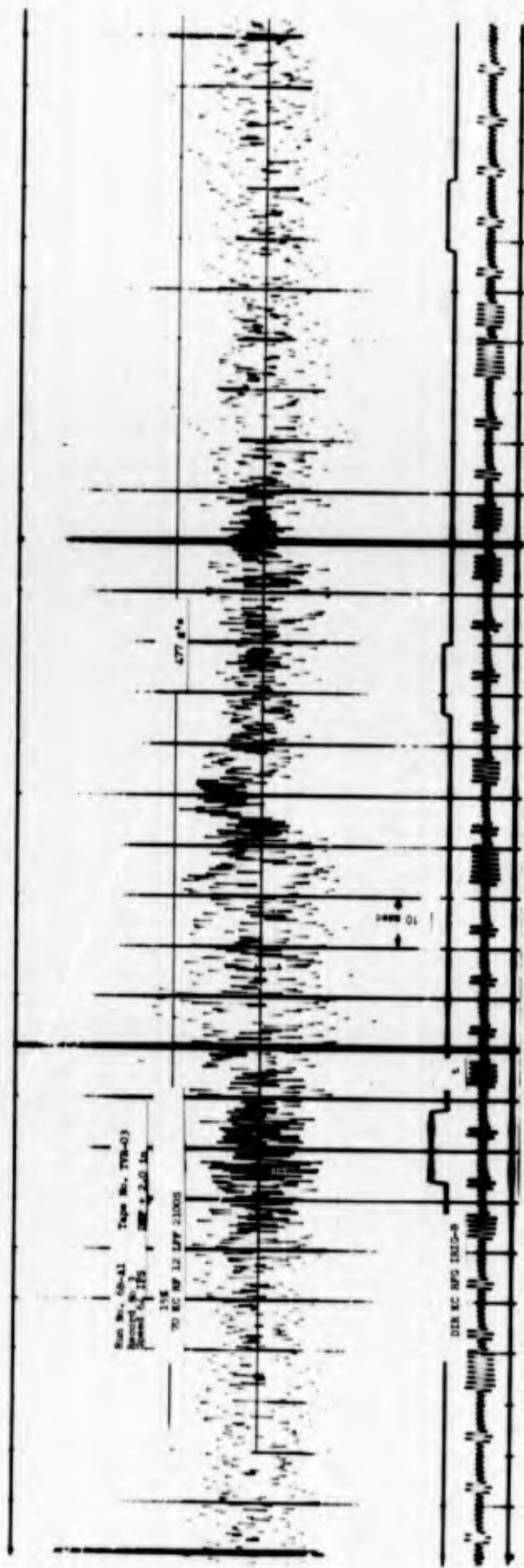


FIGURE 33 SLED LATERAL ACCELERATION AS A FUNCTION OF TIME IN THE BLAST ENVIRONMENT

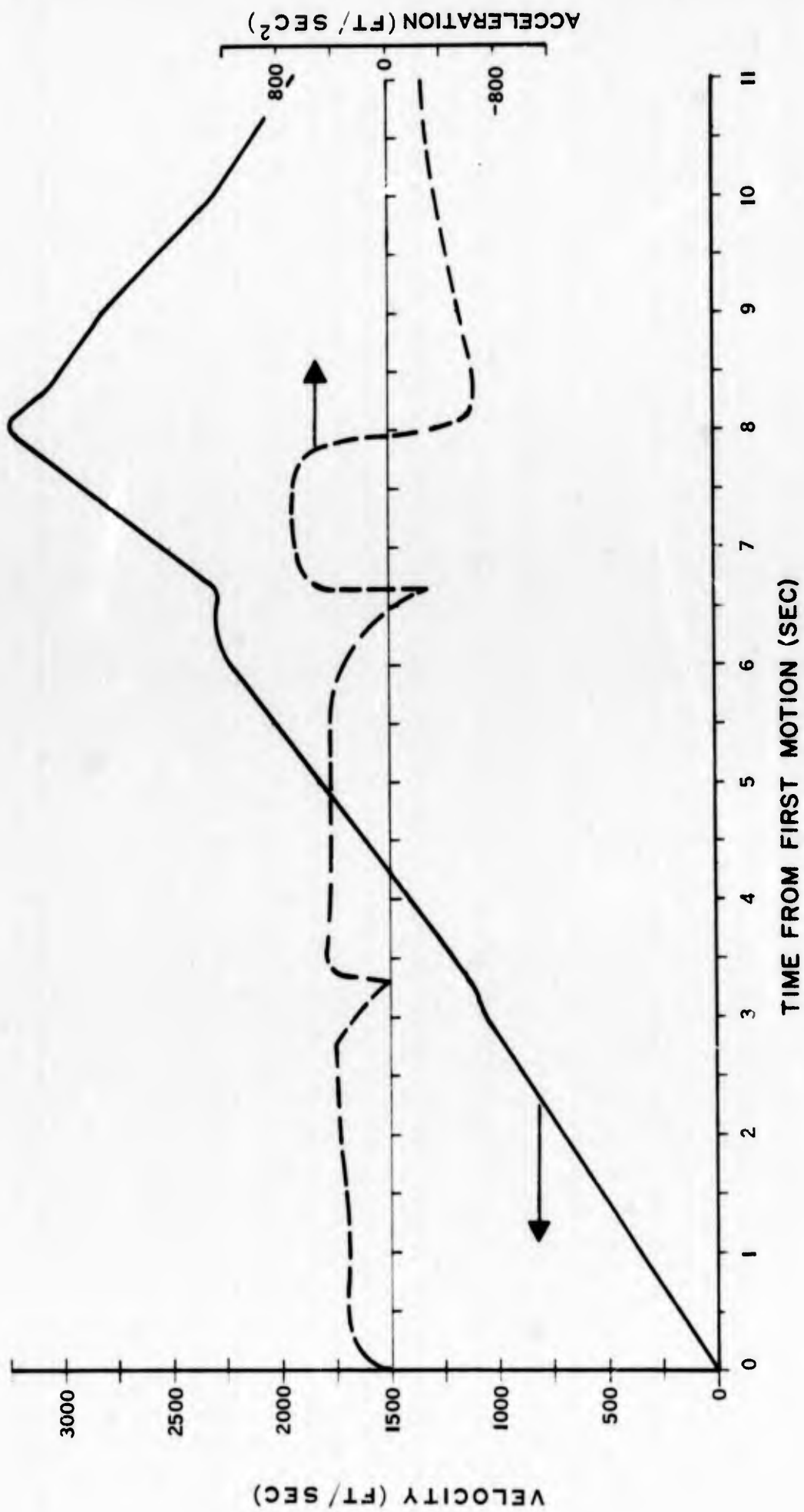
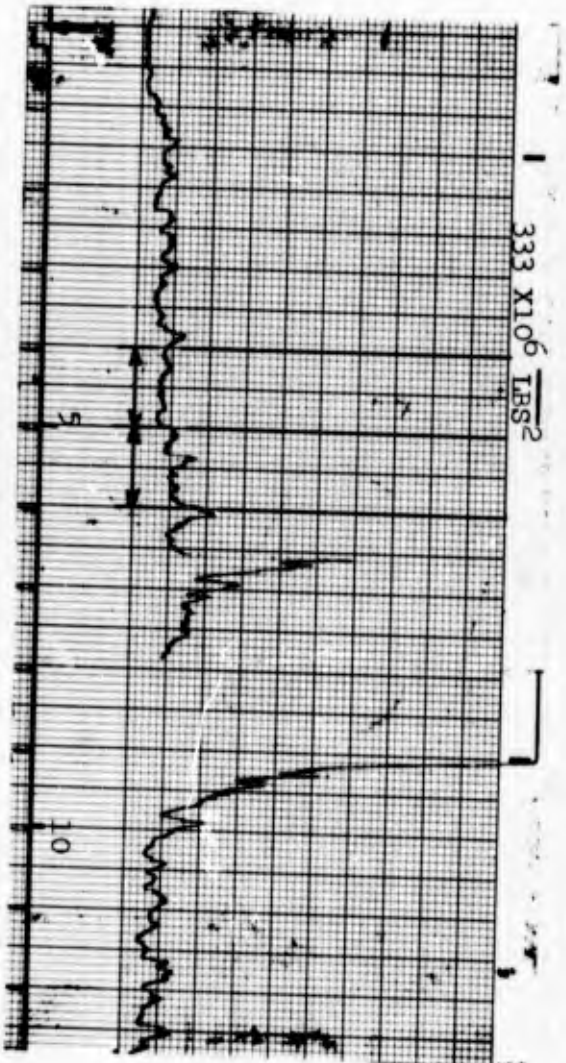


FIGURE 34

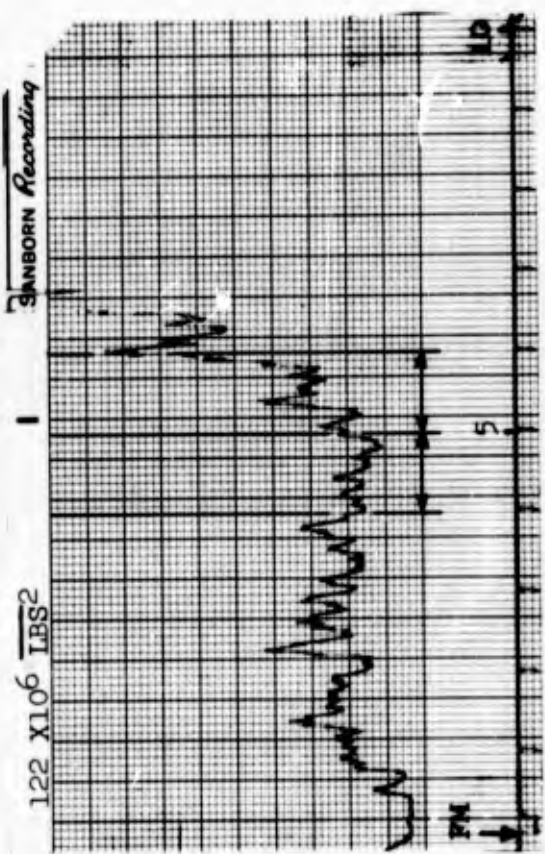
VELOCITY AND LONGITUDINAL ACCELERATION AS A FUNCTION OF TIME FOR SLED RUN 5B-GI



Track No. 7 - - - 70.0 KHz
 Low Pass Filter - - - 2100 Hz Std.
 Measurement No. 1

NOTE: Power spectral analysis
 performed on ruled intervals

FIGURE 35 SANBORN POWER VERSUS TIME (RUN NO. 5B-F1 - PORT)

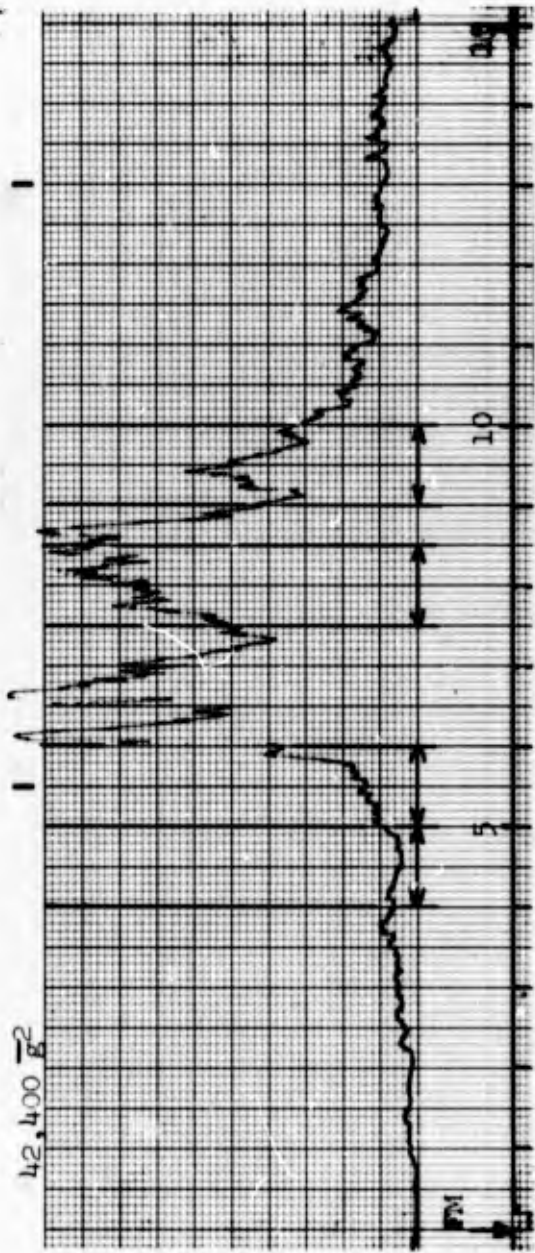


Track No. 9 - - - 70.0 KHz NOTE: Power Spectral analysis performed on ruled intervals

Low Pass Filter - - - 2100 Hz Std.

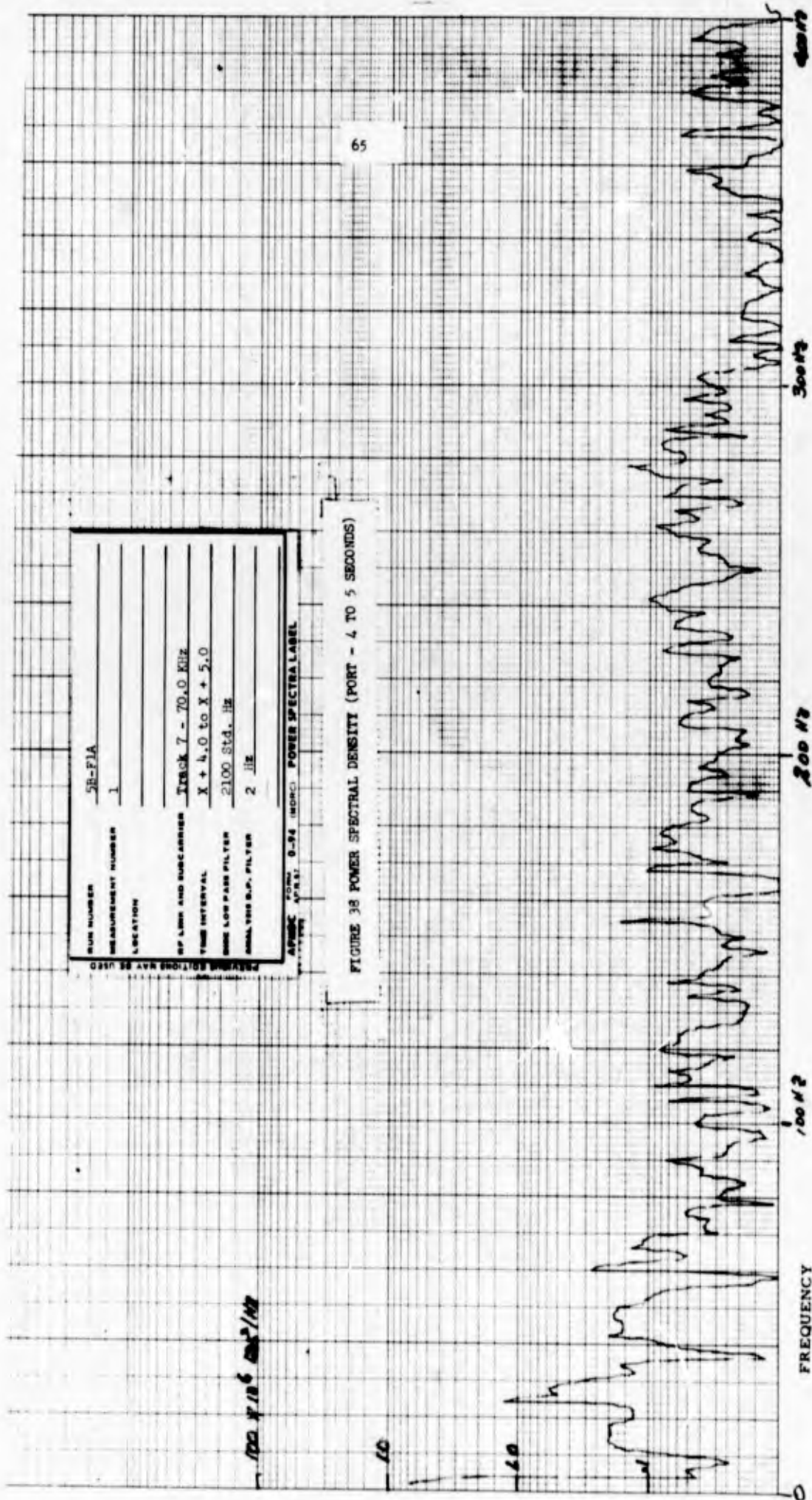
Measurement No. 2

FIGURE 36 SANBORN POWER VERSUS TIME (RUN NO. 5B-F1 - STARBOARD)



Track No. 12 - - - 70.0 KHz NOTE: Power spectral analysis performed on ruled intervals
 Low Pass Filter - - - 2100 Hz Std.
 Measurement No. 3

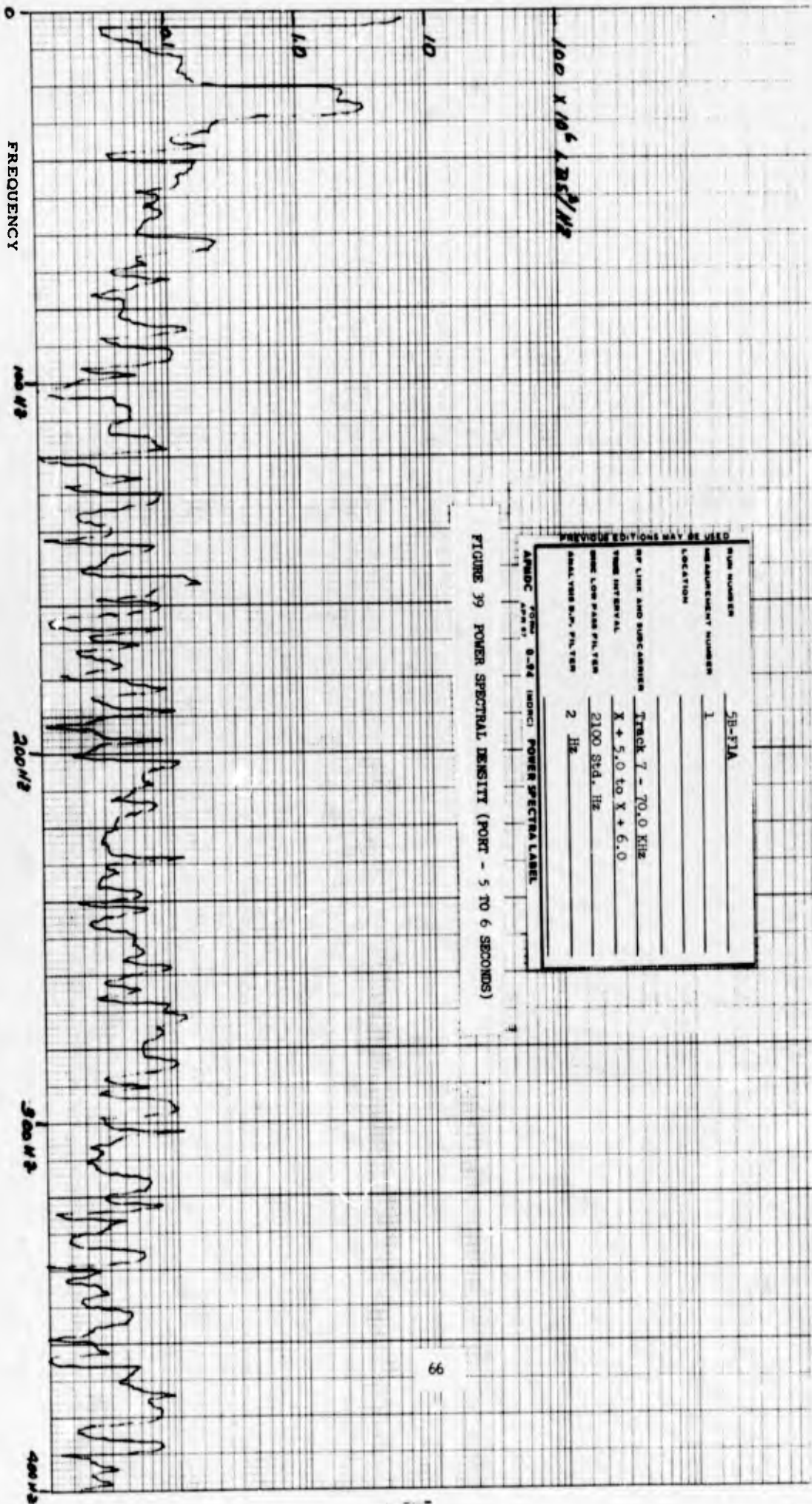
FIGURE 37 SANBORN POWER VERSUS TIME (RUN NO. 5B-F1 - ACCELERATION)



RUN NUMBER SR-F1A
 MEASUREMENT NUMBER 1
 LOCATION _____
 RF LINK AND SUBCARRIER Track 7 - 70.0 KHZ
 TIME INTERVAL X + 4.0 to X + 5.0
 BAND LOW PASS FILTER 2100 Std. Hz
 ANALYSIS BANDWIDTH FILTER 2 Hz

FORM 8-74 (MPC) POWER SPECTRA LABEL
 ARINC APPROVED

FIGURE 38 POWER SPECTRAL DENSITY (PORT - 4 TO 5 SECONDS)



PREVIOUS EDITIONS MAY BE USED

RUN NUMBER	5B-57A
MEASUREMENT NUMBER	1
LOCATION	
RF LINK AND SUBCARRIER	TRACK 7 - 70.0 KHz
VIDEO INTERVAL	X + 5.0 to X + 6.0
VIDEO LOW PASS FILTER	2100 Std. Hz
ANALYSIS BANDWIDTH	2 Hz

FORM 8-54 (REV. 1-54) POWER SPECTRAL LABEL

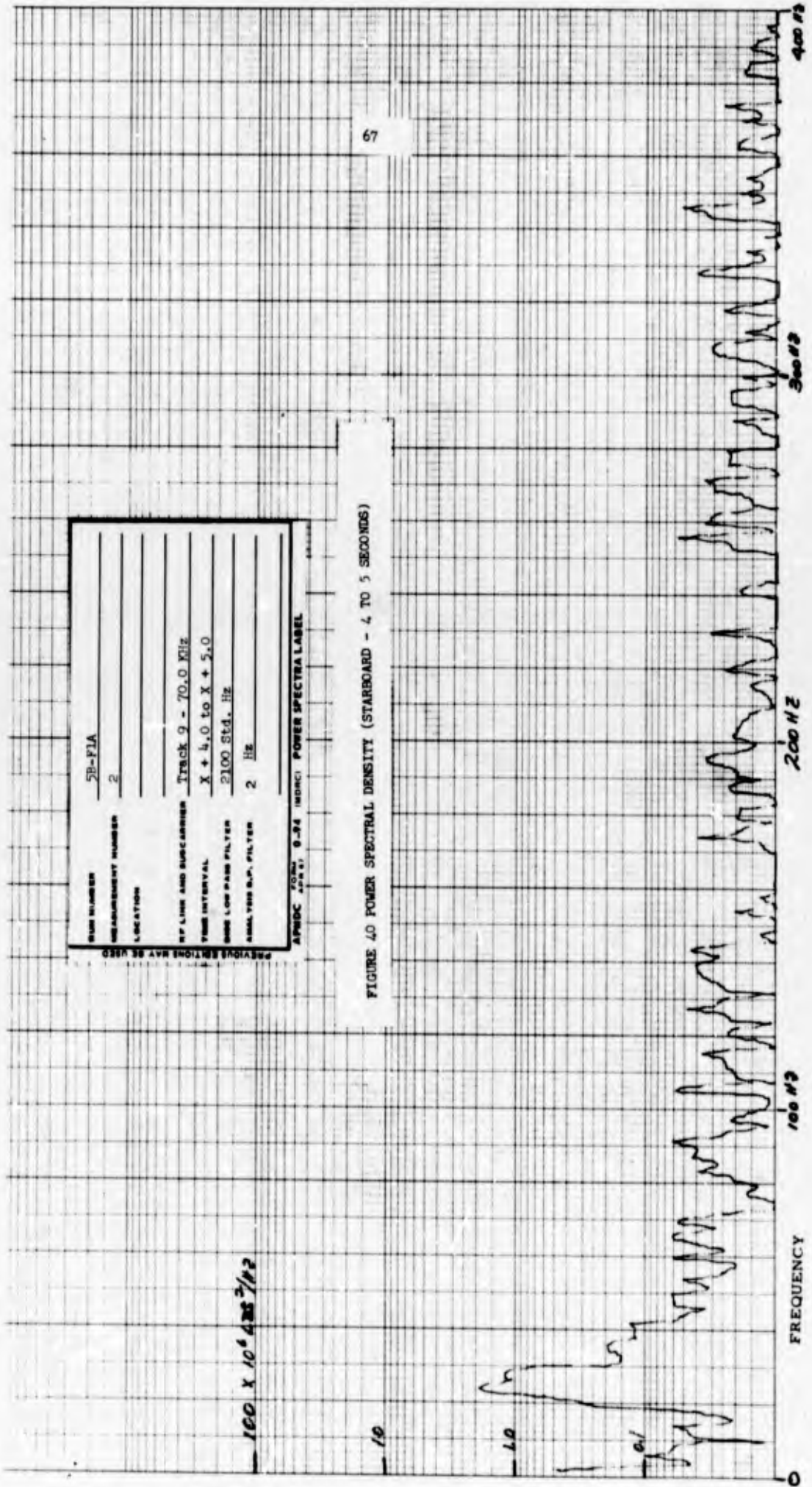
FIGURE 39 POWER SPECTRAL DENSITY (PORT - 5 TO 6 SECONDS)

PREVIOUS EDITIONS MAY BE USED

NAME NUMBER	5B-FIA
MEASUREMENT NUMBER	2
LOCATION	
RF LINK AND SUBCARRIER	Track 9 - 70.0 KHz
TIME INTERVAL	X + 4.0 to X + 5.0
BAND LOW PASS FILTER	2100 Std. Hz
SIGNAL RES. FILTER	2 Hz

APWDC FORM 8-74 (MORC) POWER SPECTRAL LABEL

FIGURE 40 POWER SPECTRAL DENSITY (STARBOARD - 4 TO 5 SECONDS)



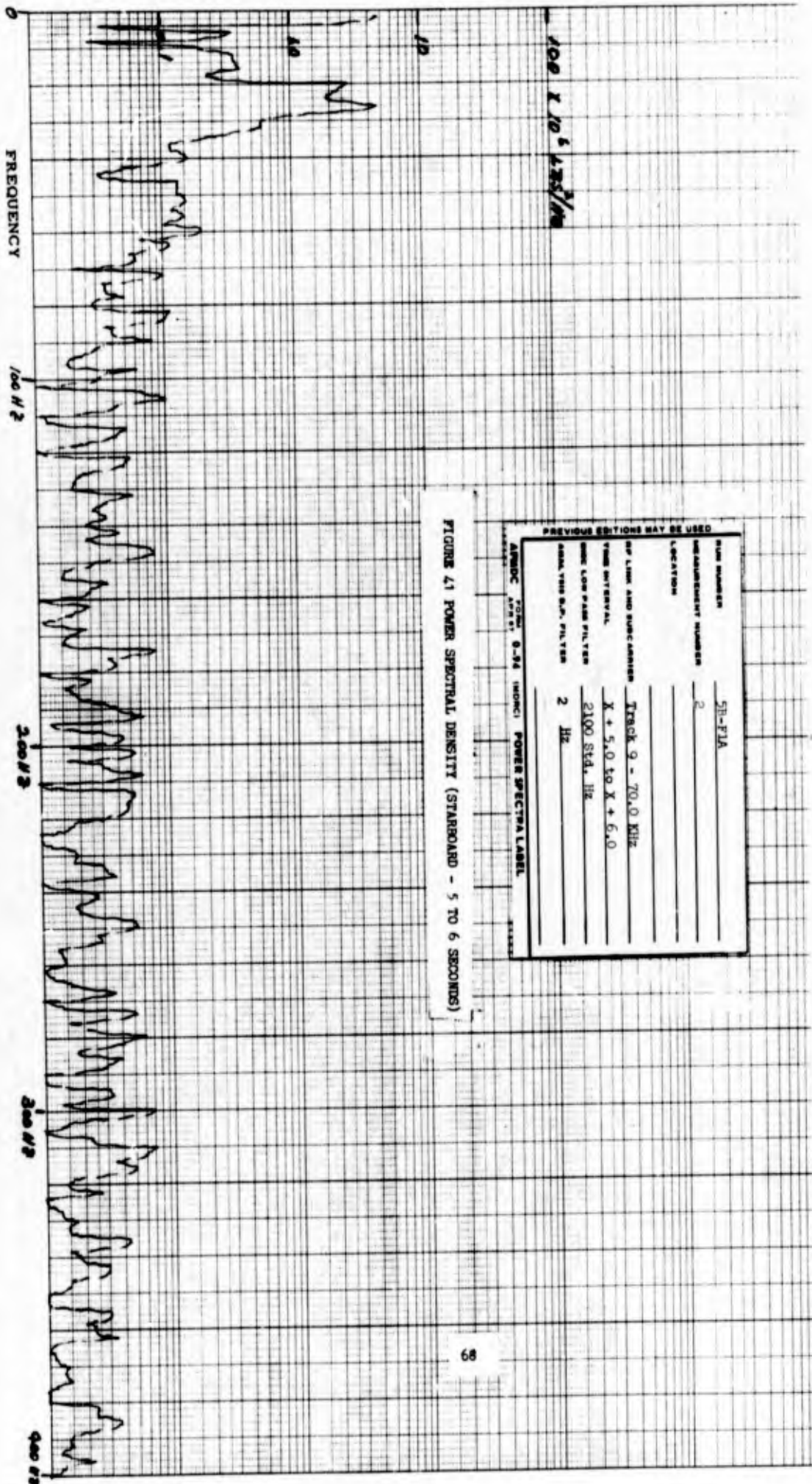
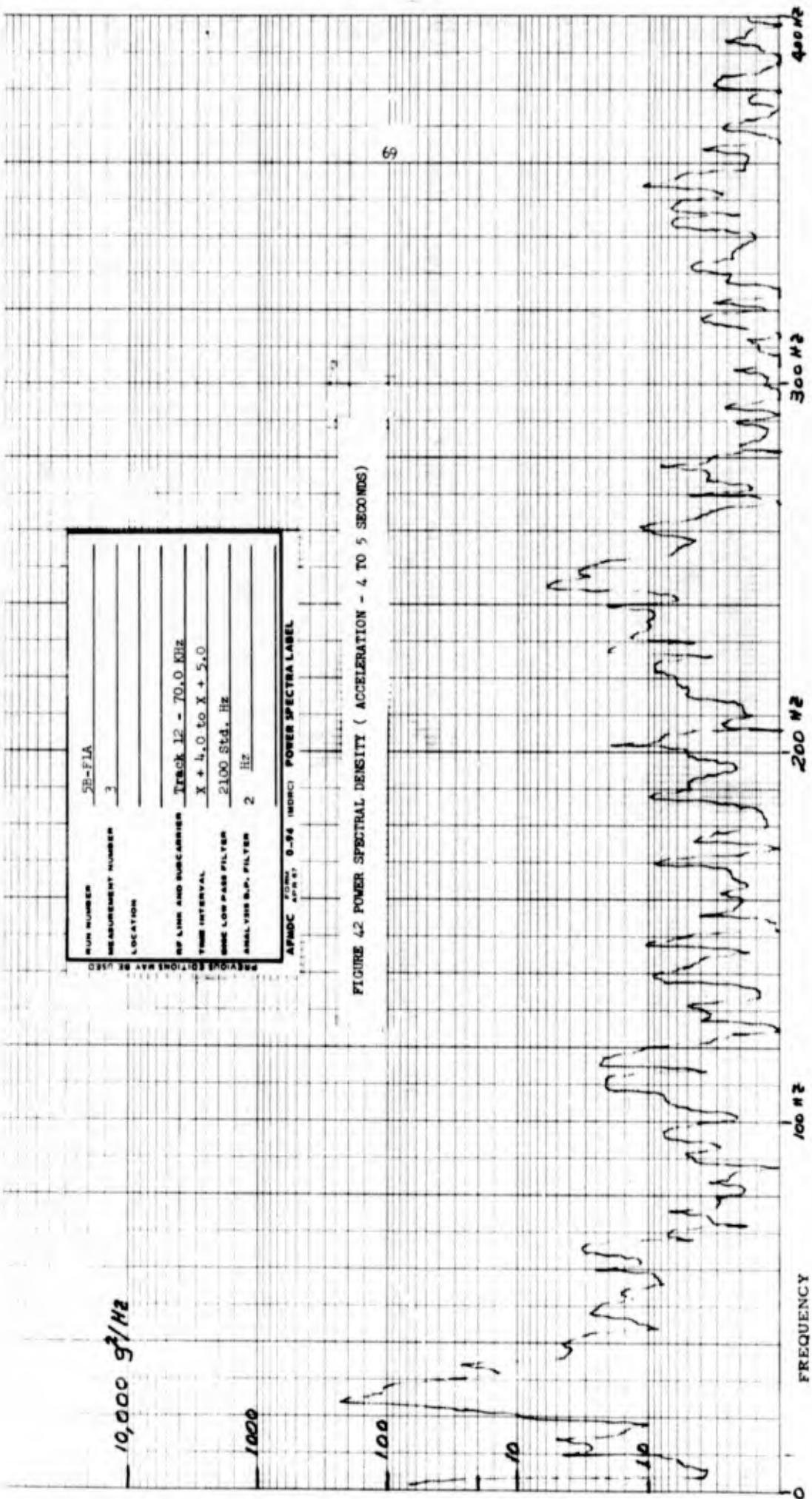


FIGURE 41 POWER SPECTRAL DENSITY (STARBOARD - 5 TO 6 SECONDS)

PREVIOUS EDITIONS MAY BE USED

RUN NUMBER	SR-FLA
MEASUREMENT NUMBER	2
LOCATION	
OP. LINE AND SUBCARRIER	Track 9 - 70.0 KHz
VIDEO INTERVAL	X + 5.0 to X + 6.0
VIDEO LOW PASS FILTER	2100 Std. Hz
VIDEO BANDWIDTH FILTER	2 Hz

FORM 8-54 (INDIC) POWER SPECTRAL LABEL



PREVIOUS EDITIONS MAY BE USED

RUN NUMBER	5E-FLA
MEASUREMENT NUMBER	3
LOCATION	
REF LINE AND SUBCARRIER	TRACK 12 - 70.0 KHZ
TIME INTERVAL	X + 4.0 to X + 5.0
BIAS LOW PASS FILTER	2100 STD. HZ
ANALYSIS B.P. FILTER	2 Hz

AFMDC FORM 8-74 (MORC) POWER SPECTRA LABEL

FIGURE 42 POWER SPECTRAL DENSITY (ACCELERATION - 4 TO 5 SECONDS)

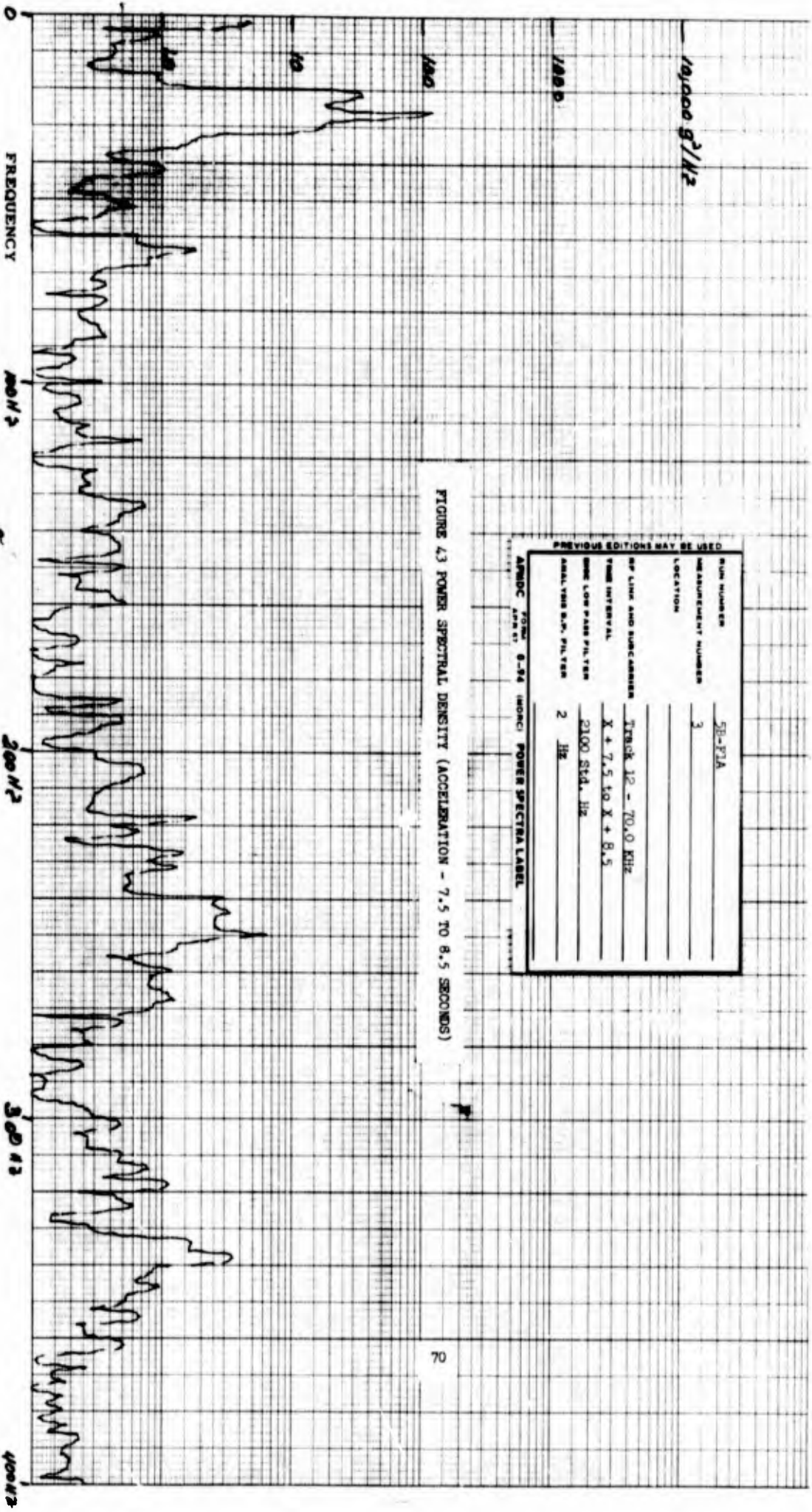


FIGURE 43 POWER SPECTRAL DENSITY (ACCELERATION - 7.5 TO 8.5 SECONDS)

PREVIOUS EDITIONS MAY BE USED

RUN NUMBER	58-P1A
MEASUREMENT NUMBER	3
LOCATION	
RF LINK AND SUBCARRIER	Track 12 - 70.0 KHz
TIME INTERVAL	X + 7.5 to X + 8.5
LOW PASS FILTER	2100 Std. Hz
ANALYSIS B.W. FILTER	2 Hz

FORM 8-54 (MORI) POWER SPECTRAL LABEL
 AMSDC APR 61



RUN NUMBER 5B-F1
 MEASUREMENT NUMBER 3
 LOCATION Accelerometer #1
 WP LINK AND SUBCARRIER Track 12 - 70.0 KHz
 TIME INTERVAL X + 4.0 to X + 5.0
 DISC LOW PASS FILTER 2100 Std. Hz
 ANALYSIS B.P. FILTER 10 Hz
 SCALE FACTOR 1:1

AFMDC 4074 8-5M (MORC) POWER SPECTRA LABEL

FIGURE 44 POWER SPECTRAL DENSITY (ACCELERATION - 4 TO 5 SECONDS)

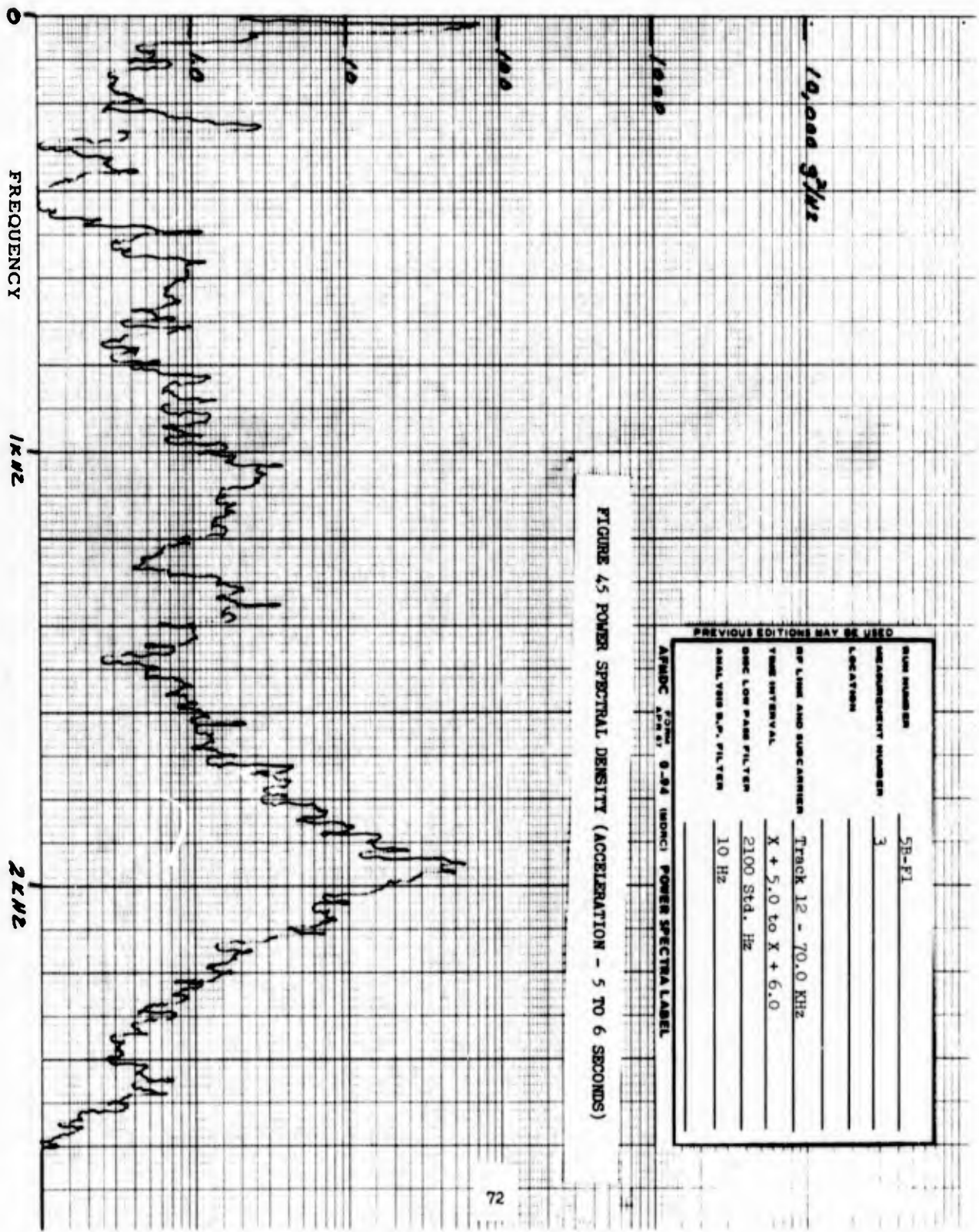
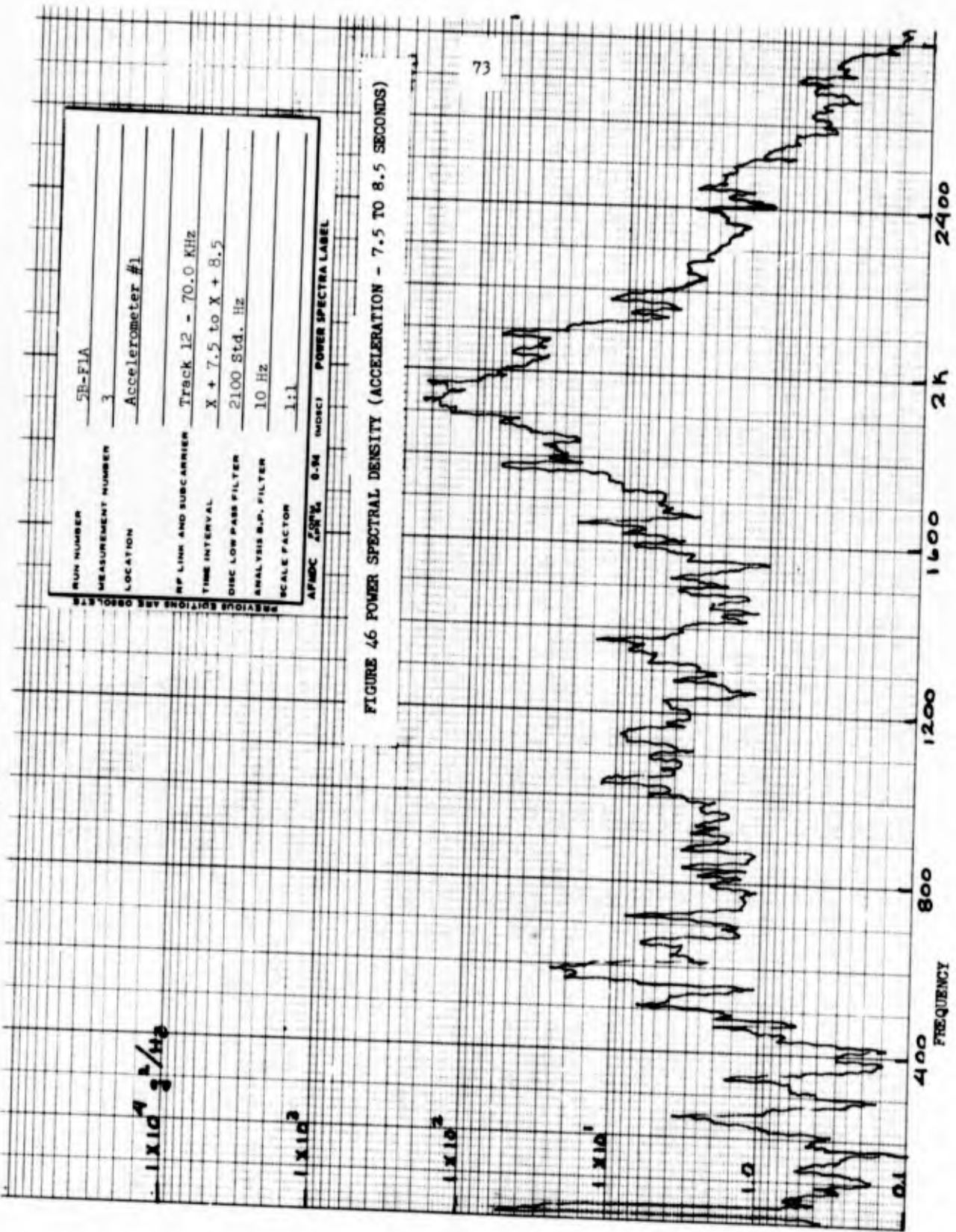


FIGURE 45 POWER SPECTRAL DENSITY (ACCELERATION - 5 TO 6 SECONDS)

PREVIOUS EDITIONS MAY BE USED

RUN NUMBER	5B-F1
MEASUREMENT NUMBER	3
LOCATION	
RF LINK AND SUBCARRIER	Track 12 - 70.0 KHz
TIME INTERVAL	X + 5.0 to X + 6.0
OSC LOW PASS FILTER	2100 Std. Hz
ANALYSIS B.P. FILTER	10 Hz

AFMDC FORM 8-64 (INDIC) POWER SPECTRA LABEL



PREVIOUS EDITIONS ARE OBSOLETE

RUN NUMBER	5R-F1A
MEASUREMENT NUMBER	3
LOCATION	Accelerometer #1
RF LINK AND SUBCARRIER	Track 12 - 70.0 KHz
TIME INTERVAL	X + 7.5 to X + 8.5
DISC LOW PASS FILTER	2100 Std. Hz
ANALYSIS B.P. FILTER	10 Hz
SCALE FACTOR	1:1

AFMDC FORM 8-54 (MORC) POWER SPECTRA LABEL

FIGURE 46 POWER SPECTRAL DENSITY (ACCELERATION - 7.5 TO 8.5 SECONDS)

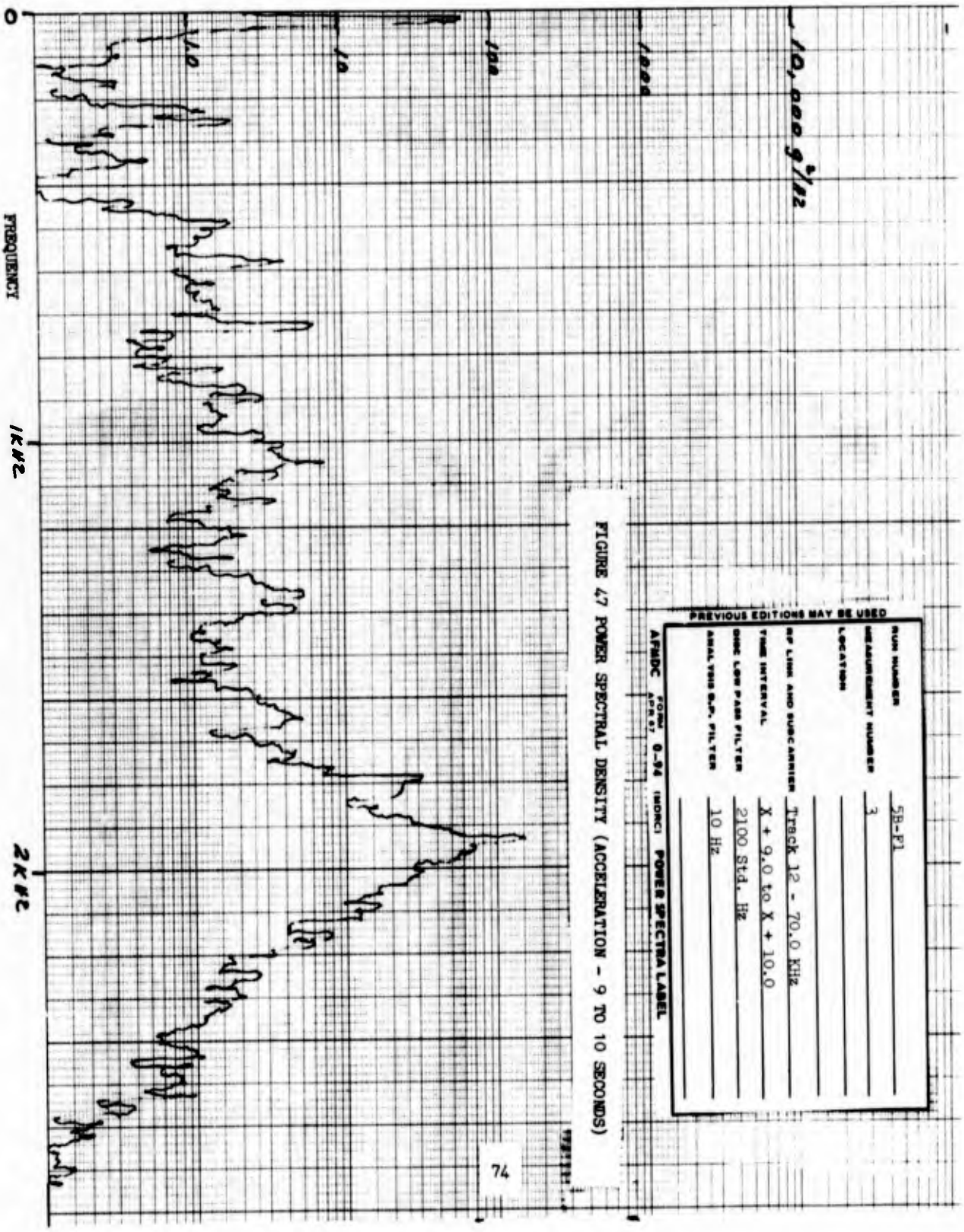
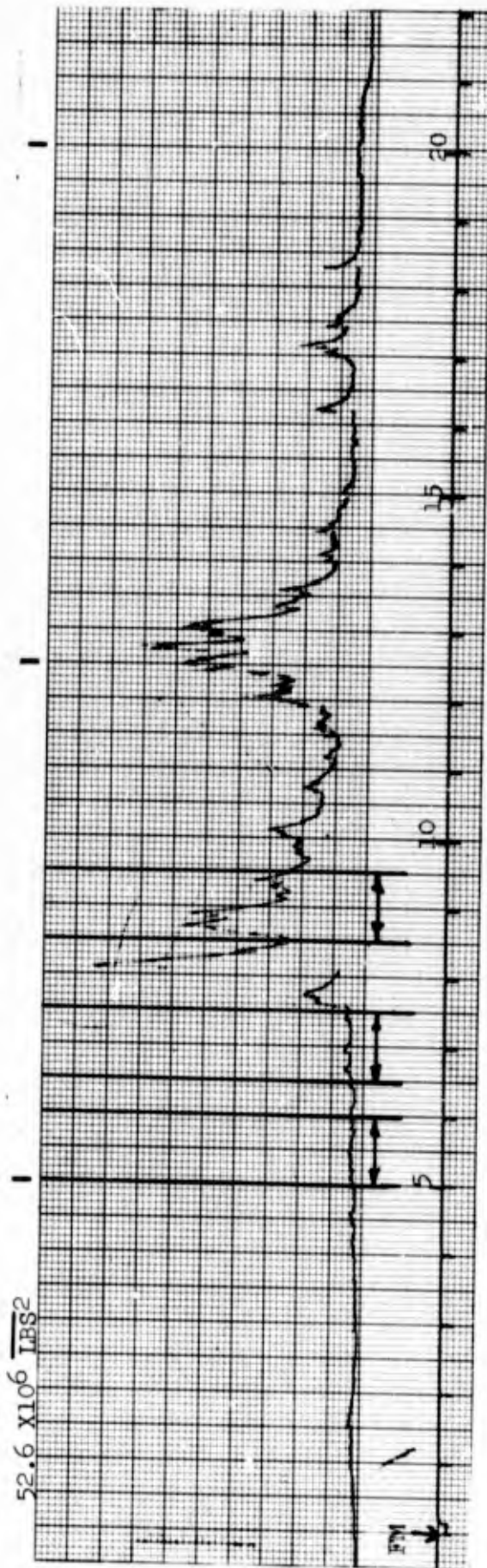


FIGURE 47 POWER SPECTRAL DENSITY (ACCELERATION - 9 TO 10 SECONDS)

PREVIOUS EDITIONS MAY BE USED

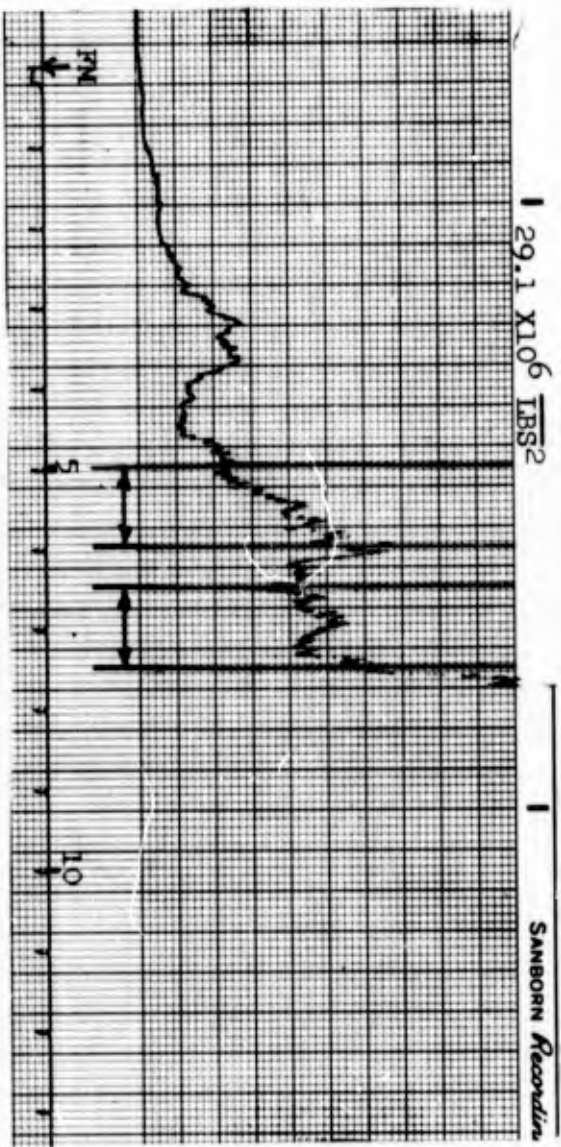
RUN NUMBER	5B-F1
MEASUREMENT NUMBER	3
LOCATION	
RF LINK AND SUBCARRIER	TRACK 12 - 70.0 KHZ
TIME INTERVAL	X + 9.0 TO X + 10.0
ONE LOW PASS FILTER	2100 Std. Hz
ANALYSIS B.P. FILTER	10 Hz

FORM 8-64 (MIL-STD-177) POWER SPECTRA LABEL
AFMDC APR 67



Track No. 7 - - - 70.0 KHz NOTE: Power spectral analysis performed on ruled intervals
 Low Pass Filter - - - 2100 Hz Std.
 Measurement No. 1

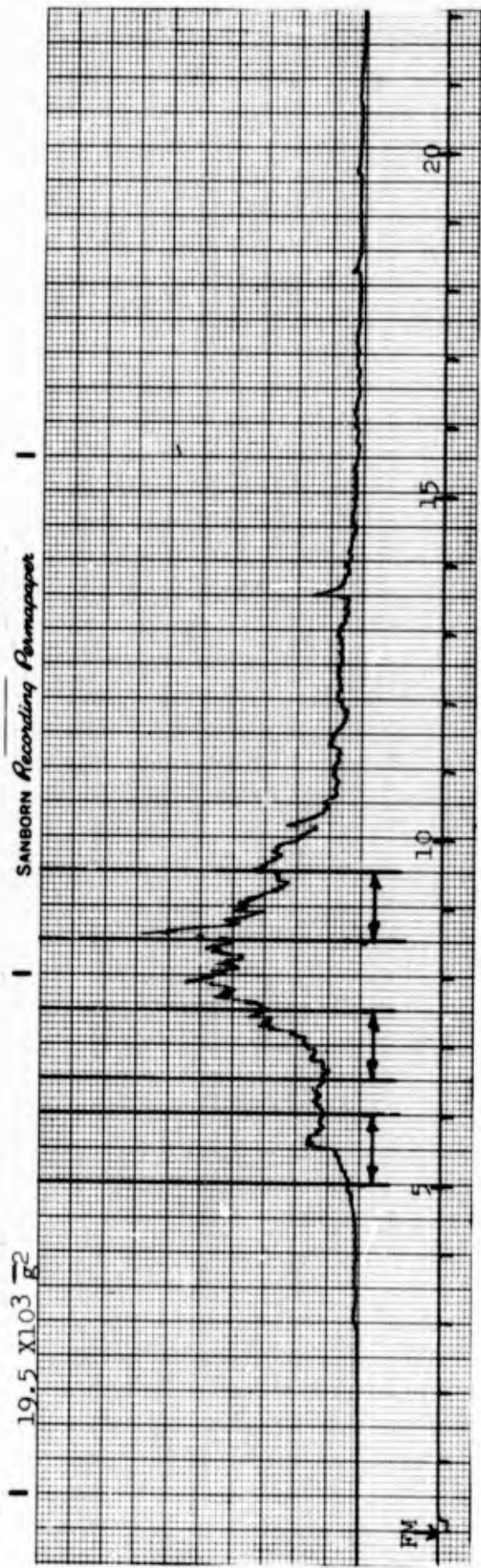
FIGURE 48 SANBORN POWER VERSUS TIME (RUN NO. 5B-G1 - PORT)



Track No. 9 - - - - 70.0 KHz
 Low Pass Filter - - - - 2100 Hz Std.
 Measurement No. 2

NOTE: Power spectral analysis
 performed on ruled intervals

FIGURE 49 SANBORN POWER VERSUS TIME (RUN NO. 5B-G1 - STARBOARD)



Track No. 12 - - - 70.0 KHz
 Low Pass Filter - - - 2100 Hz Std.
 Measurement No. 3

NOTE: Power spectral analysis performed on ruled intervals

FIGURE 50 SANBORN POWER VERSUS TIME (RUN NO. 5B-G1 - ACCELERATION)

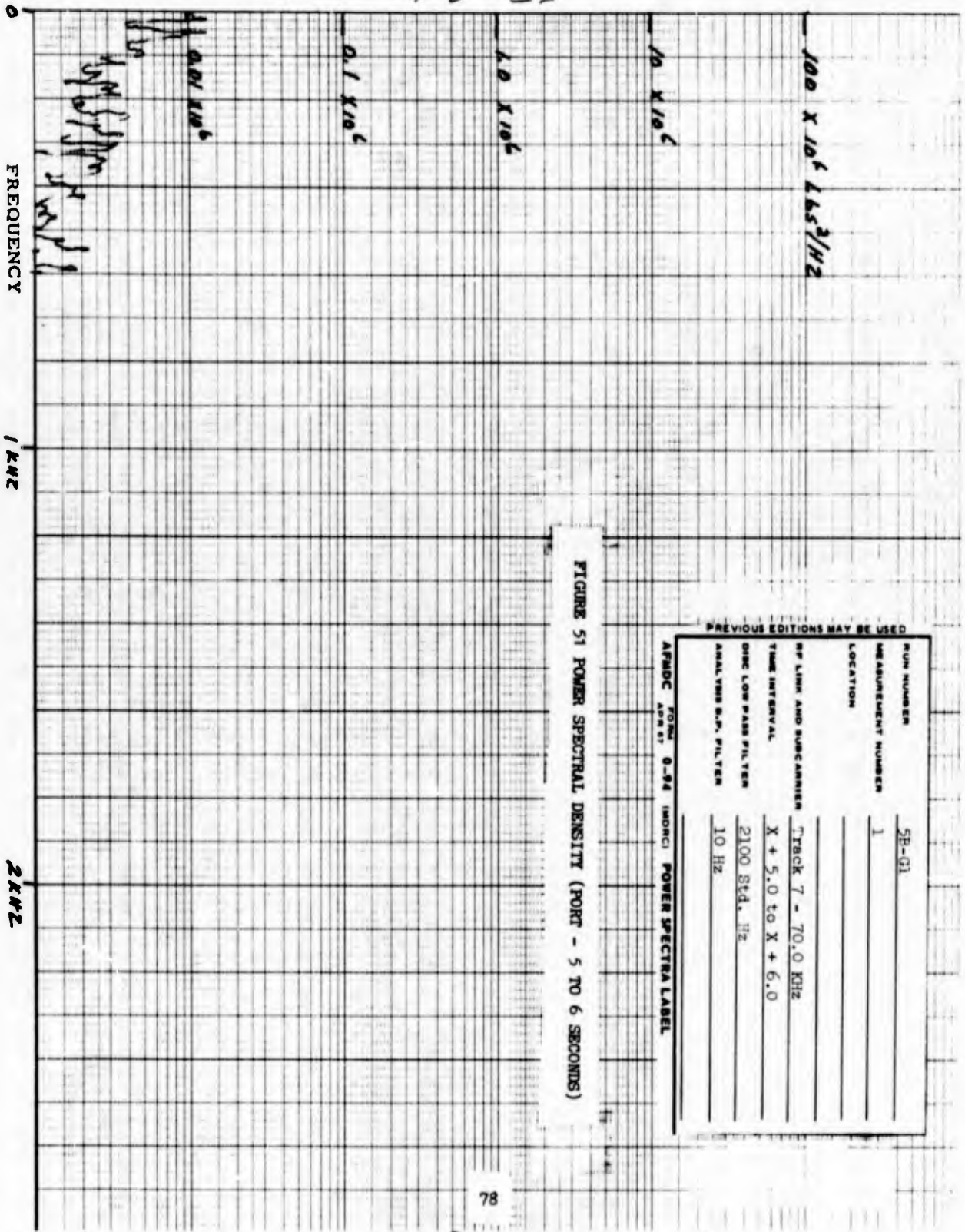


FIGURE 51 POWER SPECTRAL DENSITY (PORT - 5 TO 6 SECONDS)

PREVIOUS EDITIONS MAY BE USED

RUN NUMBER	5E-01
MEASUREMENT NUMBER	1
LOCATION	
RF LINK AND SUBCARRIER	TRACK 7 - 70.0 KHZ
TIME INTERVAL	X + 5.0 to X + 6.0
ORIG LOW PASS FILTER	2100 STD. HZ
ANALYSIS B.P. FILTER	10 HZ

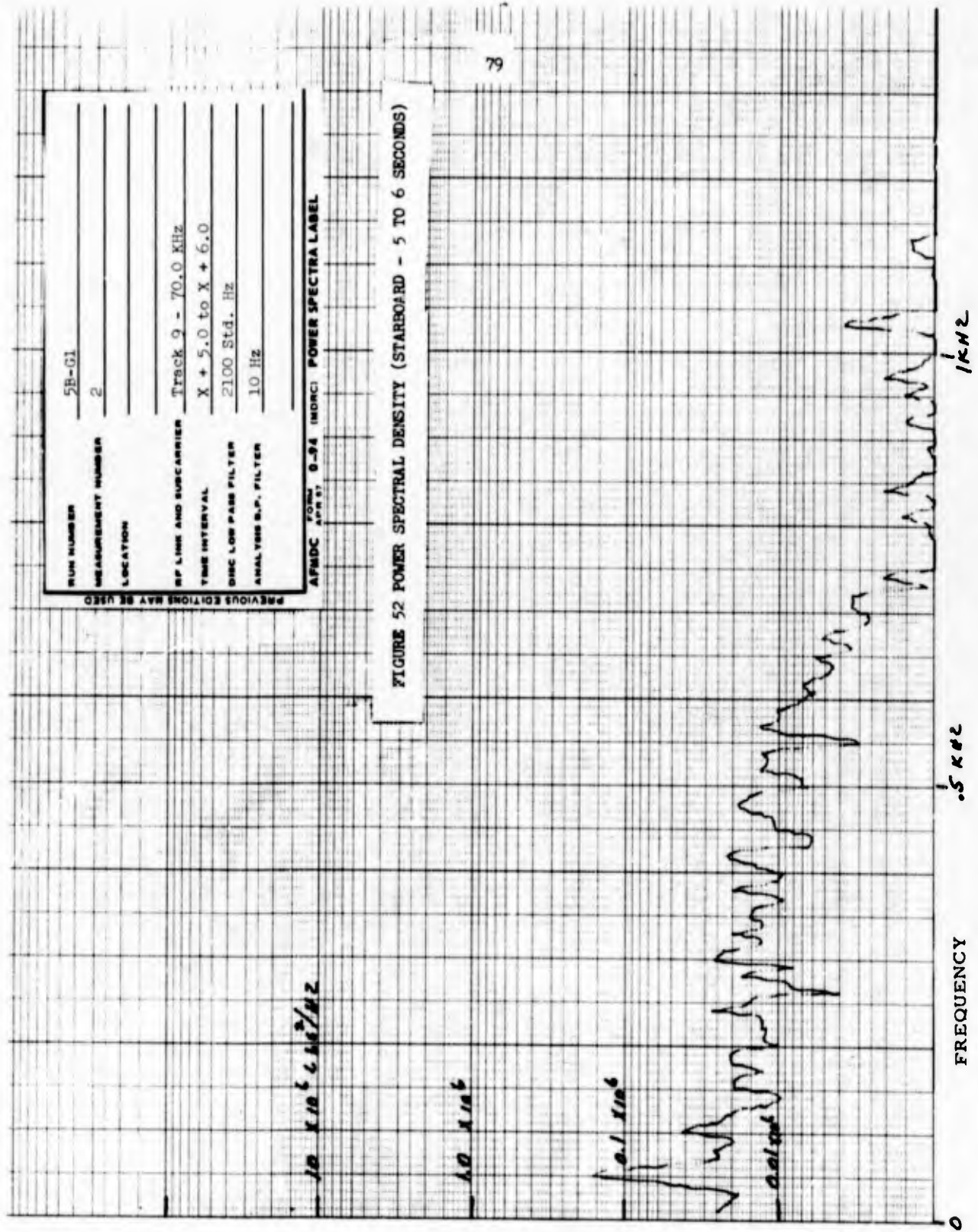
AFMDC FORM 0-94 (MORC) POWER SPECTRA LABEL
APR 67

PREVIOUS EDITIONS MAY BE USED

RUN NUMBER	5B-01
MEASUREMENT NUMBER	2
LOCATION	
RF LINK AND SUBCARRIER	Track 9 - 70.0 KHz
TIME INTERVAL	X + 5.0 to X + 6.0
DISC LOW PASS FILTER	2100 Std. Hz
ANALYSIS B.P. FILTER	10 Hz

FORM 8-94 (MORC) POWER SPECTRA LABEL

FIGURE 52 POWER SPECTRAL DENSITY (STARBOARD - 5 TO 6 SECONDS)

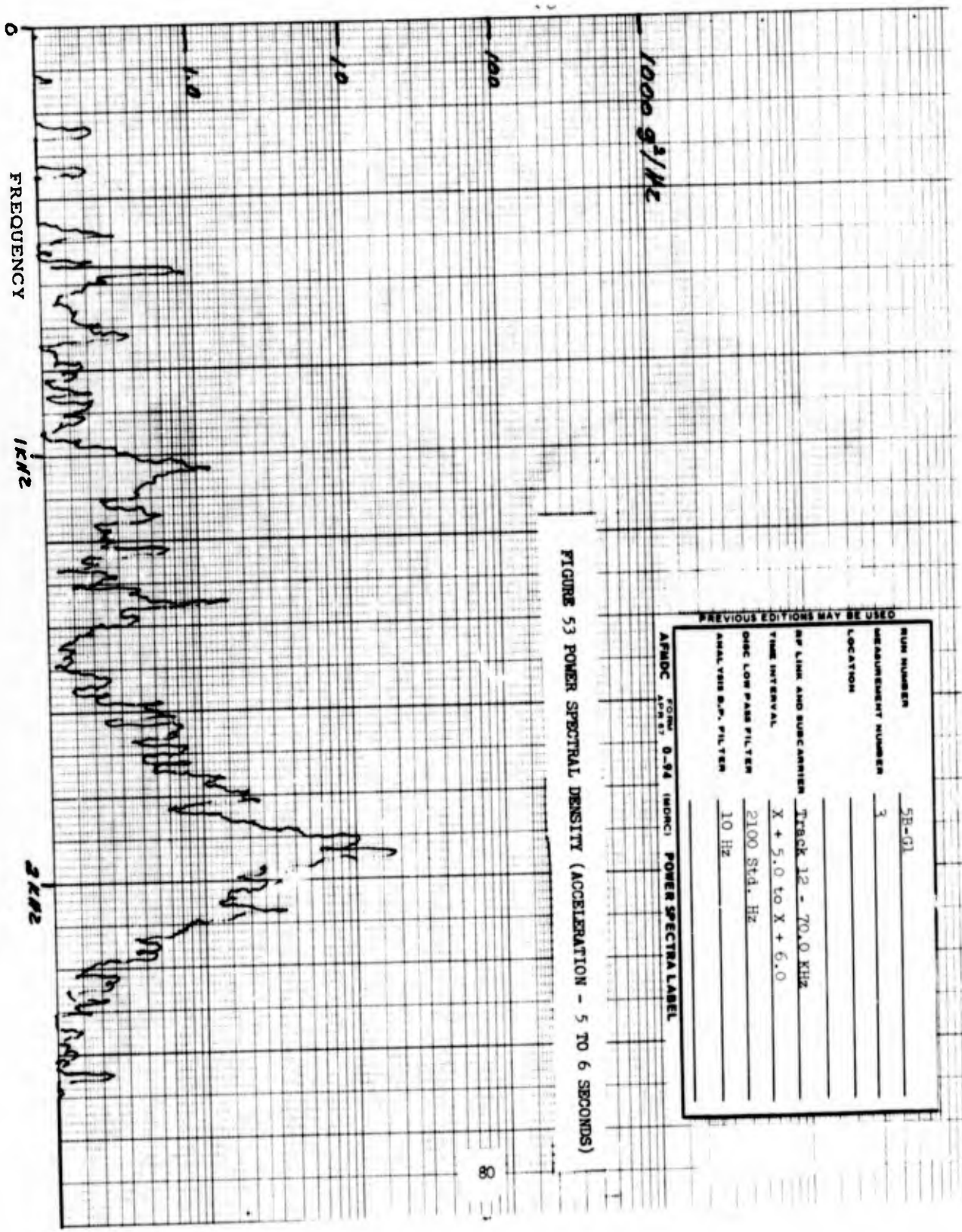


PREVIOUS EDITIONS MAY BE USED

RUN NUMBER	5E-01
MEASUREMENT NUMBER	3
LOCATION	
RF LINK AND SUBCARRIER	TRACK 12 - 70.0 KHZ
TIME INTERVAL	X + 5.0 to X + 6.0
OSC LOW PASS FILTER	2100 Std. Hz
ANALYSIS B.P. FILTER	10 Hz

AFMDC FORM 8-64 (MORI) POWER SPECTRAL LABEL

FIGURE 53 POWER SPECTRAL DENSITY (ACCELERATION - 5 TO 6 SECONDS)



PREVIOUS EDITIONS ARE OBSOLETE

RUN NUMBER	5B-01B
MEASUREMENT NUMBER	3
LOCATION	
RF LINK AND SUBCARRIER	Track 12 - 70.0 KHz
TIME INTERVAL	X + 6.5 to X + 7.5
DISC LOW PASS FILTER	2100 Std. Hz
ANALYSIS R.P. FILTER	10 Hz

AFMDC FORM 8-54 (MORC) POWER SPECTRA LABEL

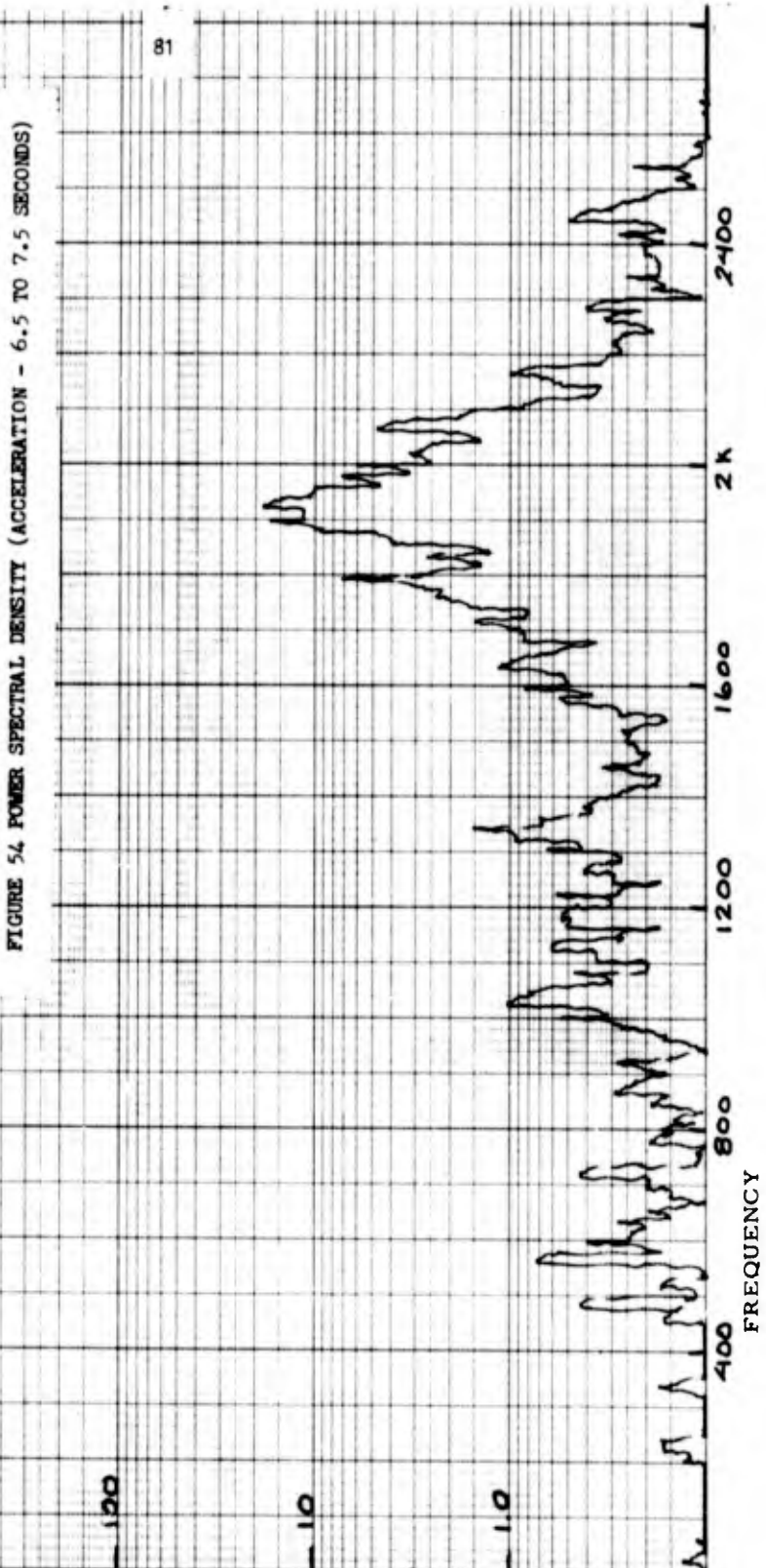
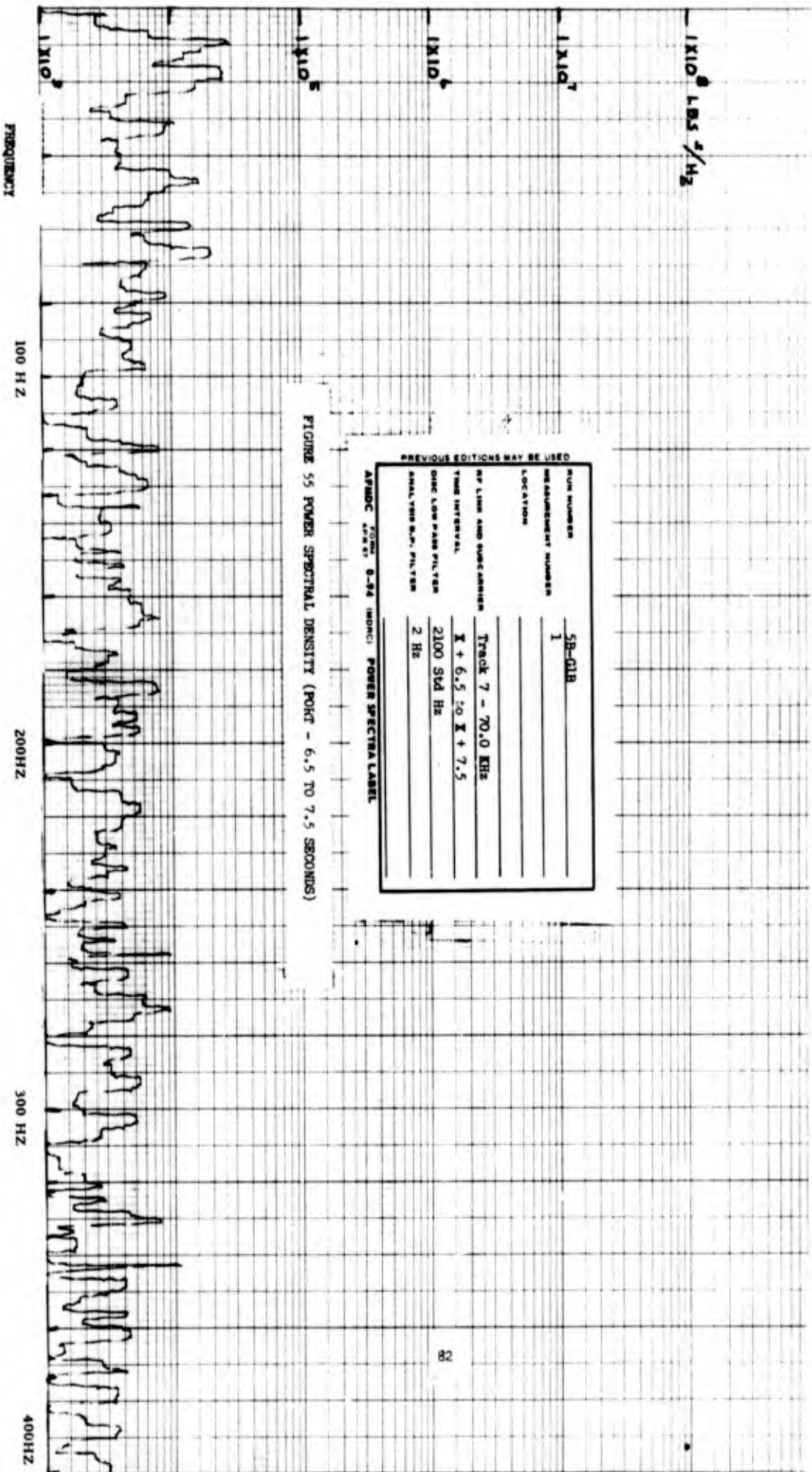


FIGURE 54 POWER SPECTRAL DENSITY (ACCELERATION - 6.5 TO 7.5 SECONDS)



PREVIOUS EDITIONS MAY BE USED

RUN NUMBER	5B-01B
MEASUREMENT NUMBER	1
LOCATION	
RF LINK AND SUBCARRIER	Track 7 - 70.0 KHz
TIME INTERVAL	$\bar{x} + 6.5$ to $\bar{x} + 7.5$
OSC LOW PASS FILTER	2100 Std Hz
ANALYSIS B.P. FILTER	2 Hz

AFMDC FORM 8-84 (INDIC) POWER SPECTRAL LABEL

FIGURE 55 POWER SPECTRAL DENSITY (POKT - 6.5 TO 7.5 SECONDS)

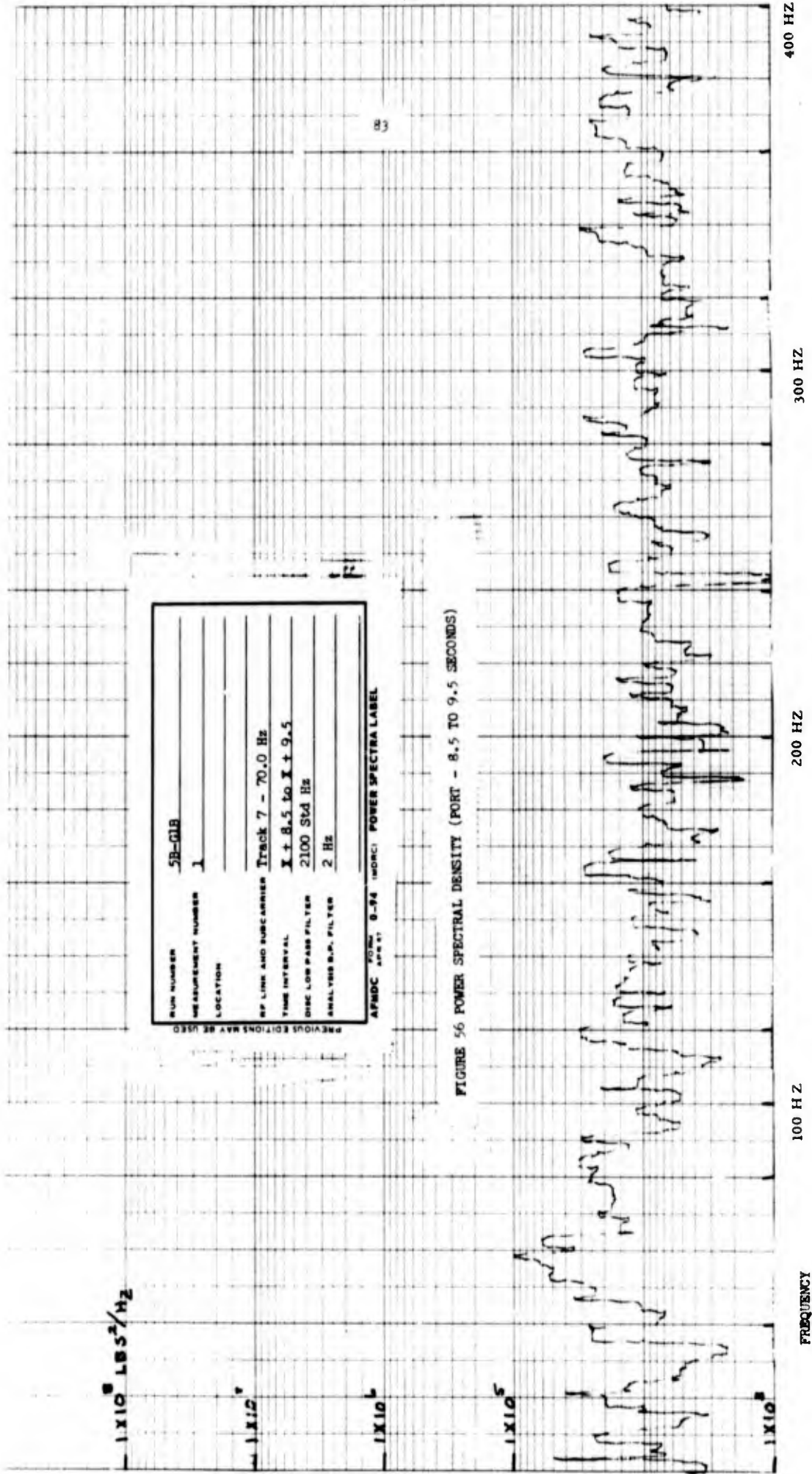


FIGURE 56 POWER SPECTRAL DENSITY (PORT - 8.5 TO 9.5 SECONDS)

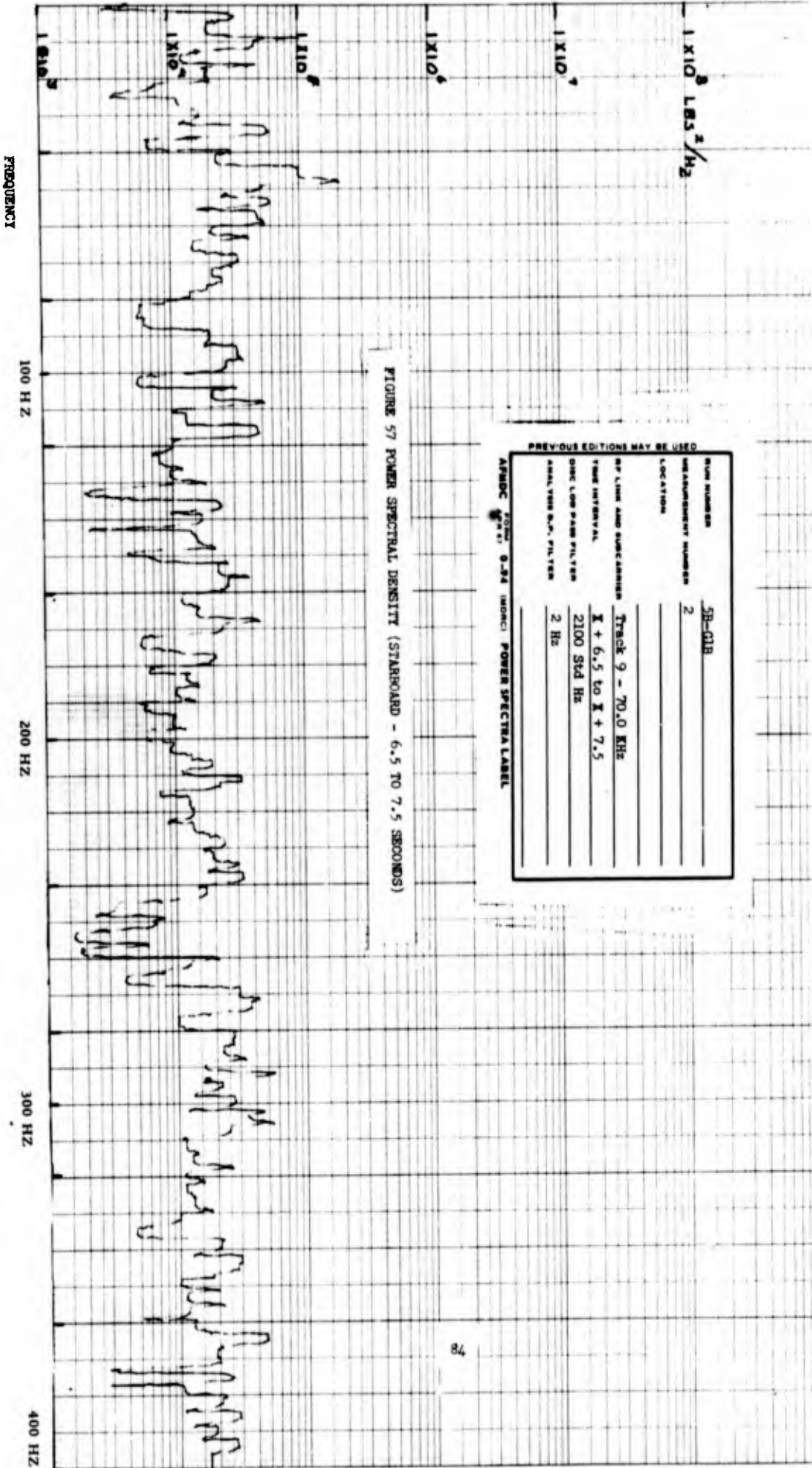


FIGURE 57 POWER SPECTRAL DENSITY (STARBOARD - 6.5 TO 7.5 SECONDS)

PREVIOUS EDITIONS MAY BE USED

RUN NUMBER	5B-01B
MEASUREMENT NUMBER	2
LOCATION	
RF LINK AND SUBCARRIER	TRACK 9 - 70.0 KHz
TIME INTERVAL	± 6.5 to ± 7.5
OSC. LOW PASS FILTER	2100 SFD Hz
ANALYSIS B.W. FILTER	2 Hz

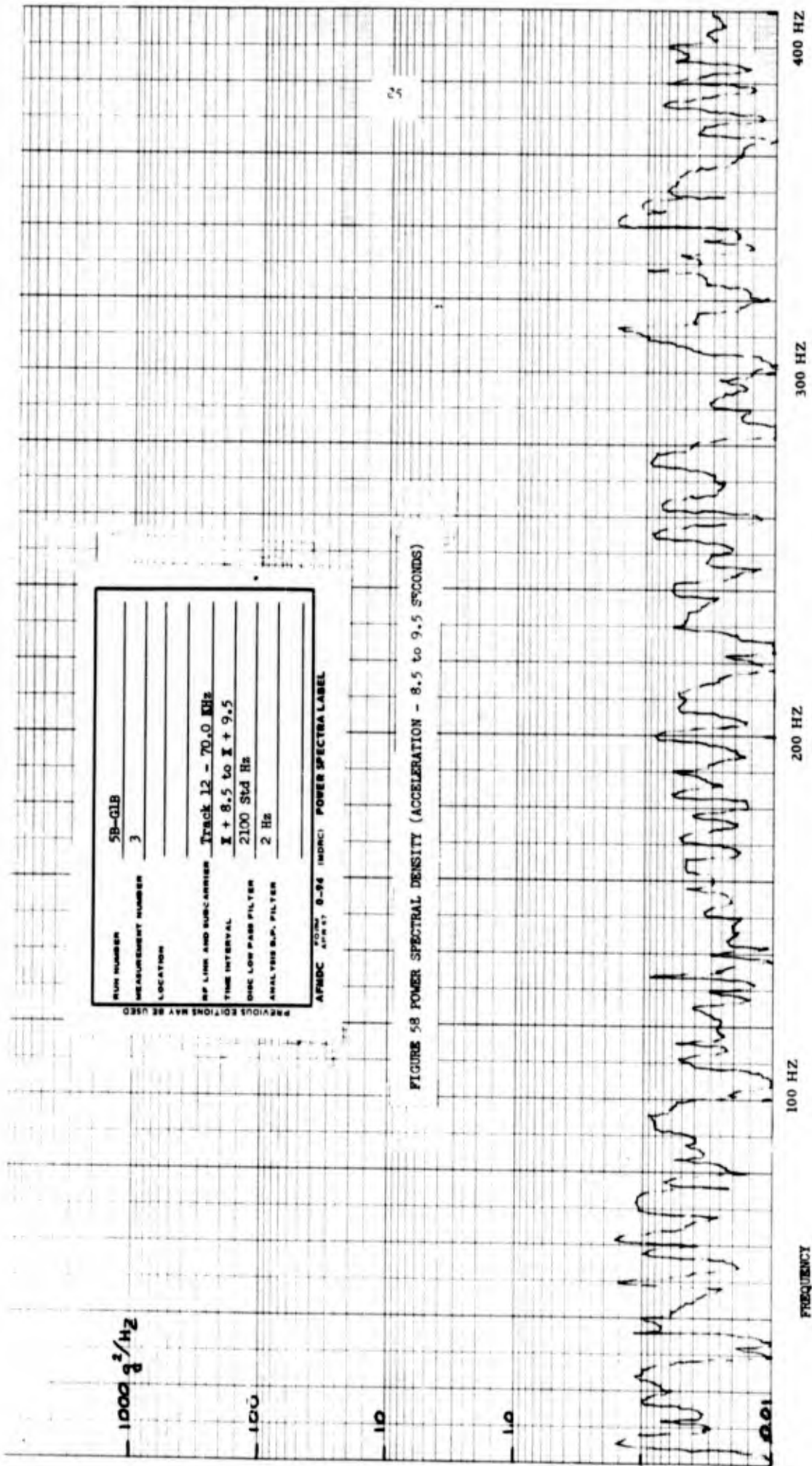
FORM 3000 9-54 (MIL-STD-177) POWER SPECTRAL LABEL

PREVIOUS EDITIONS MAY BE USED

RUN NUMBER	5B-01B
MEASUREMENT NUMBER	3
LOCATION	
RF LINK AND SUBCARRIER	Track 12 - 70.0 MHz
TIME INTERVAL	X + 8.5 to X + 9.5
OSC LOW PASS FILTER	2100 Std Hz
ANALYSIS B.P. FILTER	2 Hz

AFMDC FORM 8-74 (MORC) POWER SPECTRA LABEL

FIGURE 5B POWER SPECTRAL DENSITY (ACCELERATION - 8.5 to 9.5 SECONDS)



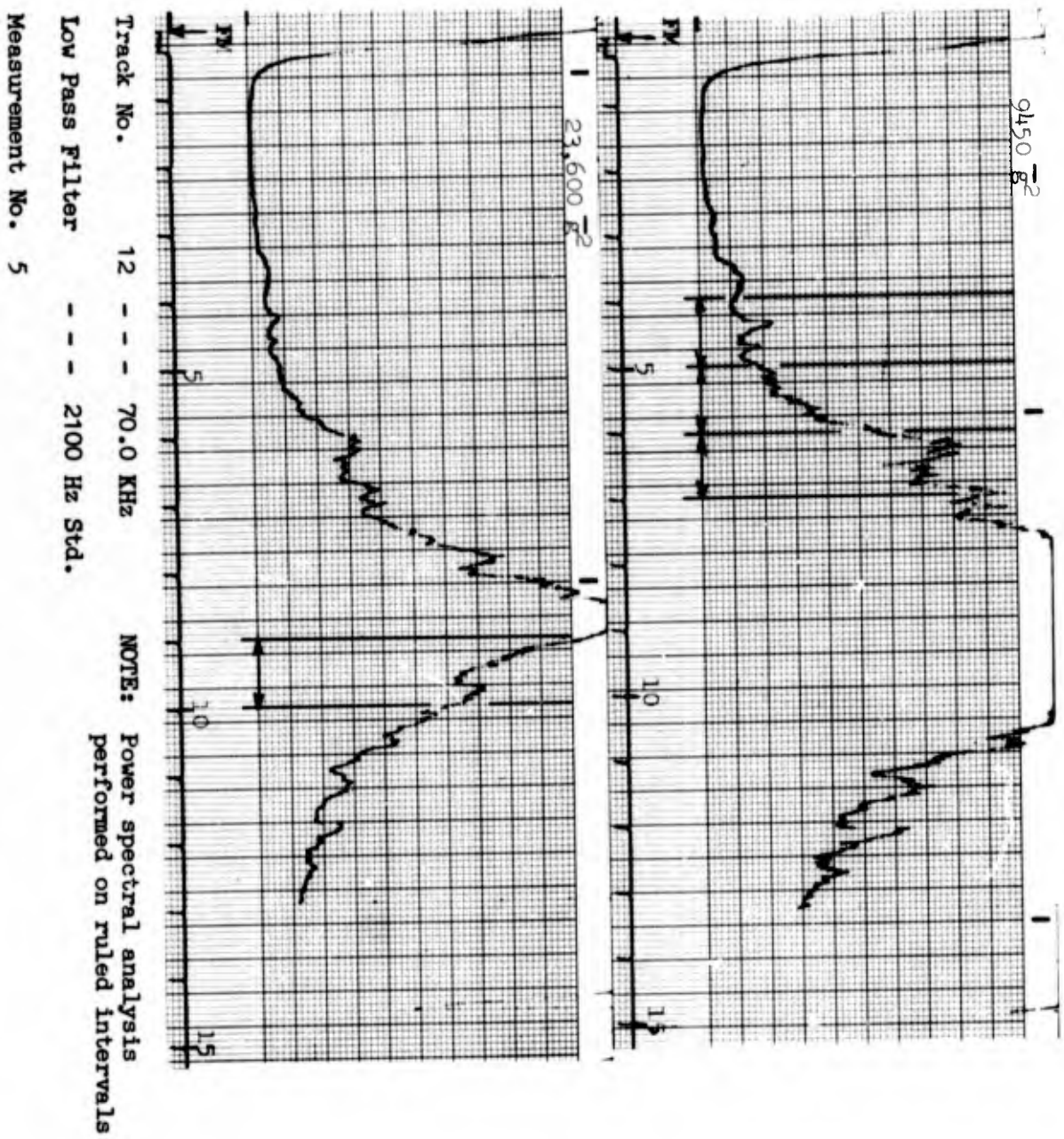


FIGURE 59 SANBORN POWER VERSUS TIME (RUN NO. 6B-A1 - ACCELERATION)

RUN NUMBER 6B-A1
 MEASUREMENT NUMBER 5
 LOCATION _____
 RF LINK AND SUBCARRIER Track 12 - 70.0 KHz
 TIME INTERVAL X + 4.0 to X + 5.0
 DISC LOW PASS FILTER 2100 Std. Hz
 ANALYSIS B.P. FILTER 10 Hz

AFMDC FORM 0-94 (MORC) POWER SPECTRA LABEL
 APR 67

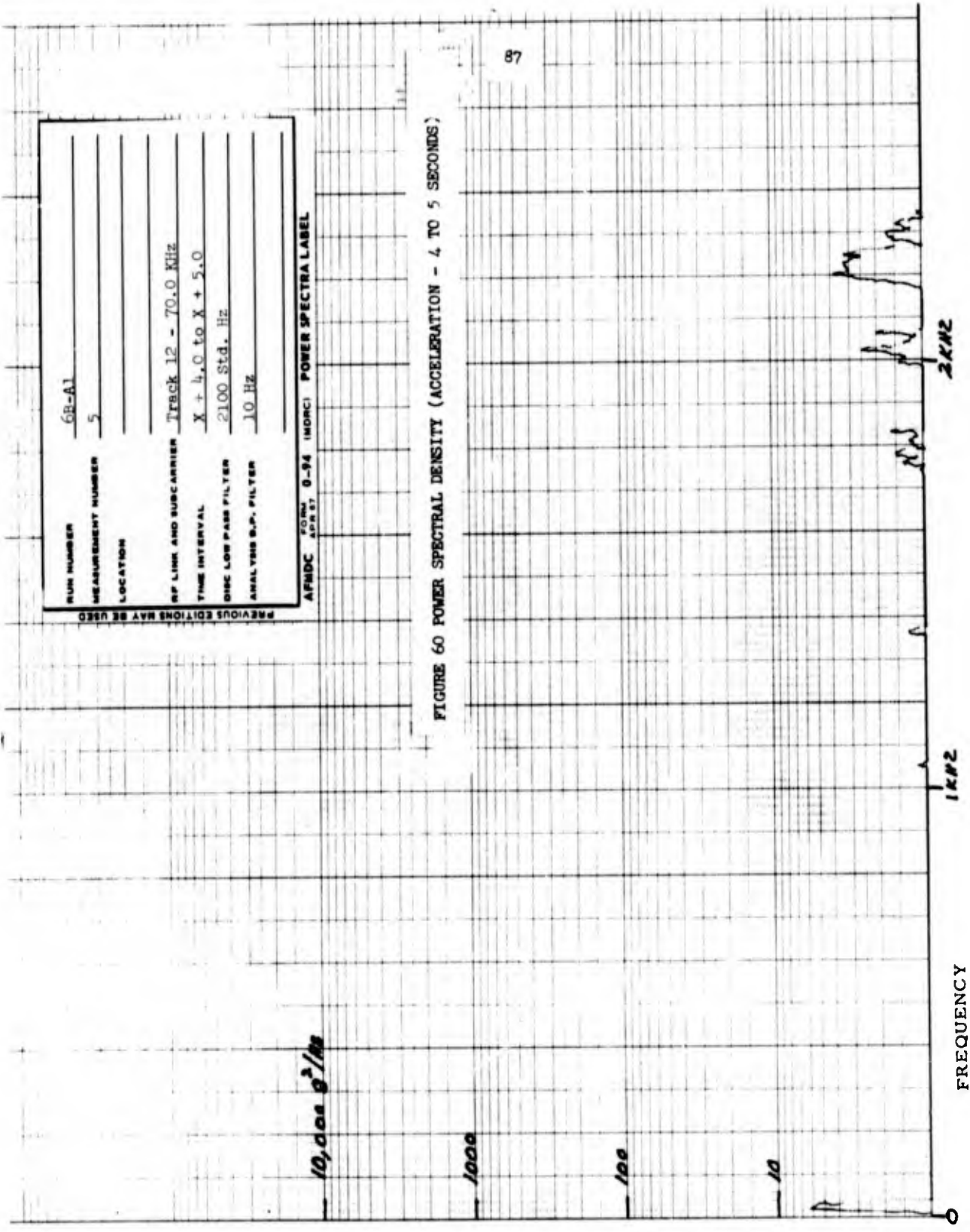


FIGURE 60 POWER SPECTRAL DENSITY (ACCELERATION - 4 TO 5 SECONDS)

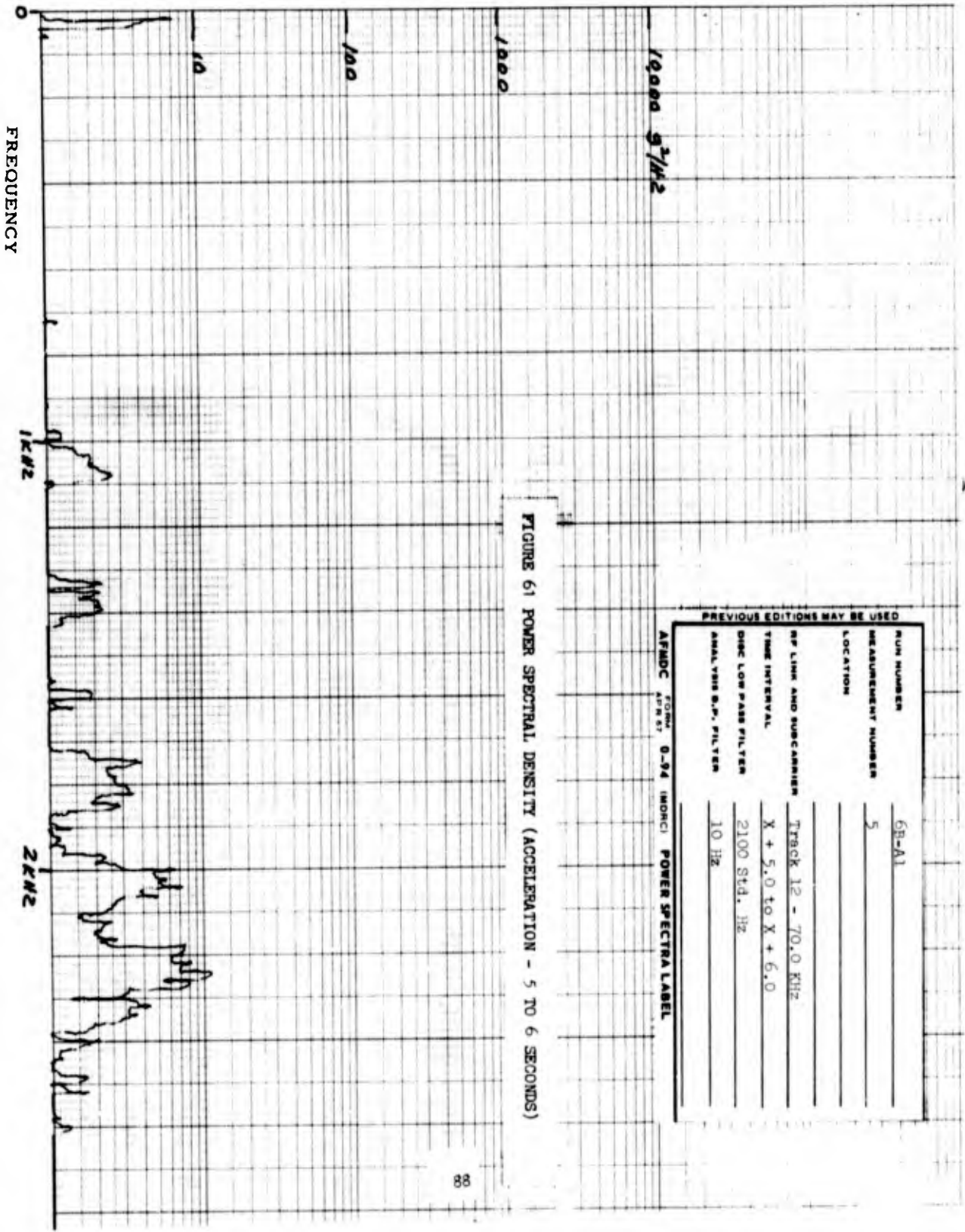


FIGURE 61 POWER SPECTRAL DENSITY (ACCELERATION - 5 TO 6 SECONDS)

PREVIOUS EDITIONS MAY BE USED

RUN NUMBER	68-A1
MEASUREMENT NUMBER	5
LOCATION	
RF LINK AND SUBCARRIER	Track 12 - 70.0 KHz
TIME INTERVAL	X + 5.0 to X + 6.0
DISC LOW PASS FILTER	2100 Std. Hz
SMALL VIBS S.P. FILTER	10 Hz

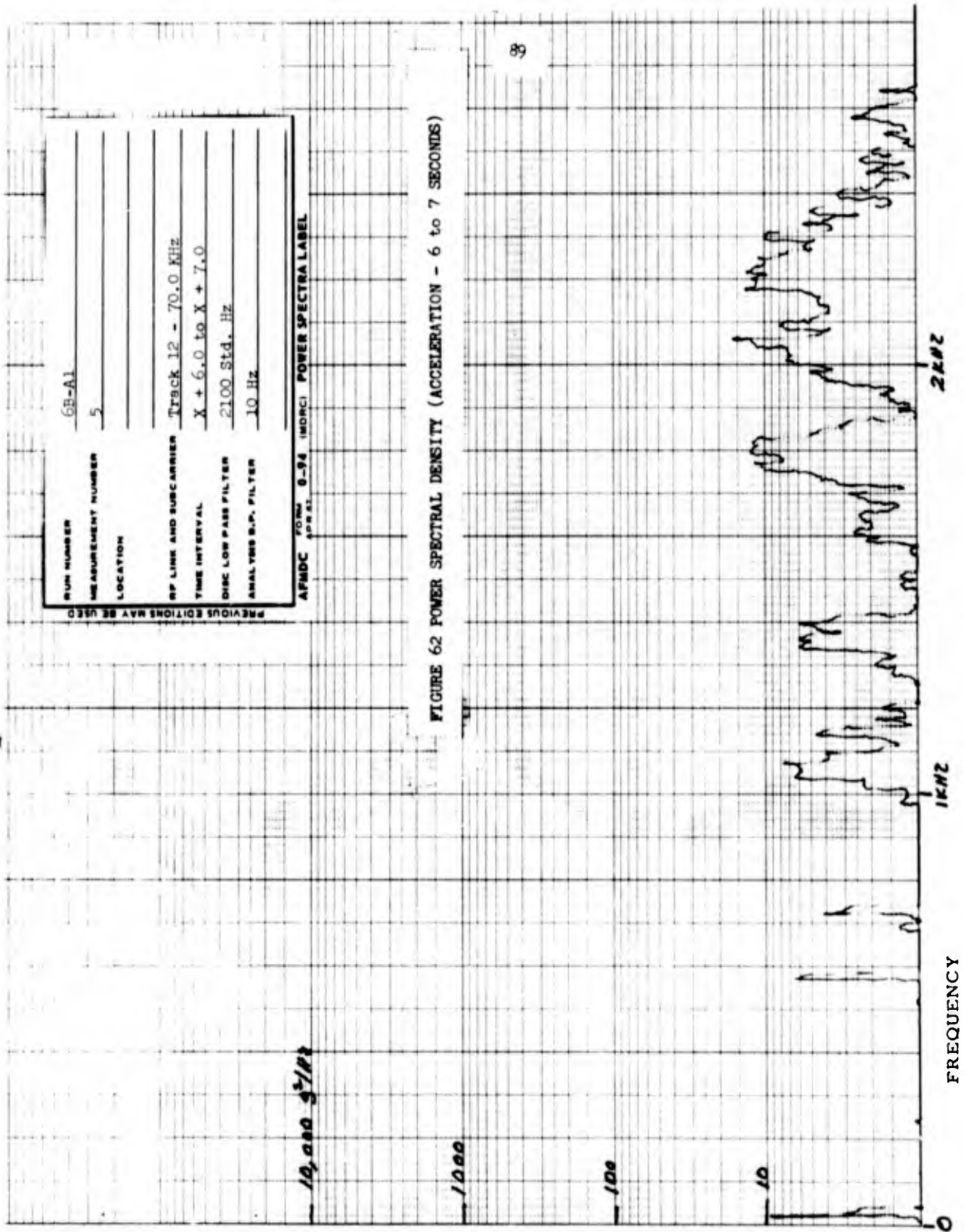
AFMDC FORM 8-64 (REV) POWER SPECTRA LABEL

PREVIOUS EDITIONS MAY BE USED

RUN NUMBER 6B-A1
MEASUREMENT NUMBER 5
LOCATION
RF LINK AND SUBCARRIER Track 12 - 70.0 KHz
TIME INTERVAL X + 6.0 to X + 7.0
DISC LOW PASS FILTER 2100 Std. Hz
ANALYSIS B.P. FILTER 10 Hz

APMDC FORM 8-74 (MORCI) POWER SPECTRA LABEL

FIGURE 62 POWER SPECTRAL DENSITY (ACCELERATION - 6 to 7 SECONDS)



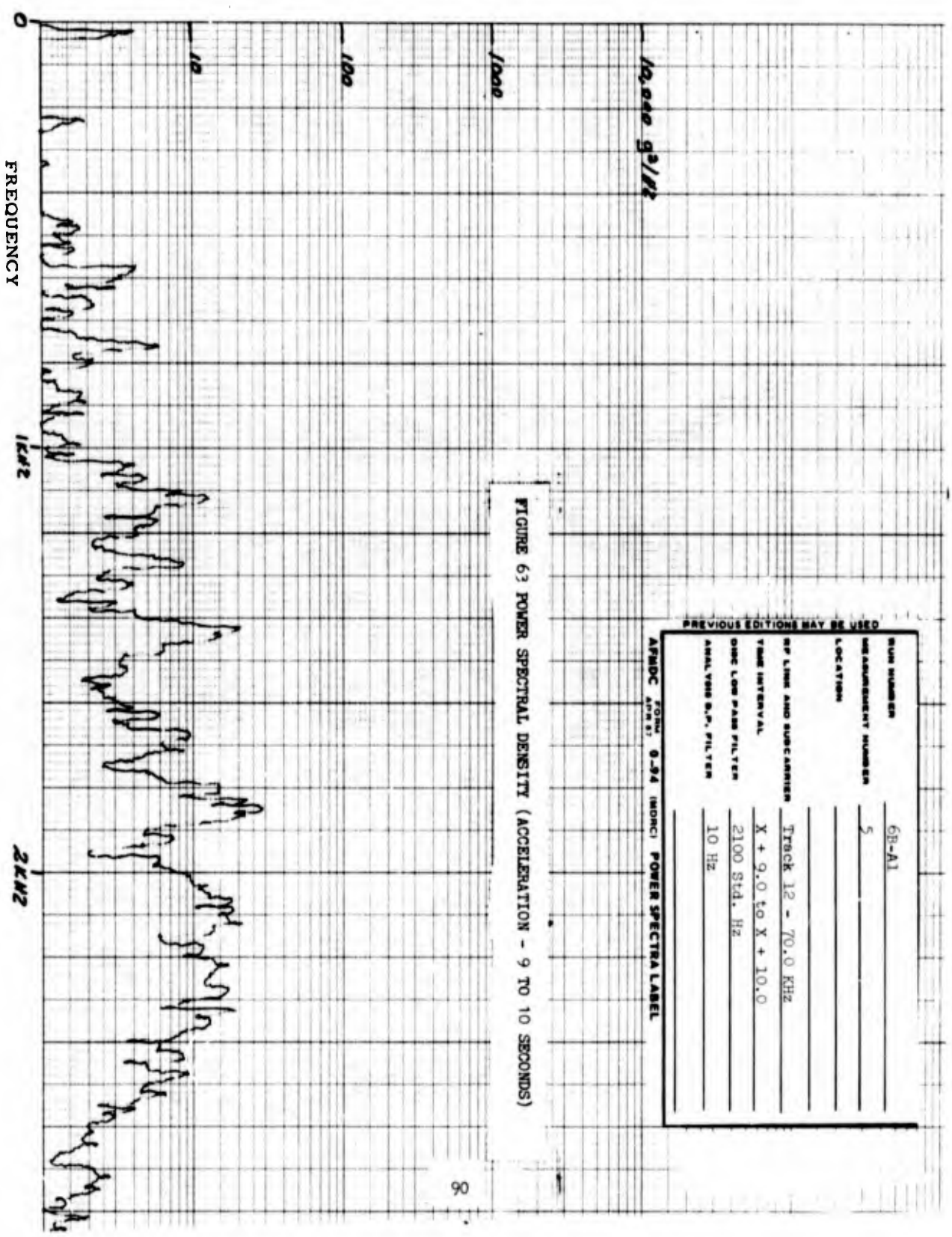


FIGURE 63 POWER SPECTRAL DENSITY (ACCELERATION - 9 TO 10 SECONDS)

PREVIOUS EDITIONS MAY BE USED

RUN NUMBER	6B-A1
MEASUREMENT NUMBER	5
LOCATION	
RF LINK AND SUBCARRIER	Track 12 - 70.0 KHz
TIME INTERVAL	X + 9.0 to X + 10.0
OSC LOW PASS FILTER	2100 Std. Hz
ANALYSIS B.P. FILTER	10 Hz

AFMDC FORM 9-54 (MAY 51) POWER SPECTRA LABEL

APPENDIX

The following computer program has been introduced for completeness. The inputs are those of Group I, λ equals 13.913. The coefficients used for the polynomials which approximate the blast parameters and aerodynamic coefficients are indicated. These polynomials, however, are not considered input parameters.

BLAST FORCES PROGRAM
 PROGRAM PRAW03
 PROJECT.....57100
 PROGRAMMER..R WARD
 DATE.....230567

INPUT PARAMETERS FOR GROUP I IN THIS REPORT

A 3.1416000000+000
 C1I -1.3900000000+000
 C2I 2.0900000000-001
 K 0.0000000000+000
 L 7.0000000000+000
 J 200
 RI 1.7026000000+002
 SI 1.2959000000+004
 DT 1.0000000000+000
 VB 3.3000000000+003
 LAMBDA 1.3913000000+001
 PHII 7.0000000000+001

EQUATION COEFFICIENTS.....

D1 9.4152999998-001
 D2 4.4615000000-001
 D3 0.0000000000+000
 D4 0.0000000000+000
 F1 1.4169872800+000
 F2 6.4676794700-001
 F3 -7.2516048900-001
 F4 -5.1111800499-001
 G1 -4.3797170899-001
 G2 -4.4041408000+000
 G3 -5.5714343900+000
 G4 -1.8323707200+000
 G5 0.0000000000+000
 G6 0.0000000000+000
 H1 1.7418572300+000
 H2 1.5848683400+000
 H3 3.0792788999-001
 H4 -8.2790775299-002
 O1 1.0923486200+000
 O2 -1.9668816800+000
 O3 -2.3819368500+000
 O4 -5.9149204900-001
 O5 0.0000000000+000
 O6 0.0000000000+000
 SP1 3.0000000000+000
 SP2 3.0000000000+000
 SP3 3.0000000000+000

$C_2 = f(C_1)$

$C_4 = f(C_3)$

$J_2 = f(C_3)$

$C_6 = f(C_5)$

$J_3 = f(C_5)$

POLYNOMIAL CONSTANTS FOR BLAST PARAMETERS

23/05/67

```

PROGRAM PRAW03
C   RICHARD A WARD
C   ROOM 116A   PHONE 4235
COMMON Y(550),Z(550),N,XJ1(550),XJ3(550),XMR(550),PDC1(550),
1PDC2(550),PDC3(550),PDC4(550),PDC5(550),PDC6(550),PHIDEG(550),
2R(550),S(550),T(550),U(550),V(550),VR(550),THETA1(550),THETA2(550),
3,THETA3(550),THETA4(550),THETA5(550),THETA6(550),RHO(550),
4PHI(550),PSI(550)
DIMENSION C1(550),C3(550),C5(550),TEXT(100),ID(14),LABEL(7),
1FOUT(7,36)
EQUIVALENCE (U,THETA1),(Z,THETA2),(XJ1,THETA3),(XJ3,THETA4),
1(C1,THETA5),(C3,THETA6),(C5,PDC1),(R,PDC2),(S,PDC3),(V,PDC4),
2(PHI,PDC5),(PHIDEG,PDC6),(Y,XMR)
DATA (LABEL=6HTIME ,6HF01 ,6HF02 ,6HF03 ,6HF04 ,6HF05
16HF06 )
C   SET PROGRAM CONSTANTS
DATA (ABAR=0.9877),(AO=1125.),(P=12.8),(RADIAN=57.2957795),
1(PI=3.1415926536),(TB=0.0),(RHOO=0.002018),
2(AA1=43.9324147),(AA2=-37.7235671),(AA3=10.1142973),
3(AA4=-.862630838),(BB1=.0798312804),(BB2=.187065866),
4(BB3=-.117832801),(BB4=.0212806959),(CC1=-.0989421312),
5(CC2=-1.96121294),(CC3=1.81792423),(CC4=-.375378495),
6(DD1=-.689392585),(DD2=1.08891493),(DD3=-.384747134),
7(DD4=.0438806198),(EE1=3425.8743),(EE2=-4691.6822),
8(EE3=2119.77639),(EE4=-300.456895),(FF1=0.0341326288),
9(FF2=-.135145185),(FF3=.0809705442),(FF4=-.0134834234),
A(GG1=403.025341),(GG2=-445.915420),(GG3=166.241063),
B(GG4=-20.6288667),(HH1=.342297313),(HH2=-.368412704),
C(HH3=.107528706),(HH4=-.00855234317),(OO1=-5.49730618),
D(OO2=12.9642358),(OO3=-7.08455938),(OO4=1.02859258),
E(PP1=-.76810477),(PP2=1.07151903),(PP3=-.426265938),
F(PP4=.0544730308),(QQ1=7.51049323),(QQ2=-8.85069614),
G(QQ3=3.05074616),(QQ4=-.326529993),(RR1=1.04864168),
H(RR2=-.969369386),(RR3=.44013466),(RR4=-.069435772)
LUO=11
CALL DATE(MDY)
C   READ OUTPUT TAPE LABEL AND SET UP ID RECORD
READ 1000,ID(1),ID(2),NSET
ID(3)=ID(7)=ID(8)=ID(9)=6H
ID(5)=MDY
ID(6)=6MPRAW03
ID(11)=0
ID(12)=7
ID(13)=36
ID(14)=6HFILE 0
READ 1101,TEXT
C   PROCESS N SETS OF DATA
DO 100 IJK=1,NSET
ICNT=NPRINT=SUMV=IOUT=0.0
C   READ IN AND PRINT OUT ONE SET OF PARAMETERS
READ 1011,A,C1,C2,XK,XL,J,RI,S1,DT,VR,XLAMBDA,PHI1,D1,D2,D3,
1D4,F1,F2,F3,F4,G1,G2,G3,G4,G5,G6,H1,H2,H3,H4,
2Q1,Q2,Q3,Q4,Q5,Q6,SP1,SP2,SP3
PRINT 1001,MDY
PRINT 1021,A,C1,C2,XK,XL,J,RI,S1,DT,VR,XLAMBDA,PHI1,D1,D2,D3,
1D4,F1,F2,F3,F4,G1,G2,G3,G4,G5,G6,H1,H2,H3,H4,

```

POLYNOMIAL CONSTANTS FOR
AERODYNAMIC COEFFICIENTS

```

201,Q2,Q3,Q4,Q5,Q6,SP1,SP2,SP3
  ID(14)=ID(14)+10000P
C   WRITE AND PRINT OUT ID RECORD
  CALL IDENT(LUO,ID,LABEL,IDFLAG)
  PRINT 1111,TEXT
C   COMPUTE RO,SO,ZI,TI OF TABLE 1
  APH11=PHI1+.0174532925
  RO=RI*SINF(APH11)
  SO=SI+RI*COSF(APH11)
  ZI=RI/XLAMBDA
  TI=(RI+C2I)/(ABAR*ZI**2*(1+C1I))
C   DETERMINE TOTAL NUMBER OF POINTS IN TIME (N)
  ITIT=XINTF(TI)
  N=ITIT+J
  IF(N.GT.550)2,6
  2  PRINT 1030,N
  N=550
C   COMPUTE TIME SERIES AND V, N TIMES EACH
  6  DO 10 M=1,N
  T(M)=M*DT
  10  V(M)=VB+XK*T(M)
C   COMPUTE SB OF TABLE 1
  DO 12 I=1,ITIT
  12  SUMV=SUMV+V(I)
  SB=SI-(SUMV+((TI-ITIT)*V(ITIT)))*.001
C   COMPUTE REMAINDER OF TABLE 2, N TIMES
  DELT=DT*.001
  RO2=RO+RO
  DO 30 M=1,N
  IF(M.GT.1)GO TO 20
  S(1)=SB+V(1)*DELT
  GO TO 22
  20  S(M)=S(M-1)+V(M)*DELT
  22  R(M)=SQRTF((S(M)-SO)**2+PO2)
  IF(SO.EQ.S(M))GO TO 25
  PHI(M)=ATANF(RO/(SO-S(M)))
  IF(SO.LT.S(M))25,27
  23  PHI(M)=PHI(M)+PI
  GO TO 27
  25  PHI(M)=1.5707963268
  27  PHIDEG(M)=PHI(M)*RADIAN
  Z(M)=R(M)/XLAMBDA
  30  Y(M)=(ABAR*R(M))/XLAMBDA
C   COMPUTE TOUT AND PRINT TABLE 1
  DO 32 M=1,N
  IF(T(M).LE.TI)GO TO 32
  EPSILON=C2I*Z(M)**ABSF(C1I)-Y(M)
  IF(EPSILON.LT.0.0)GO TO 32
  OLDEPSI=C2I*Z(M-1)**ABSF(C1I)-Y(M-1)
  TOUT=T(M-1)-OLDEPSI/(EPSILON-OLDEPSI)
  GO TO 33
  32  CONTINUE
  33  PRINT 1041,RO,SO,ZI,TI,SB,TOUT
C   PRINT TABLE 2, N LINES
  PRINT 1051,(T(M),V(M),S(M),R(M),PHIDEG(M),Z(M),Y(M),M=1,N)
C   BY NEWTONS METHOD, FIND ROOTS C1,C3,C5, N TIMES EACH

```

```

CALL DEWTON(D4,D3,D2,D1,C1,SP1)
CALL NEWTON(F4,F3,F2,F1,C3,SP2)
CALL NEWTON(H4,H3,H2,H1,C5,SP3)
C COMPUTE REMAINDER OF TABLE 3 AND PRINT OUT EACH LINE, N TIMES
DO 60 M=1,N
IF(C1(M).EQ.9999.)GO TO 35
IF(C1(M).LT.-1.228)GO TO 301
IF(C1(M).LT.-1.179)GO TO 302
IF(C1(M).LT.-1.153)GO TO 303
IF(C1(M).LT.-1.131)GO TO 304
IF(C1(M).LT.-1.025)GO TO 305,306
301 XJ1(M)=0.109649*C1(M)+0.134649
GO TO 34
302 XJ1(M)=1.020408163*C1(M)+1.253061224164
GO TO 34
303 XJ1(M)=1.925076923*C1(M)+2.317307692217
GO TO 34
304 XJ1(M)=6.818181818*C1(M)+7.961363636154
GO TO 34
305 XJ1(M)=2.6089*C1(M)+3.2006
GO TO 34
306 XJ1(M)=4.85229*C1(M)+5.5002
34 DELTAP=P*XJ1(M)
GO TO 40
35 XJ1(M)=DELTAP=9999.
40 IF(C3(M).EQ.9999.)GO TO 45
XJ2=G6*C3(M)**5+G5*C3(M)**4+G4*C3(M)**3+G3*C3(M)**2+G2*C3(M)+G1
U(M)=A0*XJ2
GO TO 50
45 XJ2=U(M)=9999.
50 IF(C5(M).EQ.9999.)GO TO 55
XJ3(M)=G6*C5(M)**5+G5*C5(M)**4+G4*C5(M)**3+G3*C5(M)**2+G2*C5(M)+G1
RHO(M)=RH00*XJ3(M)
GO TO 57
55 XJ3(M)=RHO(M)=9999.
57 NPRNT=NPRNT+1
IF(NPRNT.EQ.1)PRINT 1060
PRINT 1061,(M),C1(M),XJ1(M),DELTAP,C3(M),XJ2,U(M),C5(M),XJ3(M),
1RHO(M)
IF(NPRNT.EQ.50)NPRNT=0
60 CONTINUE
NPRNT=0
C COMPUTE AND PRINT OUT TABLE 4, N TIMES
DO 70 M=1,N
IF(U(M).EQ.9999.)GO TO 62
VR(M)=SQRTF(V(M)*V(M)+U(M)*U(M)+(V(M)+V(M))*U(M)*COSF(PHI(M)))
PSI(M)=ASINF(U(M)*SINF(PHI(M))/VR(M))*RADIAN
GO TO 63
62 VR(M)=PSI(M)=9999.
63 X3=(1+XJ1(M))/XJ3(M)
IF(XJ1(M).EQ.9999..OR.XJ3(M).EQ.9999..OR.X3.LE.0.0)GO TO 66
AR=A0*SQRTF(X3)
GO TO 67
66 AR=9999.
67 IF(VR(M).EQ.9999..OR.AR.EQ.9999.)GO TO 68
XMR(M)=VR(M)/AR

```

$$J_1 = f(C_1)$$

STRAIGHT LINE APPROXIMATIONS
FOR BLAST PARAMETERS

```

GO TO 69
68 XMR(M)=9999.
69 NPRNT=NPRNT+1
   IF(NPRNT.EQ.1)PRINT 1070
   PRINT 1071,I(M),VR(M),AR,XMR(M),PSI(M)
   IF(NPRNT.EQ.50)NPRNT=0
70 CONTINUE
   NPRNT=0
C   COMPUTE AND PRINT OUT TABLE 5, N TIMES
   DO 80 M=1,N
   IF(XMR(M).EQ.9999.)GO TO 75
   XMR1=XMR(M)
   XMR2=XMR1*XMR1
   XMR3=XMR2*XMR1
   THETA1(M)=AA4*XMR3+AA3*XMR2+AA2*XMR1+AA1
   PDC1(M)= BB4*XMR3+BB3*XMR2+BB2*XMR1+BB1
   THETA2(M)=CC4*XMR3+CC3*XMR2+CC2*XMR1+CC1
   PDC2(M)= DD4*XMR3+DD3*XMR2+DD2*XMR1+DD1
   THETA3(M)=EE4*XMR3+EE3*XMR2+EE2*XMR1+EE1
   PDC3(M)= FF4*XMR3+FF3*XMR2+FF2*XMR1+FF1
   IF(XMR1.GE.2.45)PDC3(M)=0.004981*XMR1-0.02144
   THETA4(M)=GG4*XMR3+GG3*XMR2+GG2*XMR1+GG1
   PDC4(M)= HH4*XMR3+HH3*XMR2+HH2*XMR1+HH1
   THETA5(M)=OU4*XMR3+OU3*XMR2+OU2*XMR1+OU1
   PDC5(M)= PP4*XMR3+PP3*XMR2+PP2*XMR1+PP1
   THETA6(M)=QU4*XMR3+QU3*XMR2+QU2*XMR1+QU1
   PDC6(M)= RR4*XMR3+RR3*XMR2+RR2*XMR1+RR1
   GO TO 77
75 THETA1(M)=THETA2(M)=THETA3(M)=THETA4(M)=THETA5(M)=THETA6(M)=999.
   PDC1(M)=PDC2(M)=PDC3(M)=PDC4(M)=PDC5(M)=PDC6(M)=999.
77 NPRNT=NPRNT+1
   IF(NPRNT.EQ.1)PRINT 1080
   PRINT 1081,I(M),THETA1(M),PDC1(M),THETA2(M),PDC2(M),THETA3(M),
1 PDC3(M),THETA4(M),PDC4(M),THETA5(M),PDC5(M),THETA6(M),PDC6(M)
   IF(NPRNT.EQ.50)NPRNT=0
80 CONTINUE
   NPRNT=0
C   COMPUTE AND PRINT OUT TABLE 6, N TIMES
   A12=A*.5
   A12X=A12*XL
   DO 90 M=1,N
   ICNT=ICNT+1
   FOUT(1,ICNT)=T(M)
   IF(XMR(M).EQ.9999.)GO TO 85
   RHOVR2=RHO(M)*VR(M)*VR(M)
   F01=FOUT(2,ICNT)=A12 *PDC1(M)*RHOVR2*(PSI(M)-THETA1(M))
   F02=FOUT(3,ICNT)=A12 *PDC2(M)*RHOVR2*(PSI(M)-THETA2(M))
   F03=FOUT(4,ICNT)=A12 *PDC3(M)*RHOVR2*(PSI(M)-THETA3(M))
   F04=FOUT(5,ICNT)=A12X*PDC4(M)*RHOVR2*(PSI(M)-THETA4(M))
   F05=FOUT(6,ICNT)=A12X*PDC5(M)*RHOVR2*(PSI(M)-THETA5(M))
   F06=FOUT(7,ICNT)=A12X*PDC6(M)*RHOVR2*(PSI(M)-THETA6(M))
   GO TO 87
85 F01+F02=F03+F04+F05=F06=9999.
   DO 86 I=2,7
86 FOUT(I,ICNT)=9999.
87 NPRNT=NPRNT+1

```

```

      IF(NPRNT.EQ.1)PRINT 1090
      PRINT 1091,T(M),F01,F02,F03,F04,F05,F06
      IF(NPRNT.EQ.50)NPRNT=0
C     IF BUFFER FULL, WRITE ONE RECORD ON TAPE
      IF(ICNT.EQ.36)88,90
      88  WRITE TAPE LUO,FOUT
          ICNT=0
          DO 89 I=1,2>2
      89  FOUT(I)=0.0
      90  CONTINUE
C     WRITE FINAL RECORD OF FILE ON TAPE
      IF(ICNT.GT.0)WRITE TAPE LUO,FOUT
      END FILE LUO
C     READ NEXT SET OF PARAMETERS
      100  CONTINUE
C     END PROGRAM IF ALL SETS OF DATA PROCESSED
      CALL UNLOAD(LUO)
C*****FORMATS*****
      1000 FORMAT(2A6,4X,I16)
      1001 FORMAT(1H1*BLASI FORCES PROGRAM/*PROGRAM PRAW03/*PROJECT.....57.
          1100/*PROGRAMMER..R WARD/*DATE.....*A6)
      1011 FORMAT(5E16.0/I16,4E16.0/(5E16.0))
      1021 FORMAT(///*INPUT PARAMETERS**/*A*E25.10/*C11*E23.10/*C21*E23.10/
          1*K*E25.10/*L*E25.10/*J*125/*RI*E24.10/*SI*E24.10/*DT*E24.10/*VB*
          2E24.10/*LAMBDA*E20.10/*PHI1*E22.10/*EQUATION COEFFICIENTS.....*/
          3* D1*E22.10/* D2*E22.10/* D3*E22.10/* D4*E22.10/* F1*E22.10
          4/* F2*E22.10/* F3*E22.10/* F4*E22.10/* G1*E22.10/* G2*E22.10
          5/* G3*E22.10/* G4*E22.10/* G5*E22.10/* G6*E22.10/* H1*E22.10
          6/* H2*E22.10/* H3*E22.10/* H4*E22.10/* Q1*E22.10/* Q2*E22.10
          7/* Q3*E22.10/* Q4*E22.10/* Q5*E22.10/* Q6*E22.10/*SP1*E23.10
          6/*SP2*E23.10/*SP3*E23.10,10(/))
      1030 FORMAT(/*NUMBER OF POINTS IN TIME (*I4*) EXCEEDS DIMENSION LIMIT*.
          1/)
      1041 FORMAT(9(/)* TABLE 1*//14X*RO*18X*SO*16X*ZI*18X*TI*18X*SB*16X*TOUT.
          1*//5(F16.6,4X),+16.1)
      1051 FORMAT(1H1*TABLE 2*//4X*T*17X*V*17X*S*17X*R*12X*PHIDEG*17X*Z*17X*Y.
          1*//50(F5.0,6F18.6,/)
      1060 FORMAT(1H1,*TABLE 3*//4X*T*10X*C1*10X*J1*6X*DELTAP*10X*C3*10X*J2*1.
          11X*U*10X*C5*10X*J3*9X*RHO*//)
      1061 FORMAT(F5.0,9F12.6)
      1070 FORMAT(1H1,* TABLE 4*//4X*T*19X*VR*19X*AR*19X*MR*18X*PSI*//)
      1071 FORMAT(F5.0,4F21.6)
      1080 FORMAT(1H1,* TABLE 5*//4X*T*3X*THETA1*5X*PDC1*3X*THETA2*5X*PDC2*3X.
          1*THETA3*5X*PDC3*3X*THETA4*5X*PDC4*3X*THETA5*5X*PDC5*3X*THETA6*5X*P.
          2DC6*//)
      1081 FORMAT(F5.0,12F9.3)
      1090 FORMAT(1H1,* TABLE 6*//4X,*T*15X*F01*15X*F02*15X*F03*15X*F04*15X*F.
          105*15X*F06*//)
      1091 FORMAT(F5.0,6F18.3)
      1101 FORMAT(10A8)
      1111 FORMAT(1H1/////((21X,10A8))
          END

```

```
SUBROUTINE NEWTON(PAR1,PAR2,PAR3,PAR4,PAR5,SP)
COMMON Y(550),Z(550),N
DIMENSION PAR5(550)
EPSILON=0.0001
DO 110 M=1,N
  III=1
  VARC=SP
100 FOFU=Y(M)*Z(M)**VARC-PAR1*VARC**3-PAR2*VARC**2-PAR3*VARC-PAR4
  IF(ABS(FOFU).LE.EPSILON)GO TO 109
  IF(III.EQ.1)GO TO 105
  DIFF=FOFCLAST-FOFU
  IF(FOFCLAST.LT.0.0)102,103
102 DIFF=-DIFF
103 IF(DIFF.LE.0.0)GO TO 107
105 FOFCLAST=FOFU
  III=2
  VARC=VARC-FOFU/(Y(M)*Z(M)**VARC*LOG(Z(M))-3.*PAR1*VARC**2-2.*PAR2
1*VARC-PAR3)
  GO TO 100
107 PAR5(M)=9999.
  GO TO 110
109 PAR5(M)=VARC
110 CONTINUE
  RETURN
END
```

```

SUBROUTINE NEWTON(PAR1,PAR2,PAR3,PAR4,PAR5,SP)
COMMON Y(550),Z(550),N
DIMENSION PAR5(550)
EPSILON=0.0001
C* FIND ROOTS USING NEWTONS METHOD
DO 210 M=1,N
  III=1
  VARC=SP
100 FOF=C*(Y(M)*Z(M)**VARC-PAR1*VARC**3-PAR2*VARC**2-PAR3*VARC-PAR4
  IF(ABS(FOF).LE.EPSILON)GO TO 109
  IF(III.EQ.1)GO TO 105
  DIFF=FOF-FOFCLAST
  IF(FOFCLAST.LT.0.0)102,103
102 DIFF=-DIFF
103 IF(DIFF.LE.0.0)GO TO 107
105 FOFCLAST=FOF
  III=2
  VARC=VARC-FOF/(Y(M)*Z(M)**VARC*LOG(Z(M))-3.*PAR1*VARC**2-2.*PAR2
  1*VARC-PAR3)
  GO TO 100
C* IF NO ROOT CAN BE FOUND,THEN
107 PAR5(M)=9999.
  GO TO 110
109 PAR5(M)=VARC
110 IF(PAR5(M).NE.9999.AND.PAR5(M).GT.-1.5)GO TO 210
C ELSE FIND ROOT WITH D1 = 0.46288 AND D2 = 0.127046
  III=1
  VARC=-1.0
200 FOF=C*(Y(M)*Z(M)**VARC-0.127046*VARC-0.46288
  IF(ABS(FOF).LE.EPSILON)GO TO 209
  IF(III.EQ.1)GO TO 205
  DIFF=FOF-FOFCLAST
  IF(FOFCLAST.LT.0.0)202,203
202 DIFF=-DIFF
203 IF(DIFF.LE.0.)GO TO 207
205 FOFCLAST=FOF
  III=2
  VARC=VARC-FOF/(Y(M)*Z(M)**VARC*LOG(Z(M))-0.127046)
  GO TO 200
207 PAR5(M)=9999.
  GO TO 210
209 PAR5(M)=VARC
210 CONTINUE
  RETURN
  END

```

DISTRIBUTION

Defense Documentation Center Cameron Station Alexandria, Virginia 22314	20
Air University Library Maxwell AFB, Alabama 36112	1
ASD (ASMD) Wright-Patterson AFB, Ohio 45433	1
AFFTC (FIBPP-2) Edwards AFB, California 93523	1
AFETR (ETLIG-3) Patrick AFB, Florida 32925	1
AFSWC (SWLPR) Kirtland AFB, New Mexico 87117	1
AEDC (AET) Airnold Air Station, Tennessee 37389	1
APGC (PGGT) Eglin AFB, Florida 32542	1
BGD (BSOM) Norton AFB, California 92409	1
EDS (ESTI) L. G. Hanscom Field Bedford, Massachusetts 01731	1
SAMSO (SMSDI-STINFO) AF Unit Post Office Los Angeles, California 90045	1
AFML (MAAM) Wright-Patterson AFB, Ohio 45433	1
RRD (Documents Service Center)	3
MDG	1
MDNH	1

Unclassified

Security Classification

DOCUMENT CONTROL DATA - R & D

(Security classification of title, body of abstract and indexing annotation must be entered when the overall report is classified)

1. ORIGINATING ACTIVITY (Corporate author) AFMDC (MDTE) Holloman AFB, New Mexico 88330		2a. REPORT SECURITY CLASSIFICATION Unclassified	
		2b. GROUP	
3. REPORT TITLE Predicted Forcing Functions and Force Measurements on an Outrigger Rocket Sled Traveling Through a Blast Environment			
4. DESCRIPTIVE NOTES (Type of report and inclusive dates)			
5. AUTHOR(S) (First name, middle initial, last name) Krupovage, Daniel J.			
6. REPORT DATE December 1967		7a. TOTAL NO. OF PAGES 110	7b. NO. OF REFS 11
8a. CONTRACT OR GRANT NO. N/A		9a. ORIGINATOR'S REPORT NUMBER(S) MDC-TR-68-4	
b. PROJECT NO. N/A		9b. OTHER REPORT NO(S) (Any other numbers that may be assigned this report)	
c.			
d.			
10. DISTRIBUTION STATEMENT Distribution of this document is unlimited			
11. SUPPLEMENTARY NOTES N/A		12. SPONSORING MILITARY ACTIVITY Air Force Missile Development Center Air Force Systems Command Holloman Air Force Base, New Mexico 88330	
13. ABSTRACT A technique was developed for predicting the aerodynamic forcing functions acting on an outrigger rocket sled as it traversed a blast environment. This technique was programmed on the CDC 3600 computer. In order to computerize the technique, the time histories of the blast parameters were approximated by first and third order polynomial equations. The sled trajectory was transformed into the scaled time and distance coordinates of the blast parameters. The steady state aerodynamic coefficients as a function of Mach number obtained from wind tunnel tests were approximated by third order polynomials. These steady state coefficients were used at discreet times to define the aerodynamic forces acting on the vehicle as it traversed the blast environment. The report also describes the load transducer used to measure the lateral forces acting on the front slipper of the outrigger rocket sled. The time history of these measured forces and lateral acceleration data is discussed. A maximum force on the front slipper of 76,000 pounds was recorded on one of the runs. Also included is information on the vehicle structural vibration frequencies, which was obtained from reduction of test data in the form of power spectral density.			

14 KEY WORDS	LINK A		LINK B		LINK C	
	ROLE	WT	ROLE	WT	ROLE	WT
Rocket Sleds Outrigger Sleds Blast Testing Forcing Functions Sled Forces						